National Centre for Nuclear Research

DOCTORAL THESIS

Establishment of best practices in reducing uncertainties in multigroup cross-sections with Bayesian methods

PhD Candidate Michał Jędrzejczyk

A thesis submitted in fulfilment of the requirements
for the degree of Doctor of Physical Sciences
in the National Centre for Nuclear Research

Supervisor:
Prof. dr. hab. Tomasz Kozłowski

Auxiliary supervisor:
Dr. Piotr Kopka

Acknowledgments

I would like to express my gratitude to my supervisors, Tomasz Kozłowski and Piotr Kopka, for their unwavering commitment to giving me excellent guidance and support throughout the course of my Ph.D. studies. I also would like to thank the co-author of my first publication, Dr. Basma Foad, for trusting me with the software tools of her design, which were crucial to the paper's success, and with her help in the formal analysis and writing the paper. I would like to thank Prof. Mariusz Dąbrowski and Dr. Karol Kowal for creating and running the PHD4GEN program, which made my desire to work in the field of nuclear engineering possible. I would also like to thank my family for their faith in me and their support.

Contents

List of Figures

List of Tables

Nomenclature

Greek and Latin symbols in Bayesian algorithms

α	A vector of variables representing generic model input parameters designated for Bayesian calibration
α'	Vector of posterior means of α
α_0	A vector of best estimates of generic model input parameters
$\alpha_{1:N}$	Denotes N Monte Carlo samples of α
β	Sequential Monte Carlo algorithm transition parameter
χ	Chi-statistic
δ	Distance function used for calculating the distance between distributions in SMC-ABC algorithm. In this work, it is Wasserstein distance.
ϵ	"Threshold" parameter, an auxiliary parameter in SMC-ABC that is compared to δ to determine whether a sample of α^* should be accepted or rejected
γ	A vector representing model input parameters not designated for calibration
$\gamma^{1:L}$	Denotes L Monte Carlo samples of γ
γ_0	A vector of best estimates of γ
κ	Denotes the number of a sample within a Markov Chain in SMC-ABC
π	Denotes an approximate distribution generated by SMC-ABC
*	The symbol appears when denoting variables connected to the Markov Chain stage of SMC-ABC
$C_{\alpha'\alpha'}$	Posterior relative covariance matrix of α
$C_{\alpha\alpha}$	Prior relative covariance matrix of α
$C_{k'k'}$	Posterior covariance matrix of outputs of the mathematical models
C_{kk}	Prior covariance matrix of k or outputs of the mathematical models M
C_{mm}	Covariance matrix of experimental uncertainties. Includes uncertainties from uncalibrated model parameters

d Vector of relative differences between k and m calculated as $\frac{k_0 - m_0}{/k_0}$

E_{tot} The combined value of the model's and observed data's uncertainties. Used in SMC-ABC

$F_{m/k}$ diagonal matrix with filled with m_0/k_0 ratios

I Length of m and k vectors

K Denotes the length of Markov Chains in SMC-ABC

k A vector of variables representing mathematical models' predictions of m

k' Vector of posterior means of k

k_0 A vector of the best estimates of mathematical models' predictions of m_0

M Mathematical model whose output is k

m A vector of variables representing generic experimental data

m_0 A vector of best estimates of generic experimental data

P Denotes probability distributions

Q_0, Q_m, Q' Auxiliary parameters used in the derivation of MOCABA algorithm

R A variable representing a generic integral response calculated with α and M. Similar to k, but used only in the context of presenting sensitivities.

S Vector of relative sensitivities to the α parameters

s A variable representing systematic errors in experiments

$S_{k\alpha}$ Relative sensitivity matrix

t Denotes stage of SMC-ABC algorithm

y A vector that contains both α, and k

C Covariance matrix

Greek and Latin symbols in reactor physics

BEU Benchmark Experimental Uncertainty - k_eff uncertainty of benchmark experiments presented in ICSBEP handbook

C Covariance matrix.

CS Prior cross-section value

E Error calculated with "sandwich" method.

$HEU - MET - FAST$ Highly Enriched Uranium Fast Metal System

$HEU - SOL - THERM$ Highly Enriched Uranium Thermal Solution System

$IEU - MET - FAST$ Intermediately Enriched Uranium Fast Metal System

k_{eff} Multiplication factor

$LEU - COMP - THERM$ Low Enriched Uranium Thermal Compound System

MCU Monte Carlo Uncertainty - uncertainty due to stochastic nature of SCALE calculations using Monte Carlo solver

MD Model Discrepancy - difference between model output with input values known with perfect precision (an example of that would be neutron cross-sections without uncertainty) and experimental measurements. Denotes expected difference measured in 1 standard deviation between model output and experimental outcome.

PF Perturbation factor - a relative cross-section value. Prior equal to 1.

S Sensitivity vector.

UCS Updated cross-section value

$UCSU$ Uncertainty from uncalibrated neutron cross-section and uncalibrated chi and nubar parameters

UMC Uncertainty coming from using MG neutron cross-section library instead of the more reliable CE library

chi Probability of a fission-emitted neutron to have a specific energy

nubar Average number of neutrons emitted during fission induced with neutron of a specific energy

Acronyms and names in Bayesian algorithms

$\langle \cdot \rangle$ mean or Reynolds average

ABC Approximate Bayesian Computation

ESS Effective Sample Size

GLLS Generalized Linear Least Squares

MC Markov Chain

MOCABA A General Monte Carlo-Bayes Procedure for Improved Predictions of Integral Functions of Nuclear Data

SMC-ABC Sequential Monte Carlo - Approximate Bayesian Computation

Acronyms and names in reactor physics and associated computational tools

2D Two dimensional

BONAMI A SCALE module used for basic resonance self-shielding calculations

CE Continuous Energy

CENTRM A SCALE module used for advanced resonance self-shielding calculations, specifically in the resolved resonance range

CIŚ Centrum Informatyki Świerk - a computational cluster in National Centre for Nuclear Research

CSAS5 Criticality Safety Analysis Sequence with KENO V.a; A SCALE module

CSAS6 Criticality Safety Analysis Sequence with KENO VI.a; A SCALE module

ENDF/BVII.1 Evaluated Nuclear Data File; B denotes a version and VII.1 denotes specific release

ICSBEP International Criticality Safety Benchmark Evaluation Project

KENO Monte Carlo codes for eigenvalue neutronics calculations. KENO V. denotes a specific version of the code; A SCALE module

MG Multigroup

SCALE Standardized Computer Analysis for Licensing Evaluation

Author's contribution

The thesis is partially based on the publication "Applying approximate Bayesian computation to reduce uncertainty in multigroup 235-U cross-sections using ICSBEP experimental data" by Jędrzejczyk M., Kopka P., Foad B., and Kozłowski T.. Most of the contents of this publication are in Section 4.

Abstract

The multiplication factor (k_{eff}) and its uncertainty are critical design parameters in nuclear reactors. The k_{eff} uncertainty must be considered for operation, safety, and economic reasons. Consequently, reducing uncertainty in the k_{eff} has been of interest to the nuclear industry for as long as nuclear reactors were designed. Two methods are currently in use to accomplish that: Generalized Linear Least Squares (GLLS) and A General Monte Carlo-Bayes Procedure for Improved Predictions of Integral Functions of Nuclear Data (MOCABA). Both methods can reduce the k_{eff} uncertainty by reducing uncertainty in cross-sections by assimilating measured critical systems' or nuclear reactors' operational data. However, GLLS is limited to linear models and multivariate normal prior and posterior, while MOCABA can use any (non-linear) model but is also limited to multivariate normal prior and posterior.

This work implements a universal and rigorous algorithm called Sequential Monte Carlo – Approximate Bayesian Computation (SMC-ABC) for the same application. The algorithm can calibrate parameters with any prior and any posterior distribution. The calculations were conducted on select cross-sections from the 56-multigroup library based on the ENDF/B-VII.1 nuclear data library. It is found that despite the greater reliability of SMC-ABC, all three algorithms give essentially the same results for the same problems. Therefore, it is not worth using the computationally expensive SMC-ABC for neutron cross-section calibration.

A thorough study of the uncertainty sources in experimental k_{eff} is also presented. It is investigated how the omission of the uncalibrated uncertain cross-sections during the Bayesian assimilation impacts the results. The conclusion is that omitting uncalibrated parameters in Bayesian calibration, often done by researchers, is an incorrect approach.

In the context of nuclear engineering inverse problems, a new validation technique is presented and applied for inverse problem-solving. The technique relies on so-called "synthetic experiments". Synthetic experiments are computationally generated data used in place of experiments. The method verifies whether there is a risk of overfitting the calibrated parameters (cross-sections in the case of this work) during the data assimilation. Finally, the dissertation combines all the findings of the work to establish a best-practices guide for calibrating neutron cross-sections through the assimilation of experimental integral parameters' values.

Streszczenie

Opracowanie najlepszych praktyk przy zmniejszaniu niepewności w wielogrupowych przekrojach czynnych za pomocą metod Bayesowskich

Współczynnik multiplikacji (k_{eff}) oraz jego niepewność obliczeniowa są kluczowymi parametrami związanymi z procesem projektowania reaktorów jądrowych. Niepewność współczynnika k_{eff} musi być brana pod uwagę ze względu na aspekty eksploatacyjne, bezpieczeństwa oraz ekonomiczne. Z tego powodu redukcja niepewności k_{eff} jest od wielu lat przedmiotem zainteresowania energetyki jądrowej. Obecnie osiąga się ją za pomocą dwóch metod: Uogólnionej Metody Najmniejszych Kwadratów (ang. Generalized Linear Least Squares, GLLS) oraz Uogólnionej Metody Monte Carlo-Bayesowskiej Dla Polepszonych Przewidywań Funkcji Danych Jądrowych (ang. A General Monte Carlo-Bayes Procedure for Improved Predictions of Integral Functions of Nuclear Data, MOCABA). Niepewność k_{eff} zostaje obniżona poprzez bardziej precyzyjne poznanie wartości przekrojów czynnych. W tym celu asymiluje się dane eksperymentalne układów w stanie krytycznym lub eksploatowanych reaktorów jądrowych. Metoda GLLS jest ograniczona do modeli liniowych i wielowymiarowych rozkładów normalnych a priori i a posteriori. Metoda MOCABA pozwala na użycie dowolnego modelu matematycznego (w tym modeli nieliniowych), ale również jest ograniczona do wielowymiarowych rozkładów normalnych.

W ramach pracy zastosowano uniwersalny i niezawodny algorytm Przybliżonych Obliczeń Bayesowskich w wersji Sekwencyjnej (ang. Sequential Monte Carlo – Approximate Bayesian Computation, SMC-ABC). Celem było przetestowanie nowego algorytmu dla tego samego rodzaju problemów. Metoda ta potrafi kalibrować parametry wejściowe z dowolnym rozkładem a priori i otrzymywać dowolny rozkład a posteriori. Obliczenia przeprowadzono dla wybranych przekrojów czynnych z 56-grupowej biblioteki opartej o zbiór danych jądrowych ENDF/B-VII.1. Stwierdzono, że pomimo większej niezawodności SMC-ABC, wszystkie trzy algorytmy dają praktycznie te same wyniki dla tych samych zagadnień w przypadku kalibracji przekrojów czynnych. Wyciągnięto więc wniosek, że nie ma potrzeby używać w tym celu kosztownego obliczeniowo SMC-ABC.

W rozprawie zaprezentowano także szczegółową analizę źródeł niepewności parametru k_{eff}. Przedstawiono dowody na konieczność uwzględniania niepewności niekalibrowanych przekrojów czynnych przy obliczeniach niepewności k_{eff} podczas Bayesowskiej asymilacji danych eksperymentalnych. Wyciągnięto wniosek, że zignorowanie niepewności niekalibrowanych parametrów wejściowych modelu jest nieprawidłowym zabiegiem, co jest częstą praktyką wśród badaczy.

Istotną częścią badań było przedstawienie techniki walidacyjnej polegającej na zastosowaniu tzw. "syntetycznych eksperymentów". Metody tej dotychczas nie używano przy zagadnieniach odwrotnych w fizyce jądrowej. Eksperymenty syntetyczne to generowane komputerowo sztuczne wyniki eksperymentów używane zamiast rzeczywistych zestawów danych. Metoda pozwala na

sprawdzenie, czy istnieje ryzyko nadmiernego dopasowania (tzw. "overfittingu") analizowanych parametrów. W podsumowaniu rozprawy zostały zebrane wszystkie ustalenia oraz zaproponowany został zbiór najlepszych praktyk, które mogą być wykorzystywane przy Bayesowskiej kalibracji przekrojów czynnych.

1 Introduction

1.1 IV generation nuclear reactors

Generation IV reactors are advanced reactors in various stages of development, ranging from conceptual design to small prototypes, depending on the reactor type and the country or company that works on their deployment. The interest in these reactors stems from their potential for increasing thermal efficiency, utilization for industrial heat applications, greatly improved fuel utilization, and reducing the volume and radiotoxicity of waste [1]. These features may allow the generation IV reactors to significantly aid in reducing carbon dioxide emissions, which is the goal of the one hundred and ninety-three countries that signed the Paris Agreement [2]. Each of the 4th generation nuclear reactors has unique features and applications, contributing to the advancement of nuclear energy technology with a focus on safety, efficiency, and sustainability.
The list below presents 4th Generation Nuclear Reactors that were chosen for further support in research and development by the OECD:

- Gas-Cooled Fast Reactor (GFR): A high-temperature reactor operating at 800-850°C. It uses helium as a coolant and can be used for power generation, hydrogen production, or other process heat applications. The GFR aims for breakeven breeding and employs robust nitride or carbide fuels with plutonium content of 15 to 20%. It utilizes an indirect cycle with helium for electricity generation. [3]

- Lead-Cooled Fast Reactor (LFR): A flexible fast neutron reactor that can use depleted uranium or thorium fuel matrices. It operates at temperatures up to 800°C and can enable thermochemical hydrogen production. The LFR has various unit sizes, from small grids to large plants. It utilizes liquid metal (Pb or Pb-Bi eutectic) cooling. [4]

- Molten Salt Reactor (MSR): MSR has two variants, one with fast

neutron spectrum and fissile material dissolved in the circulation fuel salt, and the other with solid particle fuel in graphite and salt as a coolant. MSR systems have unique capabilities, lower fissile inventories, and offer efficient actinide burning. [5]

- Sodium-Cooled Fast Reactor (SFR): Utilizes liquid sodium as a coolant, allowing high power density at low pressure. It can use depleted uranium as fuel and has various design variants, including modular types and pool-type versions. Sodium-cooled fast reactors have been operational in several countries. [6]

- Supercritical Water-Cooled Reactor (SCWR): Operates with supercritical water at high pressure and temperature, offering a thermal efficiency one-third higher than current light water reactors. Fuel can be uranium oxide, and it may use thermal neutron spectrum with light or heavy water moderation. [7]

- Very High-Temperature Gas Reactor (VHTR): Utilizes graphite moderation and helium cooling, operating at temperatures over 900°C. It can be used for hydrogen production, electricity generation, or high-efficiency gas turbine driving. VHTR uses TRISO fuel particles for stability and safety. [8]

These design solutions are shown in Figure 1 (the figure comes from the resources of the Generation IV International Forum (GIF) [9]) In 2013, four nuclear research institutes and engineering firms representing the Visegrád Group of Nations (V4) in Central Europe reached an agreement to establish a collaborative centre dedicated to research, development, and innovation in Generation IV nuclear reactors. This initiative gave rise to the V4G4 Centre of Excellence, a consortium comprising the Czech Republic's scientific and research engineering company, ÚJV Řež AS, Hungary's Academy of Sciences Centre for Energy Research, Poland's National Centre for Nuclear Research, and Slovakia's engineering company, VUJE AS. The

primary focus of this collaborative effort is on the development of gas-cooled fast reactors, with a particular emphasis on projects like Allegro [10]. The Polish GOSPOSTRATEG-HTR project was initiated to develop a 40 MWth High-Temperature Gas-cooled Reactor TeResa (HTGR) as a technology demonstrator. The publication [11] outlines the proposed thermal-hydraulic and neutronic core design, a result of the National Centre for Nuclear Research team's studies in fluid mechanics, heat exchange, and reactor core design support analysis, aligning with Polish research programs on non-electrical reactor applications.

In addressing the challenges posed by the multitude of Generation IV reactor projects, each featuring diverse fuel types, moderators, and structural components, advanced computational techniques, including Bayesian inference methods, play a significant role. These computational tools offer the capability to significantly mitigate uncertainties and provide invaluable support throughout the intricate reactor design process.

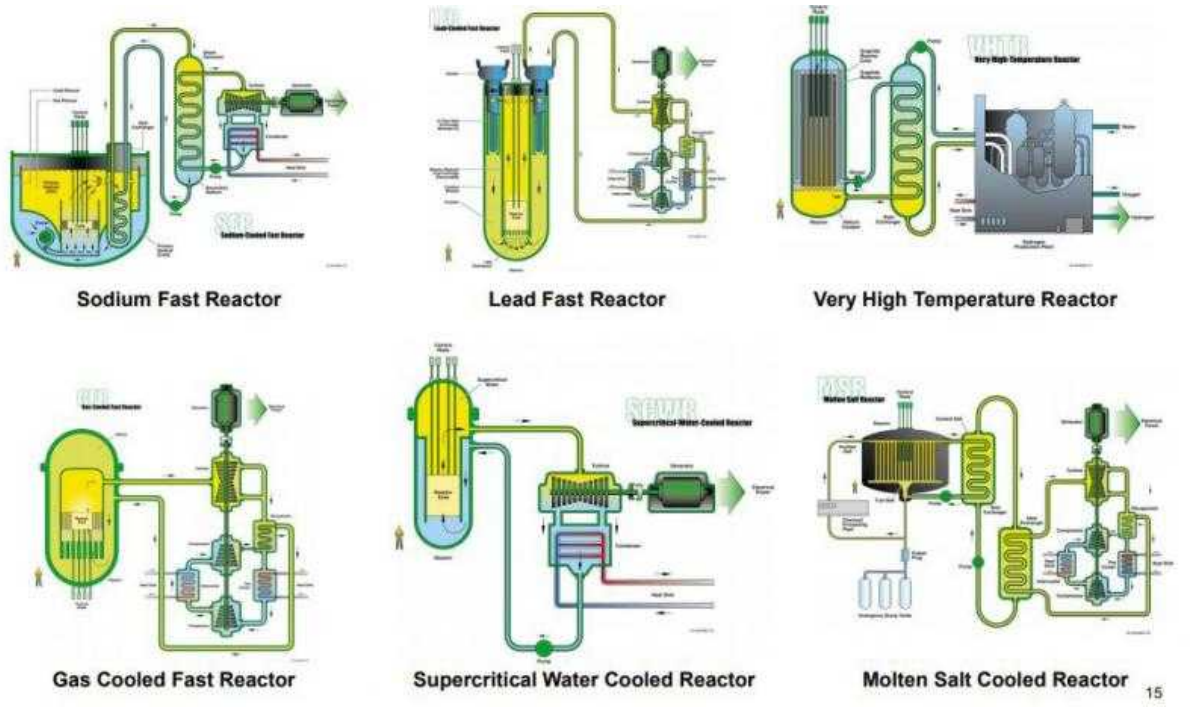

Figure 1: Conceptual technical diagrams for 6 nuclear reactors of IV generations: These include the: Gas-cooled Fast Reactor (GFR), Lead-cooled Fast Reactor (LFR), Molten Salt Reactor (MSR), Supercritical Water-cooled Reactor (SCWR), Sodium-cooled Fast Reactor (SFR) and Very High Temperature Reactor (VHTR). Figure from GIF Reports [12].

1.2 Uncertainties in simulated dynamics of nuclear reactors

One of the obstacles to developing new nuclear reactors at the most optimal design and operating them safely at the lowest possible cost is the uncertainty in the multiplication factor k_{eff} [13], [14], [15]. The multiplication factor is a crucial integral parameter describing the dynamics of a nuclear reactor or other system containing a substantial amount of fissile material. It tells us how the neutron count in a system changes in time. Its definition is presented in Eq. 1.1.

$$k_{eff} = \frac{number\,of\,neutrons\,incurrent\,generation}{number\,of\,neutrons\,in\,preceding\,generation} \tag{1.1}$$

When the k_{eff} is smaller than 1, then the reactor's power decreases, and the reactor is said to be subcritical; when it is equal to 1, then it stays constant, and the reactor is said to be "critical"; when it is greater than 1, then the

power increases and the reactor is said to be "supercritical". There are two types of supercriticality: delayed and prompt. When the reactor is delayed-supercritical, then it means that neutrons coming from fission alone are not sufficient to make the k_{eff} greater than one. What makes the k_{eff} above one in such a case comes from neutrons, which originate from the decay of the fission products. The lifetime of a generation of delayed neutrons is orders of magnitude longer than that of prompt neutrons produced during the fission process. That's why a delayed-supercritical reactor is manageable, with its power increasing steadily. A prompt-critical reactor would immediately melt or explode due to its power increasing immediately by orders of magnitude. The maximum k_{eff} for which delayed-supercriticality is possible depends on fissile material and, depending on a reactor, is in the range of 1.003 to 1.007. Preventing the reactor from achieving the prompt-criticality is the primary safety concern when designing a nuclear reactor. Having a low calculated k_{eff} uncertainty helps with this task.

One of the primary sources of k_{eff} uncertainty is neutron cross-section uncertainties. A neutron cross-section is a measure of the likelihood that an incident neutron of a specific kinetic energy will react with a nucleus in a specific way. The cross-sections are expressed in barns, where a barn is equal to $10^{-24} cm^2$. The higher the cross-section, the higher the probability of a reaction. The neutron cross-section can be defined as the area in cm^2 for which the number of nuclei–neutron reactions taking place is equal to the product of the number of incident neutrons that would pass through the area and the number of target nuclei [16].

The possible reactions are fission, absorption, elastic scattering, inelastic scattering (absorption and immediate emission of a neutron), absorption and emission of an alpha particle, and many more. There are also parameters associated with neutron reactions, which considerably contribute to the k_{eff} uncertainty. These are the probability of getting a fission neutron of specific energy, denoted as chi, and the number of fission neutrons

per fission, denoted as nubar. The latter of the two combines the parameters prompt nubar and delayed nubar. prompt nubar parameter tells us how many neutrons are, on average, emitted during fission induced by a neutron of a specific kinetic energy. delayed nubar parameter tells us how many delayed neutrons are, on average, emitted from fission products after fission induced by a neutron of a specific kinetic energy. Even though chi and nubar parameters are not technically neutron cross-sections, this thesis will sometimes refer to them with this term for conciseness.

Neutron cross-sections are measured experimentally, with measurement methods depending on the reaction type. Each measurement type has some limited precision, dependent on currently available technology. Taking U-235 as an example, its fission cross-sections are measured directly, and their uncertainties are relatively small (<0.8 %) [17]. On the other hand, the capture cross-sections are determined by measuring the ratio of fission to capture. This leads to errors from fission and ratio measurement uncertainty, resulting in larger relative uncertainty. Meanwhile, experimental energy resolution limits determine elastic and inelastic scattering uncertainties. Indirect methods have the potential to further reduce neutron cross-section uncertainties. One of such methods depends depend on solving so-called inverse problems. In such problems, a measurement of integral quantity in an experiment is used to improve the knowledge of the value of one or multiple model parameters that the calculation of the value of the experimental measurement depends on. In the case of this thesis, measurements of experimental k_{eff} values are used to improve knowledge of neutron cross-sections.

1.3 Overview of inverse Bayesian problems in nuclear engineering

For inverse problems where not only point estimates but uncertainties are important, Bayesian statistics-based tools are used. Except for cases where linear simulation models are applicable, these problems have only seen broad interest in the context of nuclear engineering since the early 2010s because they require considerable computation power. There are two general types of applications of Bayesian statistics-based methods for inverse problems: inverse uncertainty quantification (IUQ) and Bayesian calibration.

The aim of IUQ is to determine input parameters' uncertainty for parameters with only point estimates available. IUQ methods have been comprehensively reviewed in [18] for thermal-hydraulics codes. As an example, in one of the surveyed papers [19] in the publication mentioned above, Markov Chain Monte Carlo (MCMC) supported by a polynomial surrogate model for likelihood computations were used to determine the uncertainty and calibrate some of TRACE [20] physical model parameters like "wall drag coefficient" and "subcooled boiling heat transfer coefficient". The procedure used experimental data from the OECD/NEA BWR Full-size Fine-Mesh Bundle Tests (BFBT) [21] benchmark. The other type of application – Bayesian calibration, aims to calibrate parameters and reduce their known uncertainties rather than quantify uncertainties when they are entirely unknown. This is intended to reduce the subsequent difference between simulation and observation. The differences between IUQ and Bayesian calibration are subtle, except for how the prior distribution is defined. In IUQ, the prior uncertainty is usually assumed to be an arbitrarily wide uniform distribution, intended to be as uninformative as possible and only limited by constraints of laws of physics.

On the other hand, Bayesian calibration has a more informative prior described by, for example, a normal distribution. An example of work where

input parameter uncertainty was reduced instead of quantified altogether is [22]. The authors used the methodology of Cacuci and Ionescu-Bujor to reduce uncertainty in input parameters and time-dependent boundary conditions in a light water reactor thermal-hydraulic code FLICA4 [23], which allowed for achieving reduced uncertainty of computed axial void fraction distribution in forward computations.

A method called Approximate Bayesian Computation (ABC) is the most appropriate tool for Bayesian calibration or IUQ when the likelihood function is difficult or impossible to calculate. In this spirit, in [24], it was used to determine the occurrence of cracks in Advanced Gas-cooled nuclear Reactors' (AGRs') boiler spines based on the outcome of visual inspections looking for this defect. In [25], applying ABC allowed for the reduction of uncertainty in Centipede model parameters, a MOOSE framework [26] code used to predict the diffusivity of uranium and xenon for the simulation of fission gas in uranium oxide fuel. An example of the ABC method applied in the context of IUQ can be found in [27], where it was used to determine the uncertainty in model parameters for a Gamma Process describing pipe degradation in the primary heat transport system of Canada Deuterium Uranium (CANDU) reactors. The ABC method is a versatile tool that has been used by a variety of researchers with different models. The publications [28] and [29] use the SMC-ABC method to identify the source of the release, which may be important from the point of view of nuclear safety.

Reducing uncertainty in k_{eff} has long been of interest to the nuclear industry. Researchers and institutions use a couple of methods to apply Bayesian calibration for cross-section uncertainty reduction. Oak Ridge National Laboratory (ORNL) has developed the SCALE TSURFER software [30], which implements the Generalized Linear Least Squares (GLLS) [31] method. The GLLS approach considers potential variations in model input parameters (such as cross-sections) and measured integral responses

that minimize the differences in measured and calculated integral responses (such as k_{eff}) for a set of experiments. The method assumes linearity of integral responses to model input parameters' changes. Due to the method's approximate nature, it can only be used to reduce neutron cross-section uncertainties under limited conditions [32]. In 2014, a method called A General Monte Carlo-Bayes Procedure for Improved Predictions of Integral Functions of Nuclear Data (MOCABA) [33] was developed. It is a generalization of GLLS to non-linear models. Since it uses more rigorous mathematical models, it is more reliable. Like GLLS, it is limited to multivariate normal priors and only generates multivariate normal posteriors. This thesis investigates another algorithm with the potential to reduce the k_{eff} uncertainty and compares it to GLLS and MOCABA. The algorithm is called Sequential Monte Carlo – Approximate Bayesian Computation (SMC-ABC). The SMC-ABC is a universal, rigorous method of solving Bayesian inference problems, as it accepts any prior distribution and can produce any posterior distribution. This feature makes it more reliable and widely applicable than MOCABA and GLLS.

1.4 Thesis objectives

The first objective of the thesis is to compare the algorithms GLLS, MOCABA, and SMC-ABC and check whether the rigorousness and universality of SMC-ABC are worth the additional computational power required to execute the algorithm.

The second objective is to present a validation technique that hasn't been applied yet in nuclear engineering. The method is based on the so-called "synthetic experiments", which are computationally generated data used in place of experiments. This artificial data is calculated using a sample from the prior distribution of the parameters of interest (in the case of this work, a sample of relevant cross-sections) as input. The parameters in this sample are called "synthetic parameters". The artificial

data is assimilated with a Bayesian calibration algorithm, and the resulting posterior is compared to the already-known synthetic parameters. The method allows for verifying whether the data assimilation leads to overfitting.

Some researchers decide to calibrate only some of the model parameters because the others have a low influence on the results. The thesis also investigates how uncalibrated model parameters should be treated.

The author conducted a comprehensive analysis of the concepts above and formulated the following **Thesis Statement:**
There exist improvements in the methodology of conducting Bayesian calibration of neutron cross-sections, which allow for obtaining improved results with a more reliable validation.

1.5 Outline of the thesis

The dissertation consists of six chapters. The comprehensive scope of work is outlined below. Section 1 introduces the dissertation, outlining its thesis, objectives, and scope. In Section 2, three Bayesian calibration methods are described, which will later be compared in terms of neutron cross-section calibration performance. In Section 3, an overview of the simulation software used for k_{eff} calculations is provided. Section 4 is dedicated to the application and comparison of the three algorithms in calibrating 23 cross-sections that contribute significantly to k_{eff} uncertainties in highly enriched uranium fast systems. Additionally, a synthetic experiment validation procedure is presented and applied. In Section 5, the most effective algorithm is applied to calibrate 1904 cross-sections across 34 thermal systems. Furthermore, an enhanced synthetic cross-section validation procedure is introduced, along with an examination of the influence of uncalibrated cross-sections on Bayesian calibration results. The consequences of neglecting the influence of uncalibrated parameters are also investigated through the use of a toy inverse problem. Section 6 serves as a

summary, where lessons learned from Sections 4 and 5 are summarized, and a step-by-step procedure for Bayesian calibration of neutron cross-sections is proposed, incorporating the best practices established in these sections.

2 Bayesian Calibration algorithms

Bayesian calibration algorithms belong to a family of Bayesian inference methods. Two approaches for reducing this uncertainty are currently in use – Generalized Linear Least Squares (GLLS) [34] and a General Monte Carlo-Bayes Procedure for Enhanced Predictions of Integral Functions of Nuclear Data (MOCABA) [33]. Both techniques are capable of diminishing uncertainty in cross-sections by assimilating operational data from measured critical systems or nuclear reactors. These algorithms necessitate the simulation of experimental data and the description of calibrated parameters using specific statistical distributions. In this dissertation, a universal and rigorous algorithm known as Sequential Monte Carlo – Approximate Bayesian Computation (SMC-ABC) was proposed for this kind of problem. Bayesian calibration algorithms share several components needed to perform successfully. These are experimental data with measurement uncertainty, a mathematical model that can simulate the experiments, prior distributions of calibrated model input parameters, and model discrepancy estimates. The model discrepancy is the accuracy with which a model can predict experimental results. The following is an introduction to Bayesian theories for input parameter calibration. Then, in the following subsections, the algorithms used in the application part of this thesis are described in detail (see Chapters 4 and 5).

The term "calibration" [35] must be formally defined to describe these algorithms. Calibration is a process of adjusting a set of input parameters (α) in a mathematical model (M) such that the agreement of model predictions (k_α) with experimental data (m) is maximized.

All Bayesian calibration methods are based on the Bayes theorem. It states that one can update their belief on the probability or distribution of (α) considering some new observed data (m). The theorem is expressed as

follows:

$$P(\alpha|m) \propto P(m|\alpha)P(\alpha), \tag{2.1}$$

where: α - an A-dimensional vector of model parameters,
m - observed data in the form of an I-dimensional vector,
$P(\alpha)$ - prior probability distribution, belief about α without taking the data m into account,
$P(m|\alpha)$ - likelihood, joint probability of data as a function of α,
$P(\alpha|m)$ - posterior probability distribution of α given observed data m.
To be able to apply Bayesian inference and determine the posterior distribution, it is necessary to use procedures, either classic algorithms such as GLLS or typical sampling methods, e.g. ABC.

2.1 General Linearized Least Squares (GLLS)

The following description of the GLLS algorithm is based on its implementation in SCALE [30] software.
The GLLS considers potential variations in a model's input parameters and measured integral responses that minimize the differences in measured (experimental) and calculated integral responses. The method assumes linearity of integral responses to the model's input parameter variations. The linear approximation of a considered model calibrated with GLLS relates to the measured integral response and its calculated value, as shown in Eq. 2.2:

$$E = S(\frac{\alpha' - \alpha_0}{\alpha_0} - 1) * R + R + \epsilon, \tag{2.2}$$

where E is the measured quantity, S is the relative sensitivity vector, α_0 is the vector of the best estimate of prior input parameters, α' is the vector of perturbed input parameters, R is the integral response calculated with the prior input parameters, and ϵ is the error term.
Sensitivity can be either absolute or relative. The absolute sensitivity denotes the absolute change in response due to the relative change in input

parameters:

$$\tilde{S}_{\alpha_i} = \alpha_i \frac{\partial R}{\partial \alpha_i}. \tag{2.3}$$

The $\tilde{S}_{\alpha_i}$ denotes the sensitivity to a single parameter α_i. The relative sensitivity is the absolute sensitivity divided by the prior response:

$$S_{\alpha_i} = \frac{\alpha_i}{R} \frac{\partial R}{\partial \alpha_i}. \tag{2.4}$$

Further description of GLLS will be presented using the relative sensitivities. GLLS has the ability to assimilate experimental data from a series of experimental measurements, which will be denoted as an m vector of length I: $m = \{m_1, m_2, ..., m_I\}$, while m_0 designates the vector of prior best estimates of m. The set of corresponding calculated responses will be designated analogously as $k = \{k_1, k_2, ..., k_I\}$, with k_0 a vector of prior best estimates of k. The prior covariance data for relative input parameters is $C_{\alpha\alpha}$, where α is an A-long vector while C_{mm} is an $I \times I$ covariance matrix describing relative experimental uncertainties. The k values are also correlated due to correlated uncertainties in the model's input parameters. The resulting covariance matrix is designated C_{kk}. It can be computed from the following propagation of error expression:

$$C_{kk} = S_{k\alpha} C_{kk} S_{k\alpha}^T, \tag{2.5}$$

where $S_{k\alpha}$ is the relative sensitivity matrix.

GLLS requires the computation of the discrepancy parameter d, equal to the relative difference between calculated response k and measurement m. The d vector is therefore

$$d = \frac{k_0 - m_0}{k_0} = \{\frac{k_{01} - m_{01}}{k_{01}}, \frac{k_{02} - m_{02}}{k_{02}}, ..., \frac{k_{0I} - m_{0I}}{k_{0I}}\}. \tag{2.6}$$

The covariance matrix corresponding to d is designated C_{dd} and calculated with the expression:

$$C_{dd} = C_{kk} + F_{m/k} C_{mm} F_{m/k}, \tag{2.7}$$

where $F_{m/k}$ is an $I \times I$ matrix with m/k on the diagonal and zeros off-diagonal.

The essence of the GLLS method is varying the α and m values in such a way that they are as consistent as possible with their uncertainty matrices, $C_{\alpha\alpha}$ and C_{mm} respectively. To do that, the chi-square presented in Eq. 2.8 is minimized.

$$\chi^2 = [\frac{\alpha' - \alpha_0}{\alpha_0}]^T C_{\alpha\alpha}^{-1} [\frac{\alpha' - \alpha_0}{\alpha_0}] + [\frac{m' - m_0}{m_0}]^T C_{mm}^{-1} [\frac{m' - m_0}{m_0}] = [\Delta\alpha]^T C_{\alpha\alpha}^{-1} [\Delta\alpha] + [\Delta m]^T C_{mm}^{-1} [\Delta m], \tag{2.8}$$

where $\Delta\alpha = \frac{\alpha' - \alpha_0}{\alpha_0}$ and $\Delta m = \frac{m' - m_0}{m_0}$. The minimization is subject to the constraint $k' = m'$ (the posterior calculated responses have to agree with measurements) and the linearity condition $\Delta k = \frac{k' - k}{k} = S_{k\alpha}[\Delta\alpha]$. This is achieved by applying the following variations:

$$\Delta\alpha = -[C_{\alpha\alpha} S_{k\alpha}^T C_{dd}^{-1}] d, \tag{2.9}$$

$$\Delta m = [C_{mm} F_{m/k} C_{dd}^{-1}] d. \tag{2.10}$$

It is visible that the adjustments are driven by the discrepancy d. The uncertainties of α, m, and k are reduced by incorporating additional knowledge. This results in modified covariance matrices $C_{m'm'}$, $C_{\alpha'\alpha'}$, and $C_{d'd'}$, which are given by:

$$C_{\alpha'\alpha'} = C_{\alpha\alpha} - [C_{\alpha\alpha} S_{k\alpha}^T C_{dd}^{-1} S_{k\alpha} C_{\alpha\alpha}], \tag{2.11}$$

$$C_{m'm'} = C_{mm} - [C_{mm} F_{m/k} C_{dd}^{-1} F_{m/k} C_{mm}], \tag{2.12}$$

$$C_{k'k'} = C_{kk} - [C_{kk} C_{dd}^{-1} C_{kk}]. \tag{2.13}$$

If the linearity assumption is valid, the Δk value follows the relation:

$$\Delta k = F_{m/k} \Delta m - d = S_{k\alpha} \Delta\alpha, \tag{2.14}$$

which completes the GLLS calculations.

2.2 Monte Carlo-Bayes procedure for improved predictions of integral functions of nuclear data

MOCABA [33] combines Monte Carlo sampling and Bayesian updating algorithms for improved prediction of integral responses by assimilating integral experimental data. It was developed for nuclear reactor analysis problems, but just like GLLS, it has a wide range of applicability. MOCABA assumes multivariate normal prior and posterior distributions and can be applied to any mathematical model, not just the ones where the linear approximation of the influence of input parameters is valid. Under the approximation of the integral response vector by the first-order series expansion about the best-estimate input parameter vector, the GLLS formulas are obtained. Therefore, MOCABA can be interpreted as a generalization of GLLS to problems where the linear approximation may not be valid. The algorithm allows for calculating cases where the normality assumption does not hold for the prior by transforming the prior k into an approximately normally distributed vector z. There is also an option of imposing constraints on k. First, the case with no transformations will be presented in Section 2.2.1. Then, the case with transformations will be explored in 2.2.2. The case with constraints will not be explored because it is irrelevant to this thesis.

2.2.1 MOCABA without transformations or constraints

The updating of the prior distribution is based on Bayes theorem:

$$P(y|m) \propto P(m|y)P(y), \tag{2.15}$$

where y is a vector consisting of parameters α whose posterior distributions we want to find and of calculated integral responses k, so $y = \{\alpha, k\}$ with prior covariance matrix $C_{yy} = \begin{pmatrix} C_{\alpha\alpha} & C_{\alpha k} \\ C_{\alpha k}^T & C_{kk} \end{pmatrix}$. The best-estimate values of

α and k are designated α_0 and k_0, respectively. The m denotes the vector of measured values of integral responses, with m_0 being the vector of the best estimates of measurement outcomes. Since the prior $P(y)$ and the likelihood $P(m|y)$ are multivariate normal distributions, we find that the prior obeys the following relations:

$$\begin{aligned} P(y) = N(y_0, C_{yy}) \propto exp(-Q_0/2), \\ Q_0 = (y - y_0)^T C_{yy}^{-1} (y - y_0), \end{aligned} \tag{2.16}$$

while the likelihood can be described as follows:

$$\begin{aligned} P(m|y) \propto exp(-Q_m/2), \\ Q_m = (k - m_0)^T C_{mm}^{-1} (k - m_0). \end{aligned} \tag{2.17}$$

The posterior distribution $P(y|m)$ follows the expression:

$$\begin{aligned} P(y|m) = N(y_0', C_{y'y'}) \propto exp(-Q'/2), \\ Q' = Q_0 + Q_m = (y - y')^T C_{y'y'}^{-1} (y - y'), \end{aligned} \tag{2.18}$$

where $y' = \{\alpha' k'\}$ and $C_{y'y'} = \begin{pmatrix} C_{\alpha'\alpha'} & C_{\alpha'k'} \\ C_{\alpha'k'}^T & C_{k'k'} \end{pmatrix}$ are respectively the maximum-a-posteriori estimate and posterior covariance matrix of y. To calculate these parameters, the Q' has to be minimized, which leads to the following relations:

$$\begin{aligned} \alpha' = \alpha_0 + C_{\alpha k}(C_{kk} + C_{mm})^{-1}(m_0 - k_0), \\ k' = k_0 + C_{kk}(C_{kk} + C_{mm})^{-1}(m_0 - k_0), \\ C_{\alpha'\alpha'} = C_{\alpha\alpha} - C_{\alpha k}(C_{kk} + C_{mm})^{-1} C_{\alpha k}^T, \\ C_{k'k'} = C_{\alpha\alpha} - C_{\alpha k}(C_{kk} + C_{mm})^{-1} C_{kk}. \end{aligned} \tag{2.19}$$

The practical implementation of the MOCABA algorithm depends on whether we want to find the posterior distribution of input parameters or skip this step and directly calculate the posterior distribution of some integral response of interest. We denote any of the two sets of parameters as α. If we wish to calibrate the input parameters, as in the case of this thesis,

the first step is simplified, as there is no need to compute $C_{\alpha\alpha}$, since it is known from the start. We only need to create a set of samples of α.
We define a sample as a single randomized set of input parameter values for calculating all considered integral responses. If the number of input parameters is $A = 10$, a sample consists of a vector of 10 numerical values sampled from the prior distribution.
The algorithm starts by creating a set of samples of size N of input parameters α from their multivariate normal prior distribution $P(\alpha, C_{\alpha\alpha})$, so we obtain

$$\alpha_{1:N} \sim P(\alpha_0, C_{\alpha\alpha}), \tag{2.20}$$

where $\alpha_{1:N} = \{\alpha_1, \alpha_2, ..., \alpha_N\}$.
After the samples are created, the integral responses are computed with the use of appropriate mathematical models, and we obtain:

$$k_{1:N} = M(\alpha_{1:N}), \tag{2.21}$$

where $k_{1:N} = \{k_1, k_2, ..., k_N\}$ are calculated integral responses, and M denotes mathematical models used for calculating k. The number of mathematical models equals the number of integral responses I. The calculated integral responses k form a multivariate normal distribution of their own, with covariance data designated as C_{kk}.
Now the y_0, and the covariance matrix $C_{\alpha k}$ can be calculated:

$$\bar{y_0} = \{\bar{\alpha_0}, \bar{k_0}\} = \frac{1}{N}\sum_{n=1}^{N} y^n, \tag{2.22}$$

$$\bar{C_{yy}} = \begin{pmatrix} C_{\alpha\alpha} & C_{\alpha k} \\ C_{\alpha k}^T & C_{kk} \end{pmatrix} = \frac{1}{N-1}\sum_{n=1}^{N}(y^n - y_0)(y^n - y_0). \tag{2.23}$$

The experimental measurements intended for assimilation are denoted by I-long m vector. If the uncertainties of each experimental integral response are independent, then the C_{mm} matrix is diagonal. The off-diagonal elements in C_{mm} come primarily from correlated systematic uncertainties,

but this matrix must also take into account correlated uncertainty coming from any uncalibrated input parameters. We compute the C_{mm} matrix by sampling the systematic errors s from $P(s_0, C_{ss})$ and uncalibrated parameters γ from $P(\gamma_0, C_{\gamma\gamma})$ L times and calculating the integral responses with the models M:

$$\begin{aligned} \gamma^{1:L} &\sim P(\gamma_0, C_{\gamma\gamma}), \\ s^{1:L} &\sim P(s_0, C_{ss}), \end{aligned} \tag{2.24}$$

$$m^{1:L} = M(\gamma^{1:L}, s^{1:L}), \tag{2.25}$$

$$\bar{m}_{mean} = \frac{1}{N}\sum_{n=1}^{N} m^n, \tag{2.26}$$

$$C_{mm} = \frac{1}{N-1}\sum_{n=1}^{N}(m^n - \bar{m}_{mean})(m^n - \bar{m}_{mean}). \tag{2.27}$$

The Eqs.2.19 use the C_{mm} calculated in Eq.2.27, and a vector of the best estimate of measurement values m_0. Therefore, all of the RHS components of Eqs.2.19 are found, and the procedure is completed.

2.2.2 MOCABA with transformations but without constraints

For the cases where prior k fails normality tests, a vector f can be introduced, that transforms vector y into a vector z, where individual components of z are approximately normally distributed. The entire general procedure is described in detail in [36], the algorithm below is more tailored to the dissertation needs. The z components are described as follows:

$$z = (z_1, z_2, ..., z_H) = f(y) = (f_1(y_1), f_2(y_2), ..., f_H(y_H)), \tag{2.28}$$

where H is the length of the vector equal to $H = I + A$. The f transformation is invertible:

$$y = (y_1, y_2, ..., y_H) = f^{-1}(z) = (f_1^{-1}(z_1), f_2^{-1}(z_2), ..., f_H^{-1}(z_H)). \tag{2.29}$$

The z is described by a multivariate distribution:

$$\begin{aligned} P(z) = N(z_0, C_{zz}) \propto exp(-Q_0/2), \\ Q_0 = (z - z_0)^T C_{zz}^{-1}(z - z_0). \end{aligned} \tag{2.30}$$

The components of the measurement vector m also need to be transformed. Each component needs to undergo the same transformation as the corresponding k element.

$$m_z = (m_{z1}, m_{z2}, ..., m_{zI}) = f(m) = (f_1(m_1), f_2(m_2), ..., f_I(m_I)). \tag{2.31}$$

Vector m has the same length I as the k vector. After the m_z is obtained, the equations 2.19 can be applied to find the posterior distribution z'. Then, z' needs to be inverted to find the posterior y'. It might be the case that not all y components needed transformation. Then, the inverted transformation $y = f^{-1}(z)$ only needs to be applied to the transformed ones. After that inversion, the algorithm is complete.

There are many transformations that can transform a non-normal distribution into a normal one. The one that is used in this thesis is based on the Johnson distribution. This distribution has four parameters: W, E, U, and O, allowing the Johnson distribution [37] to fit into a wider range of datasets. The Johnson distribution is particularly useful because it can be transformed into a normal distribution with the use of the following transformation:

$$\begin{aligned} z_i = f_i(\tilde{y}_i) = \sinh^{-1} \frac{\tilde{y}_i - W_i}{E_i} = sinh^{-1}(r_i), \\ \text{where } r_i = \frac{\tilde{y}_i - W_i}{E_i}. \end{aligned} \tag{2.32}$$

The $\tilde{y}_i$ variable denotes the Johnson distribution fitted to the y distribution, so it is effectively the same as y. The parameters W, E, U, and O are found numerically. The y_i probability distribution function is then related to z_i in the following manner:

$$\begin{aligned} P(y_i) = \frac{U_i}{E_i} * [2\pi(1 + r_i^2)]^{-\frac{1}{2}} * exp(-\frac{1}{2}[O_i + U_i sinh^{-1}(r_i)]^2), \\ \text{with } U_i = \frac{1}{\sigma_{0i}}, O_i = -\frac{z_{0i}}{\sigma_{0i}}. \end{aligned} \tag{2.33}$$

After the Bayesian updating, the posterior y' pdf is found by replacing U and O with $U' = \frac{1}{\sigma'_{0i}}$ and $O' = -\frac{z'_{0i}}{\sigma'_{0i}}$.

2.3 Sequential Monte Carlo – Approximate Bayesian Computation

Approximate Bayesian Computation (ABC) [38], also called likelihood-free inference methods, is a group of approaches developed for inferring posterior distributions in cases where the likelihood function is intractable or computationally expensive to evaluate. This does not mean that the likelihood function is not part of the analysis, but that we are approximating the likelihood, and hence the term "approximate" in the name of the algorithm.
The Sequential Monte Carlo - Approximate Bayesian Computation (SMC-ABC) uses a modified version of the Bayes theorem:

$$P(\alpha|m) \propto P(m|\alpha)^{\beta} P(\alpha) \tag{2.34}$$

β - SMC transition step parameter. The SMC part of the algorithm proceeds by gradually increasing the value of β from 0 to 1. At $\beta = 1$, the Eq. 2.34 is equivalent to the original Bayes theorem. The SMC-ABC algorithm is described in detail in publications [39], [40]. A brief overview is given in Alg. 1.

At first, after initializing $\beta = 0$ (step 1), the N samples $\alpha^t_{1:N}$ are drawn from the prior distribution $P(\alpha)$ (step 2). These samples are used as input parameters for models $M(\alpha)$ (step 3). These models calculate integral responses $k^t_{1:N}$. The responses must be sensitive to the sampled parameters. Otherwise, the resulting posterior distribution is equal to the prior distribution. The results of calculations $M(\alpha^*) \rightarrow k^*$ for each sample are compared with corresponding experimental data m_0 by employment of a distance function $\delta(m_0, k^t_{1:N})$ (step 4). In the case of this thesis, this is the Wasserstein distance [43]. This distance approximates the likelihood,

Algorithm 1 Sequential Monte Carlo – Approximate Bayesian Computation in parallel version (The procedure is based on PyMC implementations [41] and [42], which are in the original version in the publications [39], [40])

1. Initialize $\beta = 0$ and stage $t = 1$

2. Sample from the prior $P(\alpha)$ a set of samples $\alpha^t_{1:N} \sim P(\alpha)$ of size N. When $\beta = 0$, the tempered posterior is the prior.

3. Simulate a data set $k^t_{1:N}$ using a simulator $M(\alpha^t_{1:N}) \rightarrow k$. This returns a data set of the same dimensions as the observed data set m for each sample.

4. Compare the simulated dataset $k^t_{1:N}$ with the experimental data set m using a distance function $\delta(m_0, k^t_{1:N})$. The distance function acts as a likelihood approximation.

while $\beta < 1$ **do**

5. Increase β to make the effective sample size (ESS) equal some predefined value.

6. Compute a set of importance weights $\omega^t_{1:N}$. The weights are computed as the ratio of the likelihood approximations ([42]).

7. Compute a weighted covariance matrix $C^t_{\alpha\alpha}$ from $\alpha^t_{1:N}$ and $\omega^t_{1:N}$. Obtain a new set of samples $\alpha^{t+1}_{1:N}$ by resampling $\alpha^t_{1:N}$ according to $\omega^t_{1:N}$.

for $\kappa = 1$ to K **do**

8. Run the perturbation step with N Markov Chains using a multivariate normal proposal distribution based on the $C^t_{\alpha\alpha}$ and $\alpha^t_{1:N}$ to generate a sample set $\alpha^*_{1:N}$.

9. Reject or accept each sample α^*_i to replace α^t_i after comparing the simulated dataset $M(\alpha^*) \rightarrow k^*$ with the experimental data set m_0 using a distance function $\delta(m_0, k^*_{1:N})$ and a tolerance threshold ϵ_t

10. Increase $t := t + 1$

end for

end while

11. The final result is a collection of N samples from the posterior.

which is later used to calculate new β in step 5 and the weights $\omega_{1:N}^t$ in step 6.

After steps 1-4 are complete, the algorithm loops through steps 5-10. First, in step 5, new β is determined by keeping the Effective Sample Size (ESS) at a predefined value (see [42]). Next, in step 6, a set of importance weights $\omega_{1:N}^t$ is computed, which is then used to generate a weighted covariance matrix $C_{\alpha\alpha}^t$ from $\alpha_{1:N}^t$ and to resample the samples from $\alpha_{1:N}^t$ proportionally to these weights (step 7) (see ABC procedure [41]). From this, a new resampled set denoted $\alpha_{1:N}^{t+1}$ and the weighted covariance matrix $C_{\alpha\alpha}^t$ a multivariate normal proposal distribution is constructed. This distribution is used in step 8 for sample perturbation.

A key element of the SMC part is to generate enough diversity by perturbation step 8 to explore the solution space and avoid getting stuck in local minima. In SMC-type algorithms, different versions of the sample perturbation model can ensure the appropriate level of samples' diversity. For the version implemented in the Python library PyMC [42], on which the implementation of algorithm 1 is based, we set a number of inherently parallel Markov chains (MC). At each stage, SMC will use independent MC to explore the tempered posterior (steps 8, 9, and 10) using the multivariate normal proposal distribution built in step 7 and applying the model to generate data $M(\alpha^*) \rightarrow k^*$. The algorithm either rejects or accepts proposal samples α_i^* by calculating the distance function $\delta(m_0, k_{1:N}^*)$ and comparing it to ϵ_t, known as "threshold". The parameter ϵ_t is calculated for each sample based on the input value E_{tot} (see formula 6), which constitutes the combined value of the model's and observed data's uncertainties, other parameters determined algorithmically like β, and partially randomized. Only one E_{tot} value is allowed for each set of simulations. Therefore, if data from multiple measurements with varying errors is used, it needs to be rescaled so that the sum of effects of measurement and discrepancy error always have the same value equal to E_{tot}, measured in one standard devi-

ation. At every successive stage defined by β, the ϵ_t parameter decreases from an artificially inflated value of ϵ_1 to the final value ϵ_T. As a result, we obtain a sample set of parameters α from the approximate distribution $\pi(\alpha, \delta(m_0, k^t_{1:N}) \leq \epsilon_t$ for corresponding stages defined by β. The algorithm finishes when the stage with $\beta = 1$ is completed. The final product of the algorithm is a set of samples drawn from the target posterior distribution $\pi(\alpha, \delta(m_0, k^T_{1:N})) \leq \epsilon_T$ [40] (step 11).

The discussed algorithm is presented in a simplified form in Fig. 2. The top subplot shows 4 theoretical proposal distributions at different stages t, with a proposal at stage 2 highlighted as the currently sampled one. The samples are represented by three colored dots. The bottom subplot shows simulator phase $M(\alpha) \rightarrow k$ of ABC procedure with acceptance or rejection, which depends on the distance of the simulated data k from the measurements m_0. Notice how the two samples with the shortest distance to m_0 (green circles) are accepted and used to obtain a new posterior proposal in the next stage $t + 1$. The value of β is updated to 1 when the target posterior distribution is obtained.

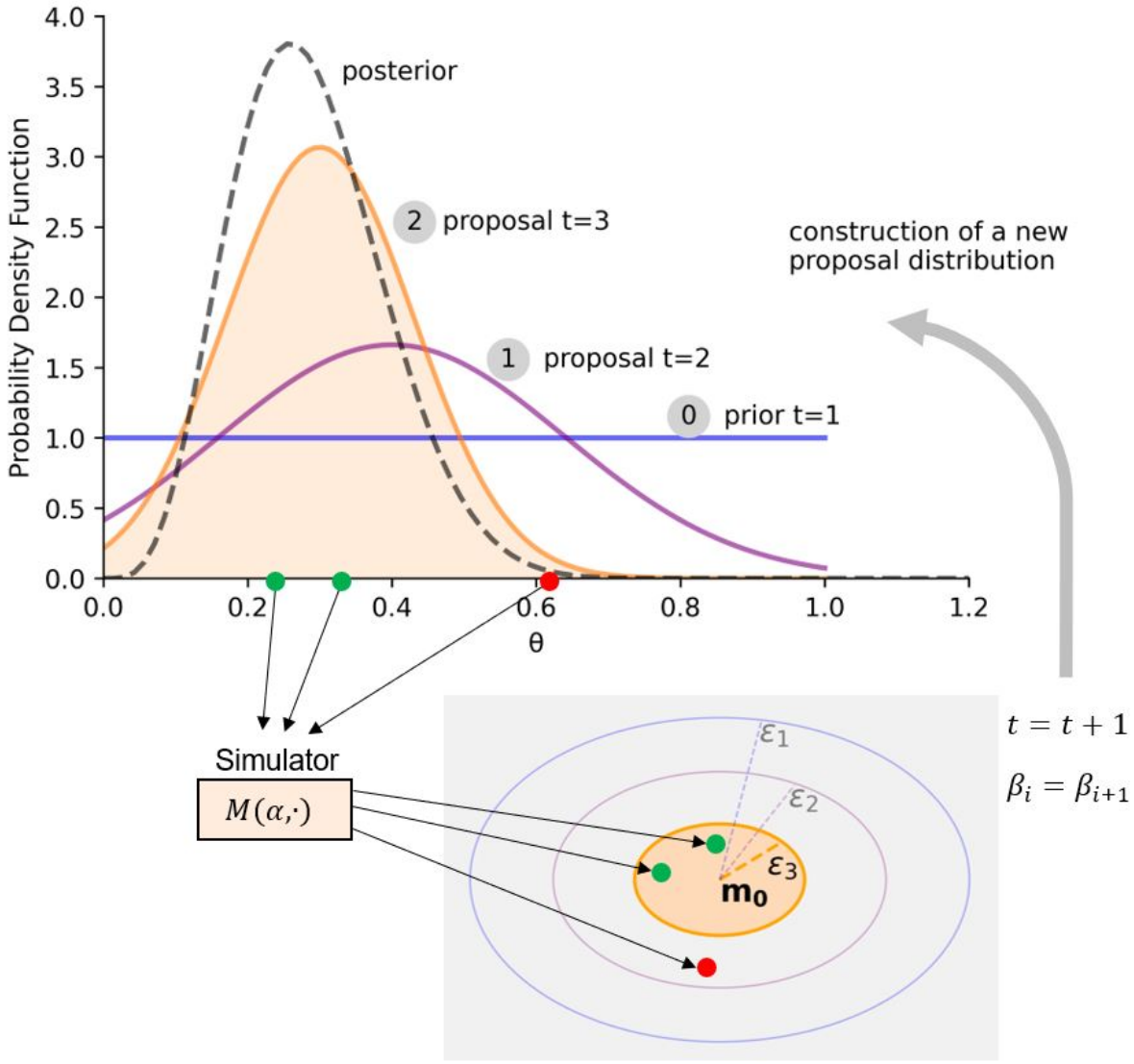

Figure 2: Illustration of SMC-ABC with an example with a uniform prior distribution. The figure was prepared based on Figure 8 from [40].

3 Criticality safety simulation software SCALE and neutron cross-section libraries

To use Bayesian methods for calibration, simulation of the experimental systems is necessary. To compare experimental data with model data, access to the model $M(\alpha)$ is required. The model should correctly reproduce the physical phenomena of critical systems. In the case of multigroup cross-sections, the appropriate program, or rather a set of modeling tools, is SCALE (Standardized Computer Analysis for Licensing Evaluation). SCALE is a comprehensive suite of tools for nuclear systems modeling and simulation. It is used by numerous regulatory bodies, research institutions, and industries across the globe. SCALE is employed for various nuclear applications, such as reactor physics, criticality safety computations, radiation shielding, radiological source term determination, radioactive waste characterization, isotopic generation and depletion, and sensitivity and uncertainty analysis concerning criticality safety computations. SCALE is organized into modules, with each module dedicated to a different, specific task. These modules can be executed in sequences, where the output from one module feeds into another, facilitating complex simulations. This enables users to employ the software for various nuclear engineering analyses. This thesis presents the modules CSAS5, TSUNAMI, and TSURFER of the SCALE program that were used in the calculations in chapters 4 and 5.

3.1 CSAS5 module

CSAS5 is a module within SCALE specifically developed for criticality safety analyses. Its primary objective is to determine the neutron multiplication factor k_{eff} of nuclear systems. The module uses a geometry processor, which is limited to combinations of several primitive structures (spheres, cylinders, shells, cuboids, etc., cylindrical holes within any of

these primitives). For more complex 3D geometries, the CSAS6 module is required. CSAS6 has higher computational costs, so it should not be used when it is not necessary. Each geometry component gets assigned isotopic composition by a user, with the atomic density of each isotope defined and the temperature of each component.

After the geometry and material composition are defined, the module processes cross-sections if a multigroup library is used and solves the neutron transport equation. There are two ways to do that: with a deterministic or Monte Carlo solver. The deterministic solver assumes a neutron source distribution, solves the transport equation, updates the neutron source distribution, and solves the transport equation again, repeating these steps until convergence is achieved. The method is limited to simple geometries. The Monte Carlo solver simulates random paths of individual neutrons as they move through the system and interact with the material. On each iteration, the neutron spatial distribution is updated. Over many such simulated iterations, a statistically meaningful result of the multiplication factor emerges. The Monte Carlo solver uses variance reduction methods to ease the computational burden of the computations. It can be used for complex geometries, making it more universal. The influence of delayed neutron on the multiplication factor is calculated by default for any solver. The SCALE's CSAS5 module is used as the model (or simulator) M in the SMC-ABC and MOCABA algorithms in Chapter 4 and in the MOCABA algorithm in Chapter 5

3.2 Cross-section library types

Calculations of criticality safety require a neutron cross-section library to be executed. Such a library contains energy-dependent cross-section values for a range of reactions and isotopes. Besides the cross-section reaction data, the libraries store additional parameters describing the behavior of neutrons. In SCALE-produced libraries, the chi parameter denotes the

probability that a neutron created in a fission process has a specific energy. The prompt nubar parameter describes the average number of neutrons emitted during neutron-induced fission for the incident neutron's specific energy. The delayed nubar denotes the average number of neutrons emitted from the decay of fission products after they were created by interaction with an incident neutron of a specific energy. The neutron cross-section libraries additionally contain photon interaction data, which play a much more minor but not insignificant influence on the k_{eff}.

There are two types of neutron cross-section libraries: the Continuous Energy (CE) and the Multigroup (MG) libraries. The CE libraries contain continuous (not discretized) cross-section values as a function of neutron energy. They are constructed by collecting direct measurements of neutron cross-sections and their interpolation. Such libraries provide the most accurate results when calculating k_{eff}, but at the cost of significantly higher computational expense. The MG libraries are step functions of neutron energy and are constructed by collapsing CE libraries into discrete cross-section values in predefined energy ranges. The MG libraries are approximations and are, therefore, less accurate than CE libraries but require much fewer computational resources. The difference in runtime for criticality calculation is not large on modern computers but becomes considerable when uncertainty calculations are performed. Given the necessity of performing uncertainty calculations for every reactor, the MG libraries are still of significant interest.

The SCALE library used in this dissertation is ENDF/BVII.1 based 56-group library, where ENDF/BVII.1 is the US version of a comprehensive collection of nuclear data that has been evaluated, processed, and compiled by experts. The collection is maintained by Brookhaven National Laboratory.

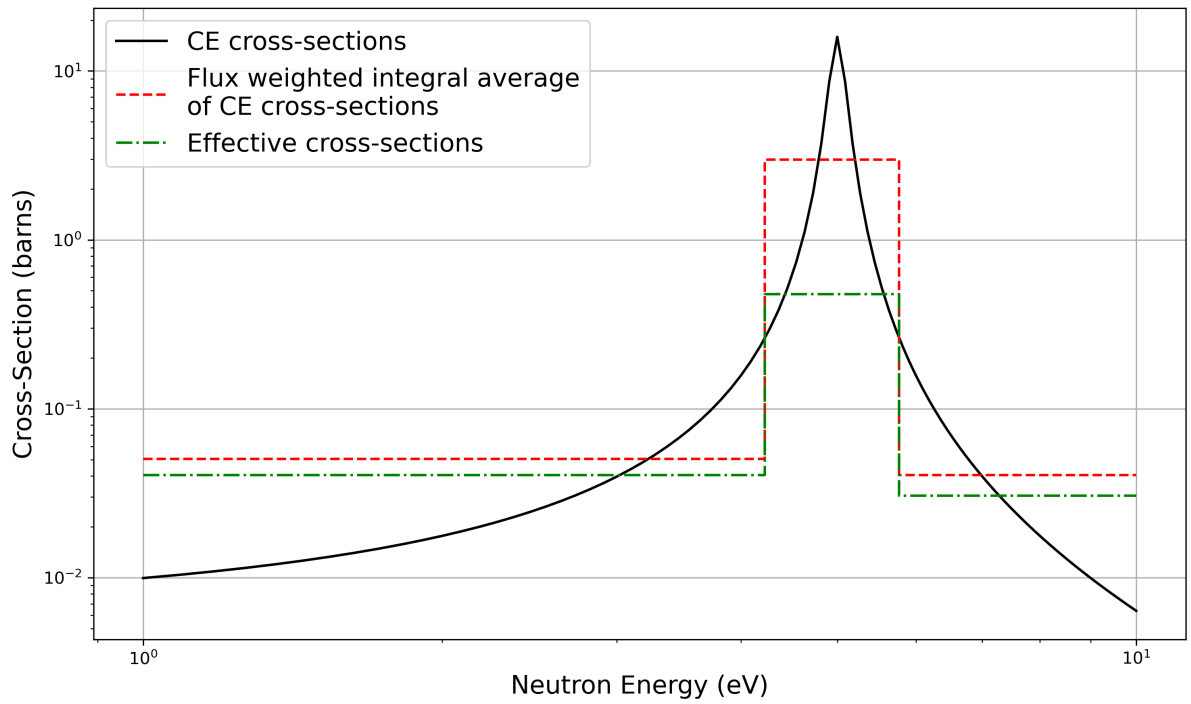

Figure 3: Comparison of CE cross-sections (black line), MG cross-sections (dashed red line), and self-shielded MG cross-sections (dashed and dotted green line)

3.3 Cross-section treatment for Multigroup library calculations

The collapse of CE cross-sections to a multigroup structure has several unfavorable consequences that necessitate additional treatment for the calculations to be reliable. In MG computations, the rates at which reactions occur are heavily influenced by the unique energy distribution of the flux specific to the problem at hand. This means that the generic MG data in the library, which isn't tailored to specific problems, should be adjusted to reflect the actual flux spectrum of the problem instead of the general spectrum provided in the library. The neutron energy distribution is particularly affected by the amount and spatial distribution of resonance absorbers. These absorbers can significantly decrease the flux at the resonance peaks of a nuclide. This reduces reaction rate and effectively lowers effective averaged multigroup cross-section values. The phenomenon is known as resonance self-shielding. Fig. 3 presents an illustration of a phenomenon on a generic resonance peak. SCALE provides a

sequence of modules that process the cross-section libraries to account for the resonance self-shielding. This sequence is a part of CSAS5, CSAS6, and TSUNAMI modules. The cross-section treatment starts by running the BONAMI module. This module applies the Bondarenko approach using cross-sections pre-computed over a range of self-shielding conditions, ranging from infinitely dilute to heavily self-shielded. Given the approximations used in the approach, the degree of self-shielding depends on a single parameter called the background cross-section or "sigma0" and Doppler broadening temperature. The procedure is applied to all materials by default. The part of geometry for which spatial effects need to be considered must be defined separately in an input block called "celldata". The geometry in such a block must belong to a limited number of geometry types for which SCALE has treatment prepared. These are arrangements of concentric spherical or cylindrical shells, fuel arrays of various configurations, slabs, doubly heterogeneous materials (like HTGR pebbles with TRISO), and others. BONAMI then analytically solves the neutron transport equation for this part of geometry and adjusts the MG cross-section values to match the resulting neutron spectrum. After the BONAMI module finishes running and the MG cross-sections are generated for each part of the geometry, either the Monte Carlo computations start or an additional treatment of the MG library is applied through the CENTRM module, whichever the user requests. CENTRM conducts a more rigorous computation compared to BONAMI by not using its main approximations, which are the neglect of resonance interference, utilization of the intermediate resonance approximation, and the equivalence theory. Resonance interference is the effect of resonances from various materials influencing each other's self-shielding in the same energy range. At the same time, the equivalence theorem calculates equivalent cross-sections for doubly heterogeneous materials. CENTRM uses the "celldata" geometry definition to solve the neutron transport equation using MG cross-section for fast and thermal

ranges to provide space-dependent slowing-down sources for CE calculations performed in the resonance range. This range covers the area where approximations used by BONAMI are not reliable enough. All simulations conducted as part of the research described in this thesis were made with the CENTRM module included in the calculation sequence CSAS5.

3.4 TSUNAMI and TSURFER modules

There are two ways of quantifying k_{eff} uncertainty. The easiest way is sampling the neutron cross-section library a few hundred times to calculate k_{eff} for the system in question. This is followed by calculating the standard deviation of the results. The method is reliable, but it does not provide good information about the sources of the uncertainty. The other way is running an adjoint calculation. SCALE has a module dedicated to that called TSUNAMI (Tools for Sensitivity and Uncertainty Analysis Methodology Implementation). It assumes that computational error is primarily caused by neutron cross-section errors. TSUNAMI first calculates sensitivities. To do that, it solves the standard neutron equation (also called forward equation) and adjoint equation. The exact procedure is mathematically complex and is presented in detail in the SCALE manual. Here, only the most general overview is provided. The forward equation describes how neutrons move and interact in a medium. While the forward equation describes how neutrons propagate from a source, the adjoint equation describes how "importance" propagates from a detector or response. Mathematically, the adjoint equation looks similar to the forward transport equation but with some terms transposed. The solution to the adjoint equation is called the adjoint flux, which represents the importance of a neutron to the desired response. After this flux is obtained, the sensitivity of k_{eff} to each neutron cross-section is calculated. These sensitivities are then used to propagate errors with the standard sandwich

method:

$$E^2 = SCS^T, \tag{3.1}$$

where E is error measured in one standard deviation, S is sensitivity vector, C is covariance matrix, S^T is the sensitivity vector transposed. The final outputs of the TSUNAMI calculation are neutron cross-section sensitivities, k_{eff} uncertainty, and forward calculation result.

It is important to note that the sensitivities generated by TSUNAMI are not guaranteed to be always calculated correctly, even if the model does not contain errors. This is stressed numerous times by the SCALE developers in the manual. To validate the sensitivities for a nuclide, the sensitivity to the total cross-section, called the "Sensitivity Coefficient for Total Reaction" in TSUNAMI output, needs to be compared to the result of the so-called direct perturbation. Direct perturbation procedure assumes that a relative change in a nuclide's density should have the same effect on k_{eff} as the same relative change in the total cross-section. Calculating this sensitivity is followed by calculating its uncertainty. If the TSUNAMI sensitivity is within two standard deviations from the direct perturbation sensitivity, the total sensitivity is validated. This provides more confidence that individual sensitivities are also calculated correctly, although a scenario where sensitivity errors compensate to give a correct result of total sensitivity is possible.

The outputs of TSUNAMI are inputs for the GLLS calculations, along with corresponding experimental data. GLLS procedure is conducted by the SCALE TSURFER (Tool for Sensitivity/Uncertainty analysis of Response Functionals using Experimental Results) module. The GLLS algorithm is implemented in this thesis by first running the TSUNAMI for each experiment model and collecting the outputs. These, along with the experimental data, are then used as inputs to the TSURFER module. The TSURFER returns relative values of calibrated cross-sections, their posterior uncertainties, and estimates of the calculated posterior k_{eff}.

4 Testing Bayesian calibration algorithms on fast enriched uranium systems

An ENDF/BVII.1 56-group library from the SCALE software package developed by Oak Ridge National Laboratory was chosen to test and compare the robustness of Bayesian calibration algorithms. The calibration would be conducted on fast systems. It is important to note that the 56-group library is not intended for fast systems. However, it was the best choice among other readily accessible MG libraries due to its low number of energy groups. Three algorithms were selected for testing and comparison. These were the multivariate-limited and based on linear approximation GLLS, the multivariate-limited but allowing for non-linear models MOCABA and the universal, non-linear SMC-ABC. The SMC-ABC's advantage of being able to update and produce as output any distribution type comes at a cost. Due to a phenomenon called the "curse of dimensionality" [44], it has much greater computational costs than GLLS and MOCABA. Therefore, a limited number of cross-sections and other relevant quantities could be calibrated. The number of calibrated parameters and the type and number of assimilated experiments were dictated by SMC-ABC's practical usability. The implementation of SMC-ABC for reducing uncertainty was carried out using the PyMC3 package [45]. However, the package had to be adapted to the analyzed problem. It needed the ability to use SCALE CSAS5 as the black box mathematical model and to be compatible with the CIS cluster architecture [46]. The Chapter also introduces two novel concepts in the field of nuclear engineering inverse problems: validation using synthetic cross-sections in Algorithm 3 and influence of error from uncalibrated cross-sections in subsection 4.6.2. The calculations and analyses from Chapter 4 were published in the article "Applying approximate Bayesian computation to reduce uncertainty in multigroup 235-U cross-sections using ICSBEP experimental data" Nuclear Engineering and Design.

4.1 Relevant cross-sections and assimilated systems

A total of 23 cross-sections were selected to reduce uncertainty in a pure, highly enriched uranium system called HEU-MET-FAST-001-001 [47] as much as possible. It means that if these cross-sections were known exactly (their standard error would be zero, and the covariance between them and other cross-sections would be zero), then the uncertainty would decrease the most. It would be computationally too expensive to check every combination of cross-sections to find the one that minimizes the error the most. Therefore, 40 cross-sections individually contributing the most to uncertainty were initially identified. They were sorted in order of uncertainty contribution. First, the 15 top ones were selected for this research. Then, from the remaining 25, 8 were selected by checking which combination contributes the most to the uncertainty reduction. All of the selected cross-sections belonged to U-235. The list of cross-sections for calibration is presented in Table 1. Following the SCALE library's formalism, the energy groups are counted from the fastest to the lowest.

Table 1: Calibrated perturbation factor list

Reaction type or quantity and energy group	Energy range [eV]
(n, gamma)4	(3.00E+06 - 1.85E+06)
(n, gamma)6	(1.50E+06 - 1.20E+06)
(n, gamma)7	(1.20E+06 - 8.61E+05)
(n, gamma)9	(7.50E+05 - 6.00E+05)
(n, gamma)10	(6.00E+05 - 4.70E+05)
(n, gamma)11	(4.70E+05 - 3.30E+05)
(n, gamma)12	(3.30E+05 - 2.70E+05)
(n, gamma)13	(2.70E+05 - 2.00E+05)
(n, gamma)14	(2.00E+05 - 5.00E+04)

Table 1: Calibrated perturbation factor list

Reaction type or quantity and energy group	Energy range [eV]
(n, gamma)15	(5.00E+04 - 2.00E+04)
(n, gamma)17	(1.70E+04 - 3.74E+03)
(n, n')4	(1.85E+06 - 1.50E+06)
(n, n')7	(1.20E+06 - 8.61E+05)
(n, n')9	(7.50E+05 - 6.00E+05)
(n, n')10	(6.00E+05 - 4.70E+05)
(n, n')11	(4.70E+05 - 3.30E+05)
(n, elastic)14	(2.00E+05 - 5.00E+04)
(n, fission)2	(6.43E+06 - 4.30E+06)
(n, fission)4	(3.00E+06 - 1.85E+06)
(n, fission)7	(1.20E+06 - 8.61E+05)
(n, fission)11	(4.70E+05 - 3.30E+05)
(n, fission)14	(2.00E+05 - 5.00E+04)
(chi)1	(2.00E+07 - 6.43E+06)

The cross-sections were not explicitly implemented for the calibration algorithm; instead, their perturbation factors were. For each cross-section, the perturbation factor started at 1. If the mean of the posterior distribution of one of the cross-sections was 1.2, then to obtain the new cross-section, one must multiply the old cross-section by the perturbation factor, as shown in Equation 4.1

$$UCS = CS * PF, \tag{4.1}$$

where UCS stands for updated cross-section value, CS for cross-section, and PF for perturbation factor. This work uses the terms "perturbation factor" and "relative cross-section value" interchangeably.

The experiments were selected for computational efficiency (simple geometry, few materials present) and high k_{eff} sensitivity to cross-sections of interest. A total of 24 experiments were selected from the International Criticality Safety Benchmark Evaluation Project (ICSBEP) Handbook [47]. These included experiments from Highly Enriched Uranium Fast Metal Systems (HEU-MET-FAST) and Intermediately Enriched Uranium Fast Metal Systems (IEU-MET-FAST). The list of experiments by their identification and brief descriptions are presented in Table 2.

Given the number of experiments, there can't be provided a more detailed description for each one because each detailed specification takes many pages in the ICSBEP report. As an example, below are short descriptions along with photographic documentation of two experiments with different characteristics and geometry: HEU-MET-FAST-001-001 and IEU-MET-FAST-001-004.

The experiment HEU-MET-FAST-001-001 consists of two halves of a sphere of a 94 wt.% 235-U. It was conducted in the 1950s in Los Alamos to determine the critical mass of this material.

Table 2: Assimilated experiment list

Experiment identification	Description
HEU-MET-FAST-001-001 shell	Bare, highly enriched uranium sphere
HEU-MET-FAST-007-004	Uranium metal slabs Moderated with Polyethylene
HEU-MET-FAST-015-001	Unreflected Cylinder of Highly Enriched Uranium
HEU-MET-FAST-016-001	Beryllium-Reflected Cylinders of Highly Enriched Uranium

Table 2: Assimilated experiment list

Experiment identification	Description
HEU-MET-FAST-017-001	Beryllium-Moderated and Reflected Cylinder of Highly Enriched Uranium
HEU-MET-FAST-018-001 simplified	Bare Spherical Assembly of ^{235}U(90%)
HEU-MET-FAST-020-001 simplified	Polyethylene-Reflected Spherical Assembly of ^{235}U(90%)
HEU-MET-FAST-021-001 simplified	Steel-Reflected Spherical Assembly of ^{235}U(90%)
HEU-MET-FAST-022-001 simplified	Duralumin-Reflected Spherical Assembly of ^{235}U(90%)
HEU-MET-FAST-025-001	A Vanadium-Reflected HEU Cylinder
HEU-MET-FAST-025-004	A Vanadium-Reflected HEU Cylinder
HEU-MET-FAST-032-001	^{235}U(94%) Sphere Surrounded by Natural-Uranium Reflector
HEU-MET-FAST-041-004	^{235}U(94%) Sphere Surrounded by Graphite Reflector
HEU-MET-FAST-065-001	Unreflected Cylinder of Highly Enriched Uranium
HEU-MET-FAST-069-001 simplified	Oralloy ^{235}U(93.2%) Metal Cylinder with Beryllium Top Reflector
HEU-MET-FAST-084-001	HEU Metal Cylinder Aluminium Reflector
HEU-MET-FAST-085-005	Highly Enriched Uranium Metal Sphere Surrounded by Copper Reflector

Table 2: Assimilated experiment list

Experiment identification	Description
IEU-MET-FAST-001-004 idealized	Bare Cylindrical Configurations of Enriched and Natural Uranium
IEU-MET-FAST-002-001	Natural Uranium Reflected Assembly of Enriched and Natural Uranium Plates
IEU-MET-FAST-003-001 simplified	Bare Spherical Assembly of ^{235}U(36%)
IEU-MET-FAST-004-001 simplified	Graphite-Reflected Spherical Assembly of ^{235}U(36%)
IEU-MET-FAST-005-001 simplified	Steel-Reflected Spherical Assembly of ^{235}U(36%)
IEU-MET-FAST-006-001 simplified	Duralumin-Reflected Spherical Assembly of ^{235}U(36%)
IEU-MET-FAST-009-001	Spherical Assembly of ^{235}U(36%) with a 5.75-cm Polyethylene Reflector

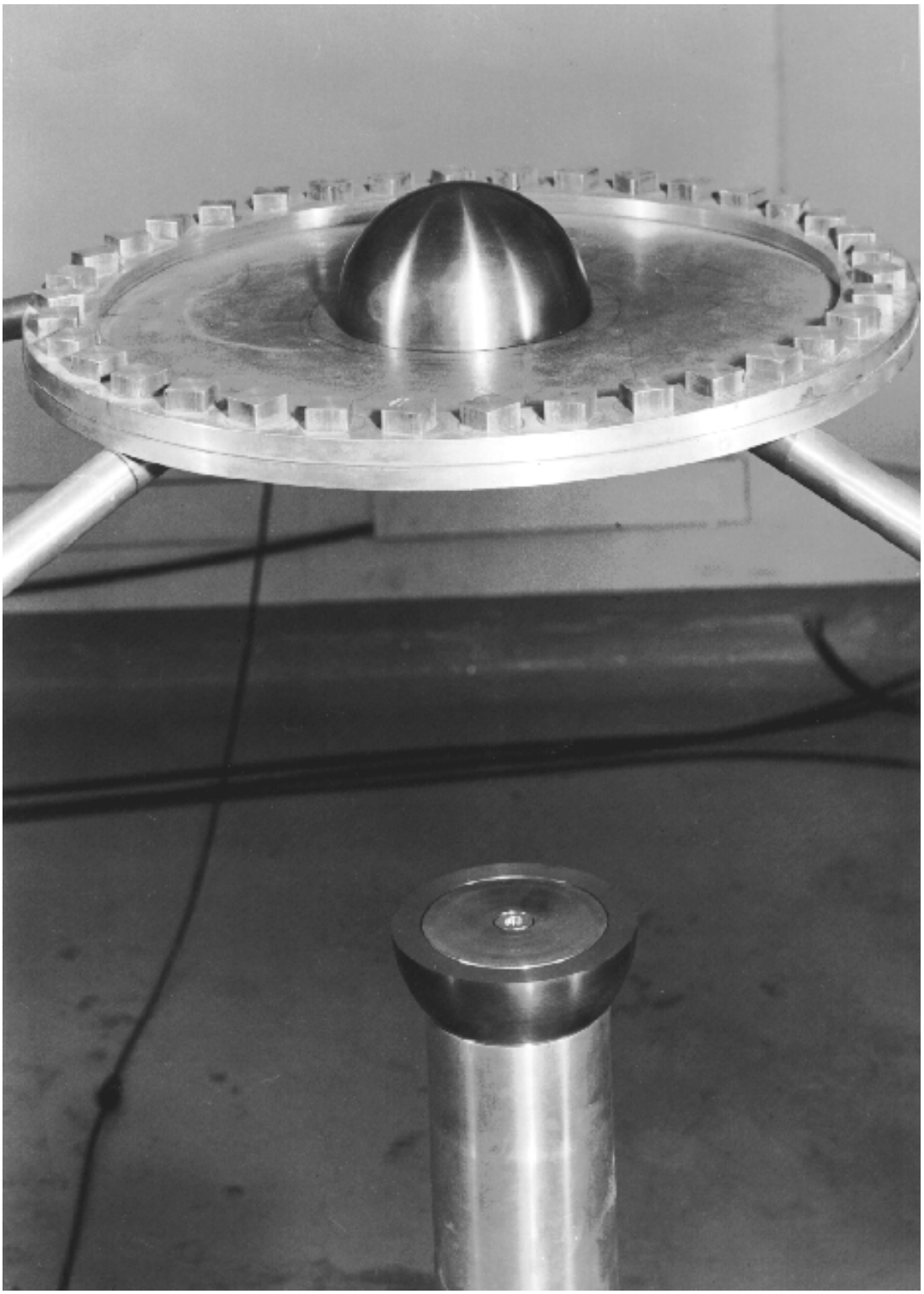

Figure 4: A photo of the experimental setup in HEU-MET-FAST-001-001 experiment.

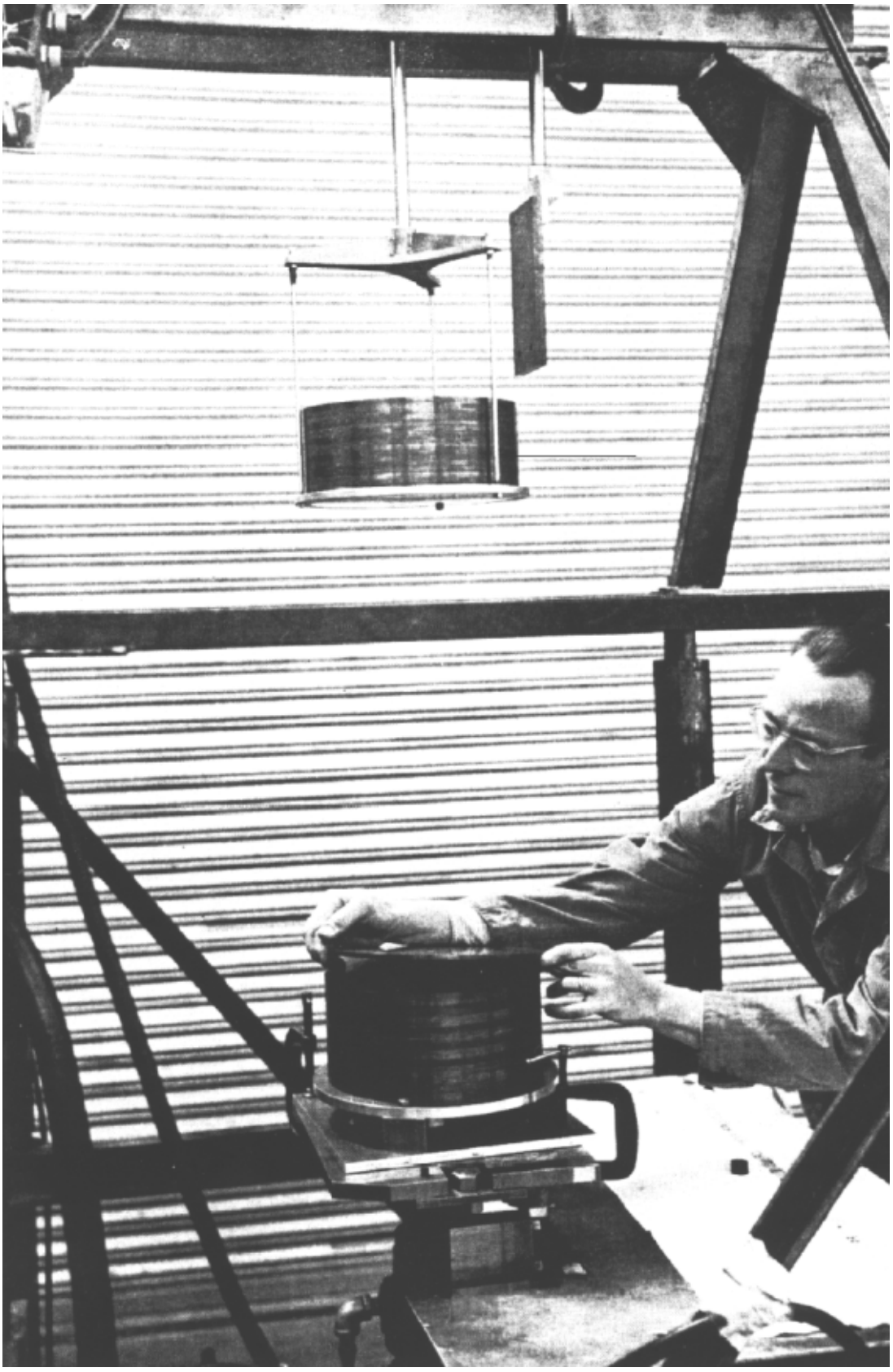

Figure 5: A photo of the experimental setup in IEU-MET-FAST-001 experimental series.

Fig. 4 presents the setup before the two halves are joined and become critical. It is visible that the sphere halves are made of shells. Inside, there is a neutron source. The benchmark model, for which k_{eff} is presented in the document, simplifies the setup substantially, leaving just the sphere and ignoring all other components, like walls and the steel diaphragm. The authors of the document did not present detailed calculations of k_{eff} uncertainty due to those simplifications but present its magnitude of 100 pcm measured in one standard deviation. The photo of the second experiment, named IEU-MET-FAST-001-004, is presented in Fig. 5. The experiment is made of a stack of uranium disks alternating between highly enriched and natural uranium. The disks had a thickness of 0.8 and 0.6 cm. The benchmark model of the experiment has a number of simplifications, whose influence was calculated by ICSBEP authors and added to the k_{eff}. Simplifications were mostly applied to the support structure of the pile, like replacing a notched aluminium boundary with a cylindrical surface. The calculated k_{eff} uncertainty due to these simplifications amounted to 30 pcm measured in one standard deviation.

4.2 Prior distribution

Prior distribution $P(\alpha_0, C_{\alpha\alpha})$ takes the form of a vector of 23 perturbation factors equal to 1, corresponding to cross-sections and quantities from Table 1, and a covariance matrix consisting of appropriate variances and covariances. These are taken from the 56-group relative covariance library from the SCALE software package. Prior is, therefore, a multivariate normal distribution. Its covariance matrix is shown in Section 4.5, in Fig. 10.

4.3 Mathematical Model and uncertainties

The software chosen for simulation of experiments in SMC-ABC and MOCABA implementation was CSAS5 module in SCALE [48] (see Chapter 3). The module calculates k_{eff} for given geometry, isotopic composition, and temperature. Simulation runs until a predefined Monte Carlo uncertainty of 0.0003 is reached. GLLS was implemented using the SCALE TSURFER module. The module requires cross-section sensitivities calculated beforehand, which was done using the SCALE TSUNAMI module. The uncertainty computation methodology presented throughout the rest of this subsection applies to all three algorithms. As discussed in Section 2, all sources of uncertainties must be quantified: the model discrepancy, measurement uncertainty (i.e., benchmark experiment uncertainty), and error stemming from uncertainty in unadjusted parameters.

Let's start with model discrepancy. The Monte Carlo statistical error is inherent in all Monte Carlo-type computations. In practical engineering applications, it is sufficient when the statistical error value of 0.0001 is reached. This kind of precision requires a substantial amount of computational time. Therefore, the simulation stops for this research when the statistical error reaches 0.0003. Another source of error is the uncertainty coming from collapsing the continuous energy library to a 56-group structure. Some uncertainty stems from averaging cross-sections across energy ranges, and some from imperfections in the resonance self-shielding process. This discrepancy is difficult to estimate. It was decided on a conservative approach summarized Alg. 2.

The resulting average absolute difference in k_{eff} between CE and MG computations was 0.0039 and will later be denoted as UMC - Uncertainty due to Multigroup Collapse. The model discrepancy error is defined in Eq. 4.2:

$$MD = \sqrt{MCU^2 + UMC^2}, \tag{4.2}$$

Algorithm 2 Model discrepancy estimation

1. Calculate k_{eff} for all experiments used in the Bayesian algorithms using the 56-group library.

2. Calculate k_{eff} for all experiments used in Bayesian algorithms using a CE library.

3. Calculate the absolute difference in k_{eff} for each pair of results.

4. Calculate the average absolute difference in k_{eff} for all experiments combined.

5. Assume that the average absolute difference in k_{eff} is the model discrepancy component, measured in one standard deviation.

where MD stands for the model discrepancy, MCU is Monte Carlo uncertainty, and UMC is uncertainty due to multigroup collapse. Uncertainty from unadjusted parameters (cross-sections and other quantities) comes from the fact that only some cross-sections are calibrated. This uncertainty can be computed using the standard error propagation "sandwich" method [49], as shown in Eq. 3.1. The covariance matrix C is the covariance matrix for 56-group library from SCALE software package, but with variances and covariances coming from calibrated parameters assigned a value of zero, as these cross-sections will be adjusted (calibrated). Sensitivity vectors were calculated using the SCALE TSUNAMI module (see Chapter 3.4). The last source of uncertainty is benchmark experiment uncertainty. This uncertainty comes from two sources. Firstly, a model of any system will have some idealizations and simplifications. Therefore, any model is not expected to reproduce the exact k_{eff} value measured in a laboratory setting. The model is instead expected to predict k_{eff} of a system resembling the real one but with influences from simplifications present. For example, mathematical models usually ignore the room return phenomenon, inevitably underpredicting k_{eff} value. The effect of these simplifications can be estimated along with its uncertainty with error propagation methods. The second source of benchmark experiment uncertainty is input uncertainties. These can be, for example, the imprecision with which uranium enrichment is known, geometrical uncertainties, or imperfect knowledge of temperature and how it varies across geometry.

The procedure of estimating how the k_{eff} for the model will be different from the measured one and computing corresponding uncertainty, as well as uncertainty coming from input uncertainties, was done for every experiment in the ICSBEP handbook by the document's authors.

Combining all the uncertainty sources, the total uncertainty for each experiment is shown in Eq. 4.3.

$$E_{tot} = \sqrt{MD^2 + BEU^2 + UCSU^2} \tag{4.3}$$

where BEU stands for benchmark experimental uncertainty, and UCSU stands for uncalibrated cross-section uncertainty and is equal to E from Eq. 3.1. It is important to note that this approach neglects the correlations between experimental uncertainties. Since most experiments did not have correlated systematic errors (except the two HEU-MET-FAST-025 experiments), this correlation mostly comes from uncalibrated parameters. The reason for this neglect is that SMC-ABC does not have an option for considering such uncertainties. Sections 4.6.2 and 5.5.3 investigate the potential influence of correlations on the results.

4.4 Bayesian algorithm settings

4.4.1 GLLS

In contrast to SMC-ABC, there are few adjustable settings because the GLLS procedure consists of a couple of straightforward mathematical transformations. Some options of low significance are available in its TSURFER implementation, like the treatment of unavailable covariance data, minimum sensitivity criteria, or manually setting target chi-square for consistency acceptance. These were not important for the research concerning this thesis, so they were set to default, described in detail in [30]. The computation of posterior distributions of the considered perturbation factors takes a few seconds on a desktop computer with Intel Core i5-4690 CPU and 8 GB RAM.

4.4.2 MOCABA

There are two notable algorithm settings for MOCABA: the number of sampled cross-section libraries and the transformation function f, in case the prior k (i.e. the k_{eff}) is not normally distributed. It was decided to create 2,000 samples since this number provided a low enough Monte Carlo uncertainty. The computations took about 24,000 core hours using Intel Xeon E5-2680 v2 processors. After these computations, a normalcy test could be run on each generated k_{eff} distribution. It was determined with D'Agostino's K-squared normalcy test that over half of the distributions were not normal. An example of such a distribution is the HEU-MET-FAST-021-001S, for which the sampled distribution versus a fitted normal distribution is presented in Fig. 6. It is visible that the prior k_{eff} distribution for HEU-MET-FAST-021-001S is slightly skewed to the right.

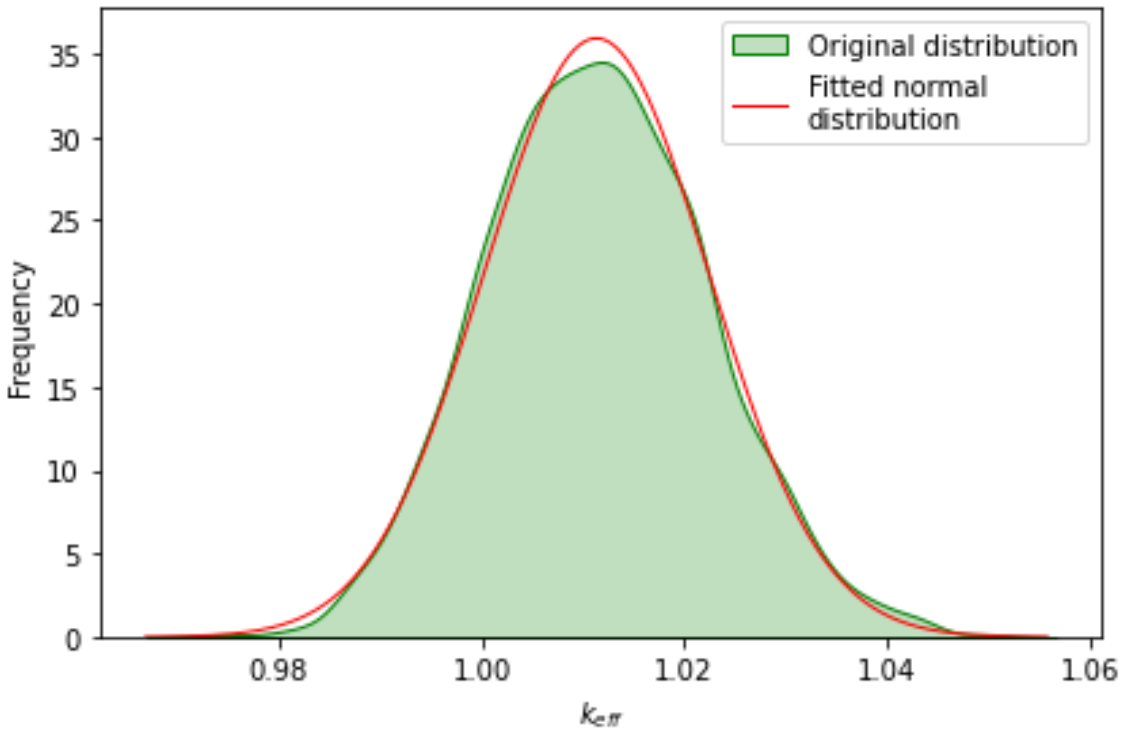

Figure 6: The sampled k_{eff} distribution for HEU-MET-FAST-021-001S and a fitted normal distribution.

4.4.3 SMC-ABC

Based on separate pre-calculations, it was decided to set $N = 20,000$ parallel, $K = 10$ iterations long Markov chains for each β stage. Therefore, samples in number 20,000 can be drawn simultaneously in one instance, allowing for significant parallelization of the computations. Given 20,000 simultaneous samples and 24 SCALE inputs describing the 24 experiments, 480,000 simulations must be performed for each instance. These simulations can be done in parallel, limited only by the number of available CPU cores. They were conducted on the Świerk Computing Centre (CIŚ) cluster. Simulation for each input took ∼3–5 min, depending on the core. The algorithm went through 3 stages of β, resulting in 31 instances of 20,000 samples. A rough estimate of resources spent on computations is 744,000–1,240,000 core hours using Intel Xeon E5-2680 v2 processors.

4.5 Results

Figs. 7 and 9 show each cross-section's perturbation factors and relative standard deviations before and after the GLLS, MOCABA with transformations, and SMC-ABC calibrations. Additionally, a plot with MOCABA results without transformation will be presented in Fig. 8 to illustrate how the neglect of the skew of the prior distribution affects the results.

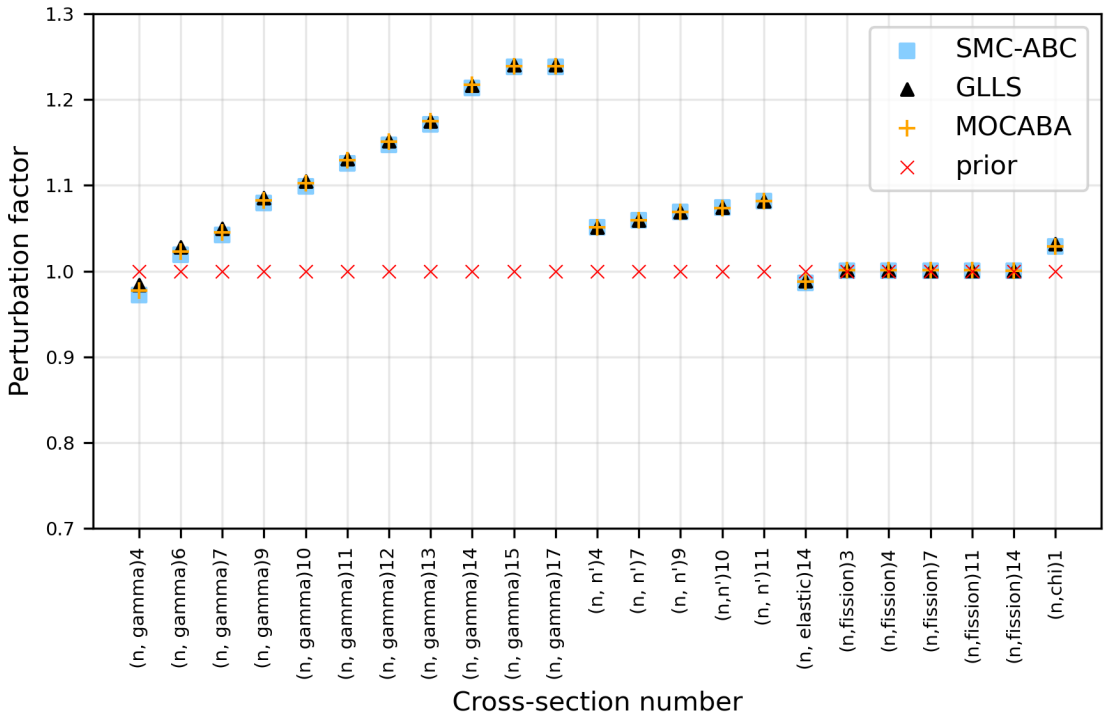

Figure 7: Mean of prior and posterior perturbation factor values for GLLS, MOCABA with transformations, and SMC-ABC.

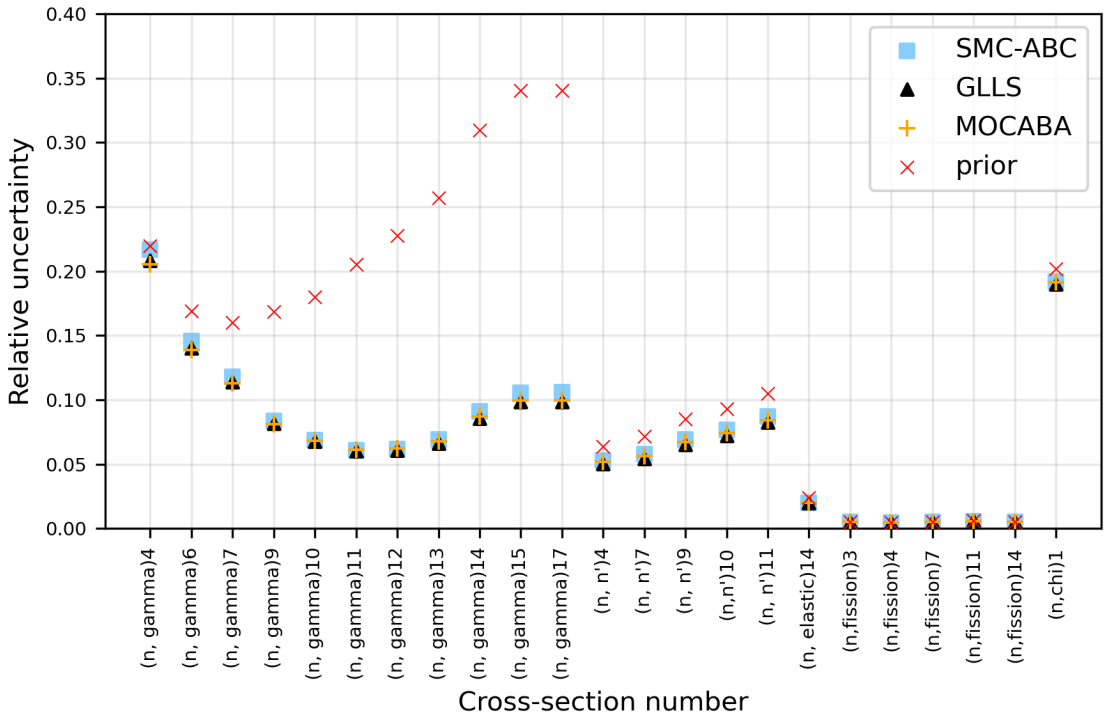

Figure 9: Standard deviation of prior and posterior perturbation factor values for GLLS, MOCABA without transformations, and SMC-ABC.

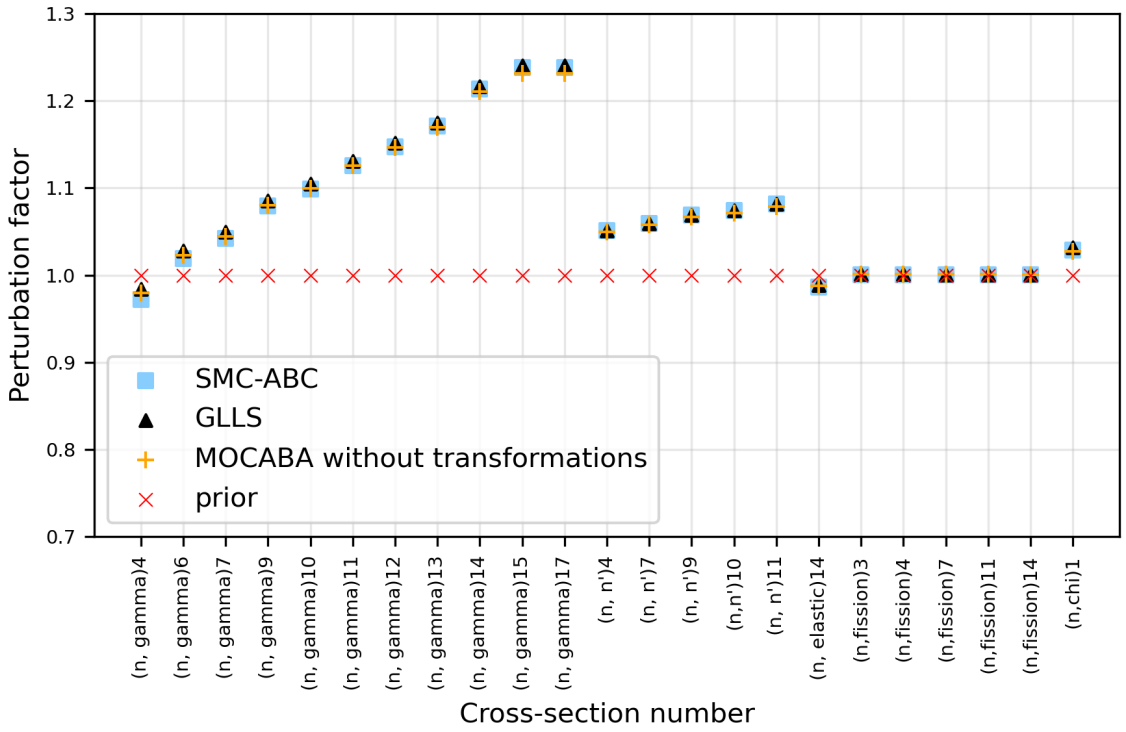

Figure 8: Mean of prior and posterior perturbation factor values for GLLS, MOCABA without transformations, and SMC-ABC.

It is visible, especially for the cross-sections (n, gamma)15 and (n, gamma)17, that the neglect of transformations shifts the posterior means a little in the direction away from SMC-ABC, which is considered the most reliable among the methods. The finding reinforces the necessity of transforming the prior distributions that don't pass the normalcy test due to even a relatively minor skew. The comparison will not be repeated for the posterior uncertainties because, in that case, the difference is barely noticeable.

The numbers beside the reactions denote the energy groups selected from the 56 energy groups of the SCALE code library, where energy group 1 is the fastest neutron energy group (20 MeV - 6.4 MeV), and energy group 56 is the slowest neutron energy group (4e-03 eV - 1e-05 eV), and n' means inelastic scattering. All of the cross-sections belong to the U-235 isotope. In general, cross-sections with high prior relative standard deviations are significantly affected by calibration. For example, the relative

difference between U-235 prior and posterior capture cross-section at 17 energy groups (17 keV - 3.7 keV), which has a maximum relative standard deviation of about 0.35, is about 25% for the mean and 71.5% for the relative standard deviation, then it decreases as prior relative standard deviation decreases. On the other hand, calibration has negligible influences on U-235 fission cross-sections since their prior relative standard deviations are almost zero.

From Figs. 7 and 9, we can see that the posterior cross-section results are consistent between the three applied methods and often practically the same. The posterior uncertainty is also very similar. It is very slightly underestimated by GLLS and MOCABA for the (n,gamma)14∼17 cross-sections, which witnessed the most significant changes, and for (n,n') reactions when GLLS is used. The differences reside, however, within the Monte Carlo uncertainty of SMC-ABC calculations. The Monte Carlo uncertainty for SMC-ABC was roughly estimated by running a simplified 1D version of the algorithm a couple of times with different starting seeds. A somewhat baffling finding is that the linear GLLS method gives the same posterior mean results as the non-linear SCALE-based MOCABA and SMC-ABC, even though the skew in the prior k_{eff} values suggest slight non-linearity of the sensitivities. This is most likely due to the sensitivities corresponding to calibrated cross-sections being linear close to their prior value and non-linear far away. Some cross-sections have large uncertainty, and during MOCABA sampling, they could be randomized to be even twice larger than the prior ones. These extreme samples are likely the origin of the skew in prior k_{eff} seen in 4.4.2. This non-linearity in samples with values far from the prior is not relevant, however, when GLLS is applied.

The standard deviation of the posterior distribution for each perturbation factor presents incomplete information about posterior uncertainty. Posterior covariance must also be considered. Since only 23 cross-sections were calibrated while the rest stayed unchanged, a unique method had to

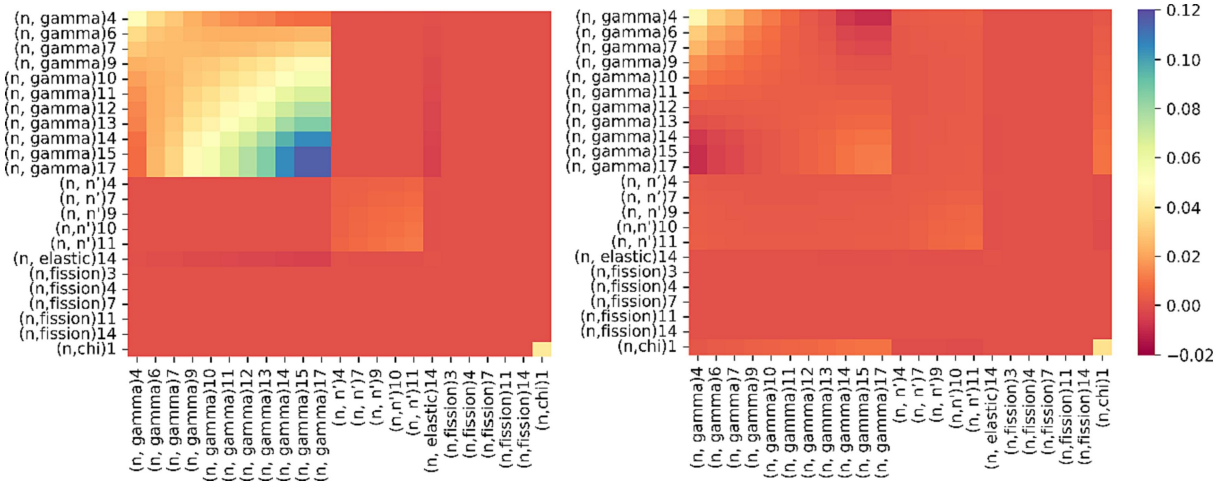

Figure 10: Prior (on the left) and posterior (on the right) covariance of perturbation factors.

be developed to calculate the posterior covariance between calibrated and uncalibrated cross-sections. Given the formula for covariance shown in Eq. 4.4:

$$Cov_{ij} = Corr_{ij} * \sigma_i * \sigma j \tag{4.4}$$

where Cov_{ij} and $Corr_{ij}$ are, respectively, covariance and correlation between cross-sections i and j, and σ_i, σj are their standard deviations, the standard deviation of the calibrated cross-section changes while the rest of the variables stay the same. The correlation component should also change (its absolute value should decrease), but it is impossible to calculate it with how the calibration was implemented. Keeping the correlation values constant is a conservative approach to not underpredict the posterior uncertainty of k_{eff}.

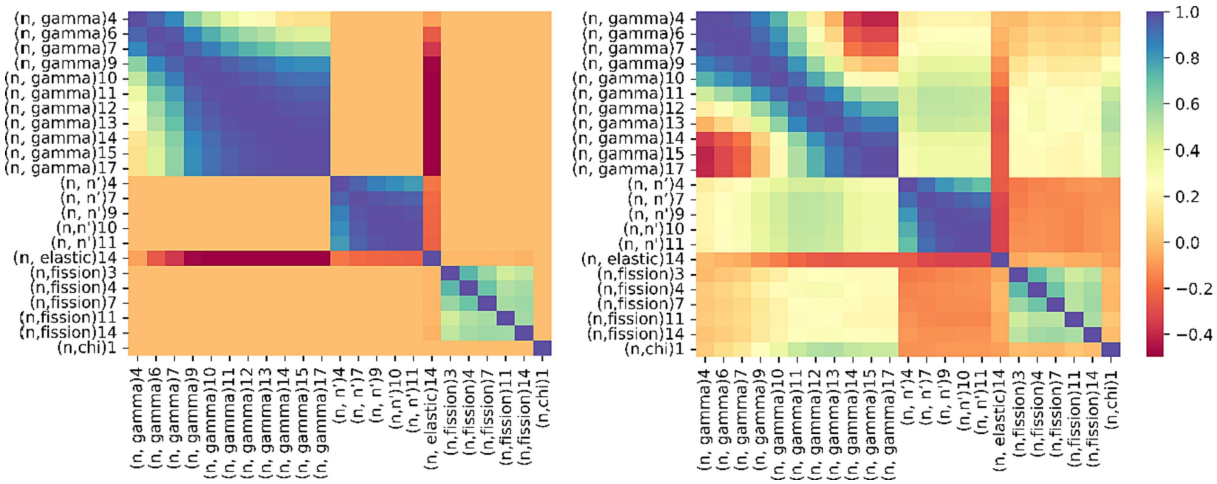

Figure 11: Prior (on the left) and posterior (on the right) correlation matrix of perturbation factors.

The prior and posterior covariance matrices of the SMC-ABC calibrated perturbation factors (i.e., prior and posterior relative covariance matrix of cross-sections) are presented in Fig. 10. The GLLS and MOCABA-produced posterior covariance looks qualitatively the same as the SMC-ABC-produced one. The prior covariance matrix has the multivariate distribution taken from the SCALE software package, where the diagonal matrix elements are the squares of the prior relative standard deviations. As can be seen in Fig. 10, the posterior covariance matrix elements are smaller than the prior ones, and this is due to the reduction in the relative standard deviation. To deeply understand the influence of calibration on the covariance matrix, which is the squares of the relative standard deviations multiplied by the correlation matrix, the prior and posterior correlation matrices are described in Fig. 11.

Before calibration, all reactions have positive correlations except the elastic scattering at the 14 energy group, which is anticorrelated to all capture and inelastic cross-sections. It can be seen that the calibration converts some weak positive correlations to anticorrelated ones, such as the correlations between (n,gamma)14∼17 and (n,gamma)4∼7 cross-sections. The calibration also changes some zero correlations to positive ones, such as

the correlation between capture cross-sections and fission spectrum 'chi', inelastic scattering, and fission cross-sections, where the correlation increases as the number of energy groups increases. It can be concluded that calibration does not only affect the relative standard deviations but also disturbs the correlations between different reactions and energy groups. Posterior distribution (solid lines) and fitted normal distributions (dotted lines) are presented in Fig. 12 for three perturbation factors. The posterior distributions resemble normal distributions but are less smooth. Given the fixed number of samples from which the posterior is created (20,000), the posterior distribution would be coarser if more cross-sections had been calibrated or smoother if fewer cross-sections had been calibrated.

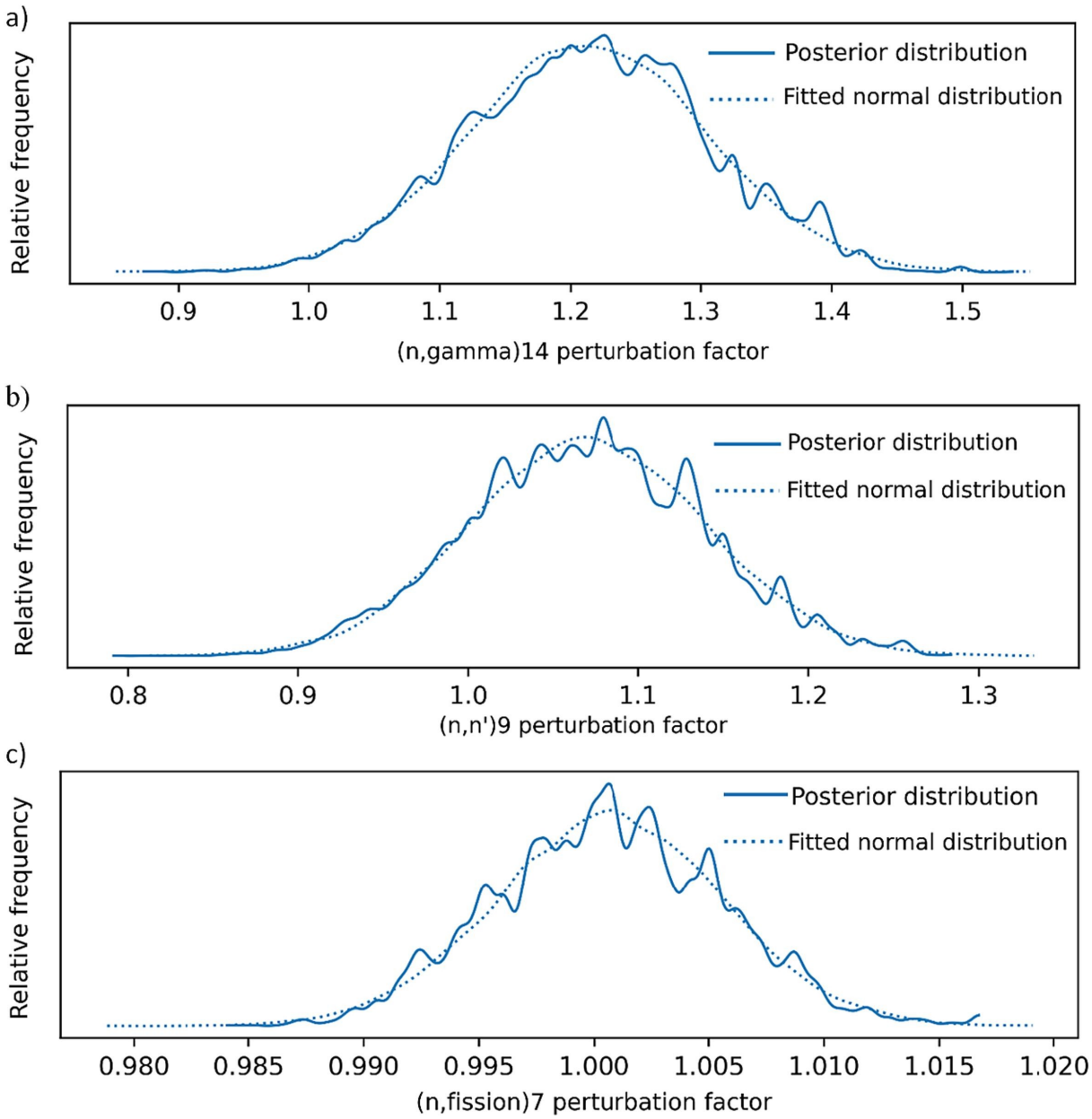

Figure 12: Comparison between the posterior distribution and a fitted normal distribution for the perturbation factor of: a) (n, gamma)14, b) (n,n')9, c) (n,fission)7. for the SMC-ABC posterior

4.6 Validation

4.6.1 Verifying whether goals of Bayesian calibration were accomplished

The goals of Bayesian calibration in the context of this work are successful inference of true values of neutron cross-sections, subsequent reduction of k_{eff} uncertainty, and improved ability to accurately predict benchmarks

k_{eff}. Three procedures are applied to verify whether these goals have been fulfilled:

(a) Comparing k_{eff} computed using cross-sections before and after calibration for experiments not used in the SMC-ABC calibration process.

(b) Checking if the calculated and experimental k_{eff} values lie within 3 standard deviations of each other for each system.

(c) Using so-called "synthetic experiments", which are computationally generated reference ("experimental") results.

To conduct procedure (a), 17 new experiments (not used for calibration) were chosen based on their dominant source of uncertainty. If a relative uncertainty contribution from any reaction from any isotope other than U-234, U-235, and U-238 was larger than 0.02 %, then the experiment was not included in the comparison. The reason for this exclusion is the possibility that the cross-section uncertainty effect on k_{eff} from uranium and other elements could cancel each other out. This would lead to calculated k_{eff} results closer to the experiment before calibration, despite calibrated cross-sections' values being improved. The comparison of k_{eff} results between using the original (uncalibrated) and perturbed (calibrated) 56-group library are presented in Fig. 13. The mean absolute difference between experimental and computational k_{eff} has been reduced from 0.0049 to 0.0025 (reduction of 49%). The average posterior uncertainty is lower than the prior uncertainty by 47.6 %.

The calculated k_{eff} is expected to lie within three standard deviations of calculated uncertainty from the experimental one 99.7 % of the time, regardless of the system's isotopic composition and geometry. A set of new experiments was chosen to check whether this remains true after calibration. The k_{eff} and its uncertainty were calculated for each experiment

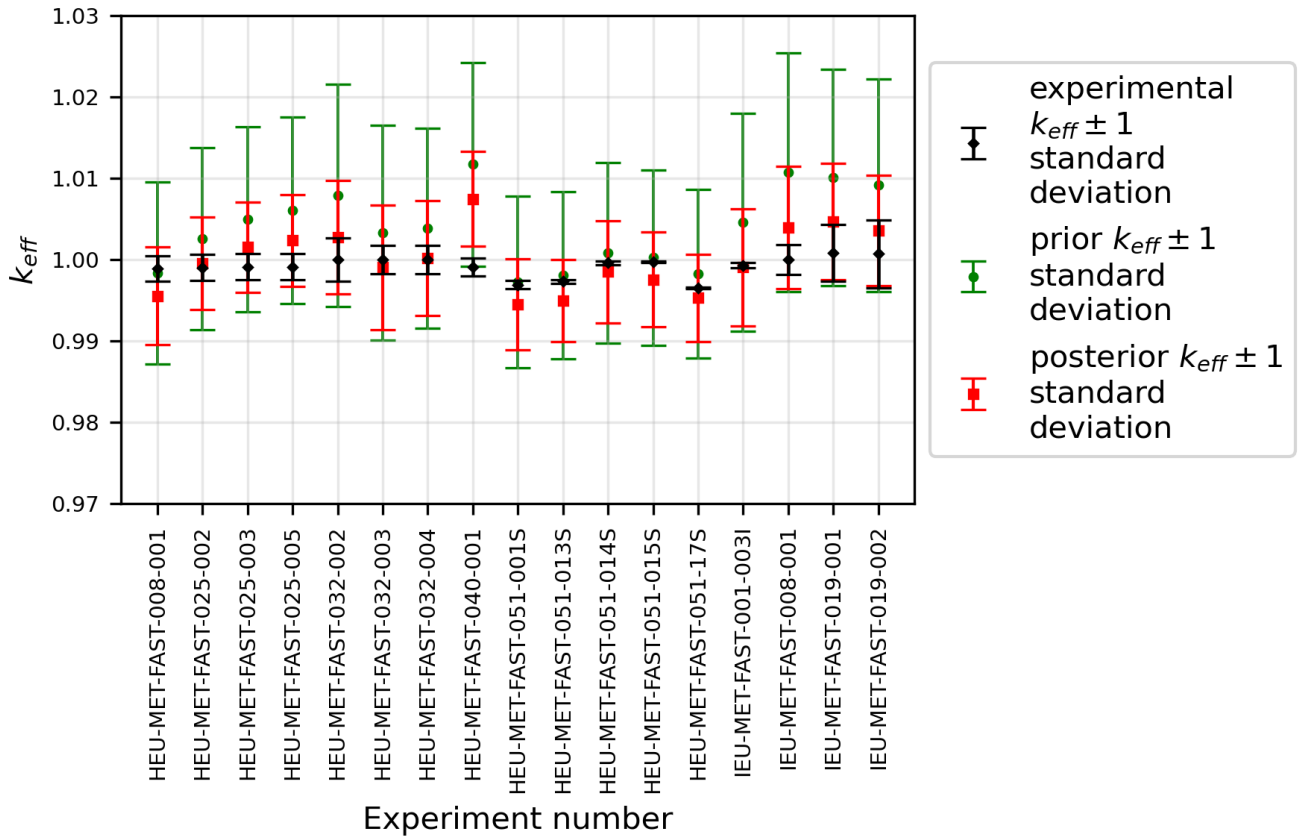

Figure 13: Comparison of k_{eff} results obtained using unperturbed 56-group library (prior) against perturbed 56-group library (posterior) and experiment for experiments with a very small fraction of uncertainty coming from any isotopes other than U-234, U-235, U-238.

using posterior cross-sections and posterior covariance matrix. Model discrepancy (discussed in Section 4.3) was added to the uncertainty to take into account all computational errors. The comparison between experimental and computed k_{eff} is presented in Fig. 14. Note that the plot in Fig. 14 has an error expressed in three standard deviations, as opposed to Fig. 13, where one standard deviation is used. The experimental k_{eff} distribution overlapped significantly with the calculated one for every experiment.

Procedure (a) shows that the goals of reducing k_{eff} uncertainty and improvement of agreement of k_{eff} with experimental results have been achieved. Step (b) provides additional confidence that there were no signi-

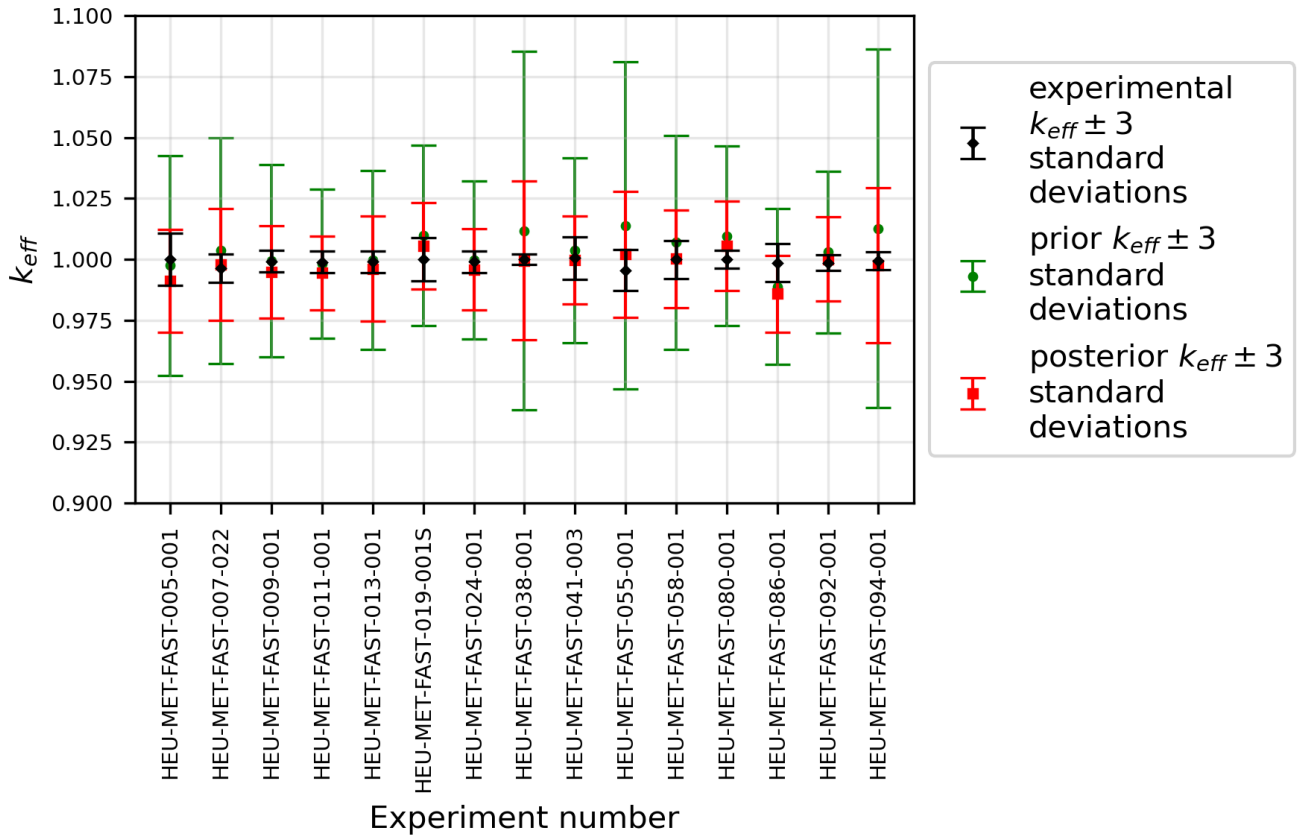

Figure 14: Comparison of k_{eff} results obtained using unperturbed 56-group library (prior) against perturbed 56-group library (posterior) and experiment for experiments with large portions of uncertainties coming from other sources than in the case of the assimilated ones.

ficant errors in the application of Bayesian calibration, for example, underestimation of the total experiment uncertainty E_{tot} (see definition of E_{tot} in 4.3). However, these procedures do not rule out the possibility that cross-sections were overfitted. The improvement of results shown in Fig. 13 could be achieved by modification of many combinations of cross-sections. The problem of potential overfitting or inability to infer true posterior values is referred to in the literature as a "non-identifiability problem" [50]. It may arise if experimental data is inadequate or not sensitive enough to calibrate parameters. To check whether it is possible to infer true posterior values of cross-sections, the authors of this paper implemented method (c). This method uses so-called "synthetic experiments". These are calculated

values of measurable quantities using synthetically generated parameters. In the current study, these are k_{eff} values computed using a synthetically generated cross-section library.

A perturbed 56-group library from one of the SCALE SAMPLER module libraries was used for this purpose. All the perturbation factors in this library were created by taking a sample from a multivariate normal distribution (the multivariate normal distribution is defined by a vector of perturbation factors equal to one and 56-group covariance library).
To conduct the validation, a linear metamodel consisting of k_{eff} computed with unperturbed cross-sections and sensitivities generated by the TSUNAMI module was created. The metamodel has been proven to work well by conducting the same SMC-ABC procedure as described in Section 4.4.3. The results were very similar to the TSURFER ones, with the difference within statistical uncertainty. Procedure (c) is described in Algorithm 3. The algorithm is less computationally expensive since a linear metamodel is used instead of SCALE CSAS5. It takes 20 min on a desktop computer with Intel Core i5-4690 CPU and 8 GB RAM to finish. The comparison between the synthetic and posterior cross-sections is presented in Fig. 15. It is visible in Fig. 15. that all the synthetic cross-sections are very close to the SMC-ABC results.Most are within one standard deviation of the posterior distribution, with one case 1.2 standard deviations away. Fifteen cross-sections have shifted considerably in the direction of their corresponding synthetic values.

Algorithm 3 Validation using synthetic cross-sections.

1. Choose a 56-group library from SAMPLER libraries provided in the SCALE software package.

2. Calculate k_{eff} for the 24 experiments using SCALE CSAS5 with the library chosen in step (1).

3. Implement the resulting k_{eff} values in the SMC-ABC algorithm as observed data.

4. Assume the same uncertainties for k_{eff} in step (3) as for real experiments from ICSBEP.

5. Collect sensitivity data for the 24 experiments from TSUNAMI results (using the standard 56-group library).

6. Implement metamodel based on sensitivities to the SMC-ABC algorithm.

7. Set the same SMC-ABC algorithm parameters as described in Section 4.4.3.

8. Run the algorithm using the PyMC library version 3.11.4.

9. Compare the resulting posterior cross-sections with the cross-sections from step (1).

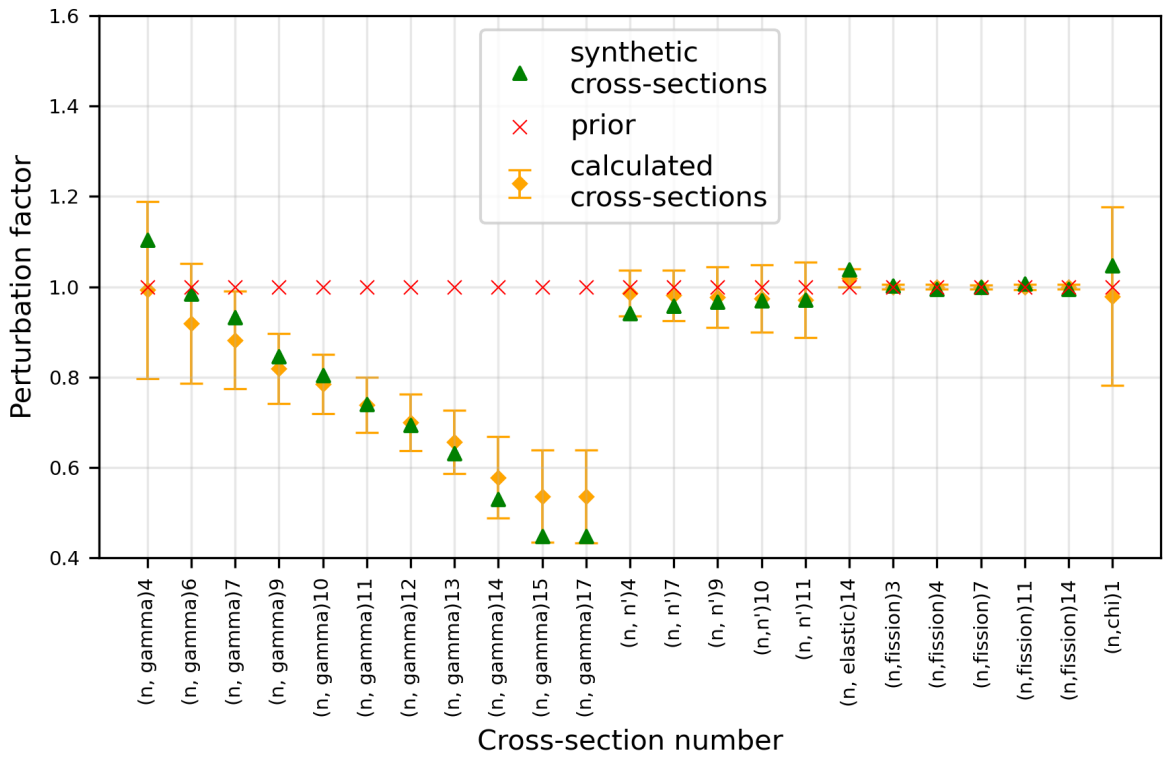

Figure 15: Comparison between synthetic cross-sections and calculated cross-sections.

The remaining eight have either stayed constant or minor overfit took place. The largest overfitting occurred for U-235 (n, gamma)6, but it is still within one standard deviation of the posterior distribution to the

synthetic cross-section value. The degree to which posterior cross-sections are close to synthetic cross-sections informs us whether the inference of true cross-section values is possible given available experimental data. The agreement between posterior and synthetic cross-sections presented in Fig. 15 is satisfactory, although it is likely that the assimilation of a larger number of experiments with parameters other than k_{eff} would improve this agreement.

4.6.2 Study of the potential influence of error correlations due to uncertainty from uncalibrated cross-sections

PyMC implementation of SMC-ABC has no in-built capability to consider correlations between errors in experimental data. Such correlations can arise when only some of the input parameters are calibrated. Neglecting these correlations comes with the risk of artificially reduced posterior uncertainty. To investigate the effect of these correlations in this work, TSURFER was run with settings described in 4.4.1, but correlations between experiments errors were included. The reliability of TSURFER for calibrating the considered cross-sections despite the assumption of linear responses was proven in Section 4.5. The correlations were computed using the Monte Carlo method. For that, linear metamodels were used to calculate the influence of sampled uncalibrated U-234, U-235, and U-238 cross-sections, while independent uncertainty sources like benchmark experiment uncertainty were set as random variables. Two thousand calculations were made for each considered experiment. The resulting correlations were in the range of -0.18 to 0.5. The comparison with SMC-ABC results is presented in Fig. 16. The posterior uncertainties' comparison is presented in Fig. 17. The new posterior cross-sections have only slightly different values. The posterior uncertainty values are also quite similar, although SMC-ABC slightly underestimates the posterior uncertainty for some cross-sections.

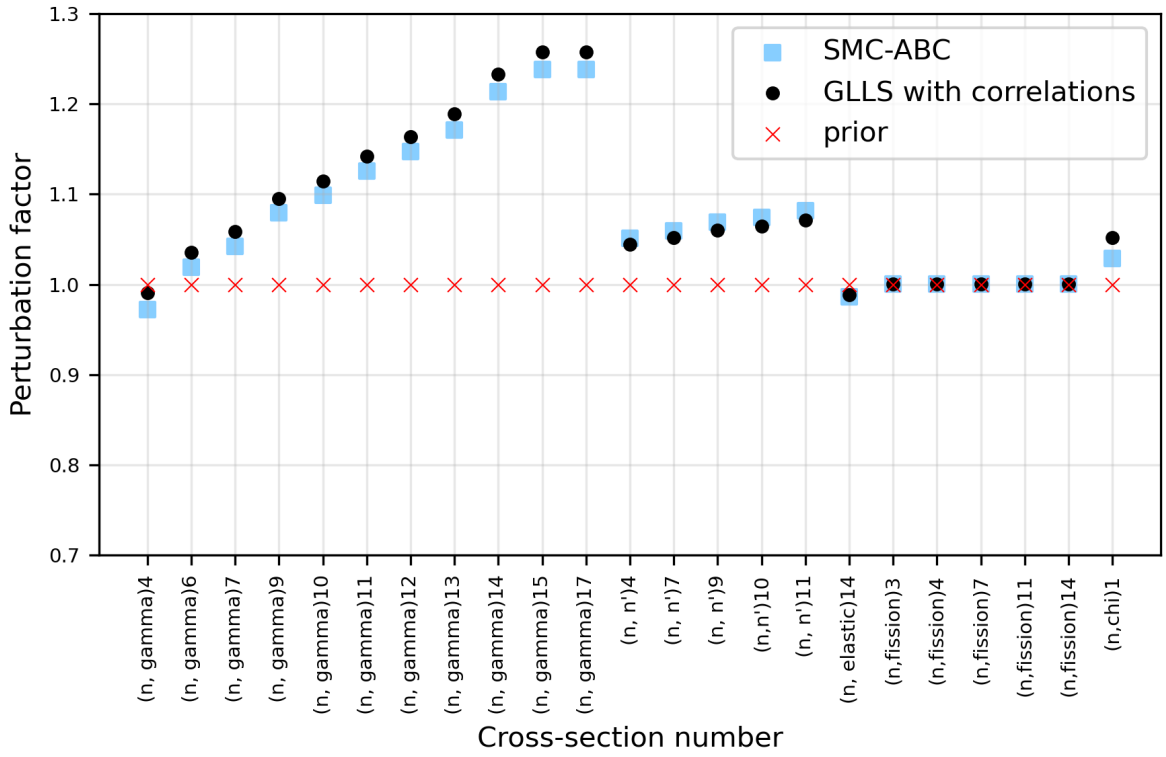

Figure 16: Comparison between posterior cross-sections calculated by SMC-ABC without correlations and by GLLS with correlations.

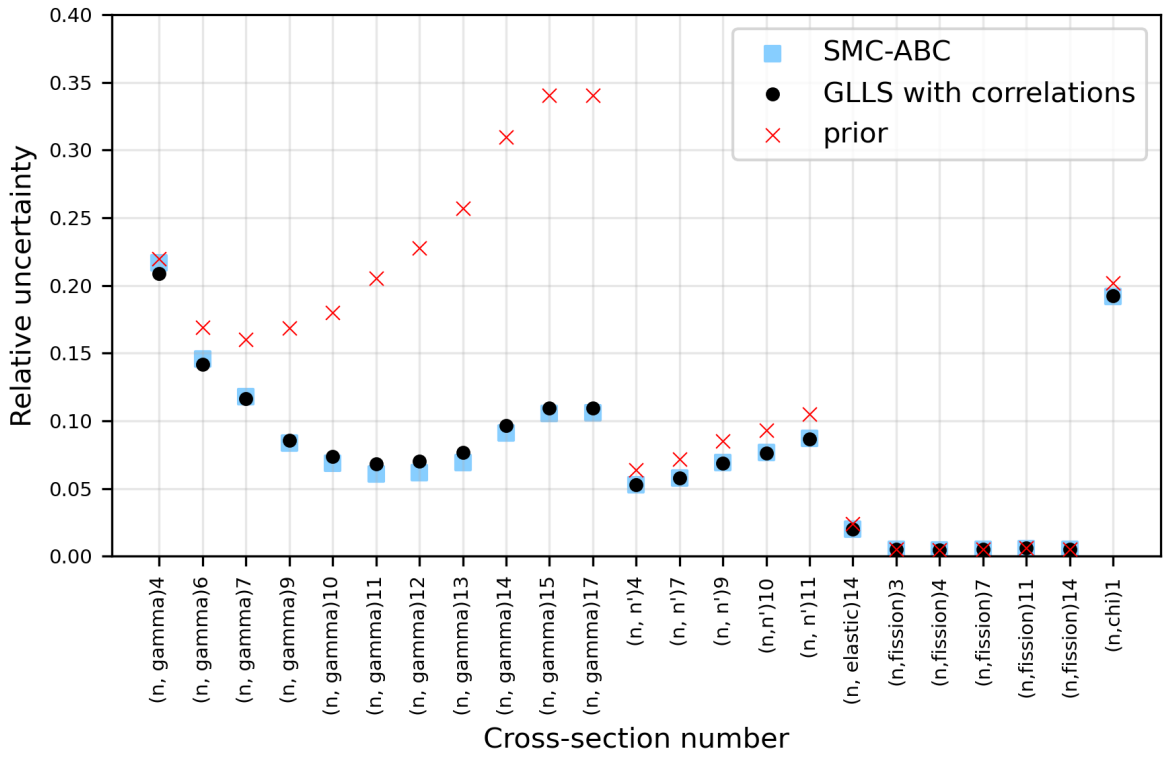

Figure 17: Comparison between posterior uncertainties calculated by SMC-ABC without correlations and by GLLS with correlations.

Figs. 16 and 17 prove that correlations between uncalibrated parameters have an influence on results, and although this influence was not large in this study, it could be when using a different set of experiments or if another Bayesian calibration problem was being solved. A more thorough analysis of the influence of the uncalibrated parameters' uncertainties and correlations from uncalibrated experiments is presented in Section 5.5.3.

4.7 Summary of the GLLS, MOCABA, and SMC-ABC comparison

The comparison conducted in this chapter shows that the SMC-ABC method is an effective but computationally expensive tool to reduce uncertainty in select multigroup neutron-cross sections. The algorithm's implementation in the PyMC Python library also needs an improvement in the form of the built-in capability to include correlations between experimental uncertainties. The GLLS method implemented in the SCALE TSURFER code is a much faster and similarly reliable tool for U-235-based fast systems. The minor differences in posterior uncertainties of cross-sections are likely due to SMC-ABC Monte Carlo error. MOCABA is also much faster than SMC-ABC and gives practically the same results, with posterior uncertainties within Monte Carlo error from each other. MOCABA also enables the use of non-linear models and allows for the possibility of not relying on sensitivity calculations. The adjoint-based sensitivity calculations are not always reliable, as explained in Chapter 3.4. It was decided that for calculations concerning thermal systems in Section 5, the MOCABA procedure would be used. It was shown that the posterior distributions are multivariate normal anyway, so there is no need for SMC-ABC. On the other hand, it is uncertain whether the GLLS's linear approximation of cross-section sensitivities is valid for thermal systems where resonances occur.

5 Application of MOCABA to reduce uncertainty in cross-sections relevant to HTGRs

After the comparison analyses of the algorithms in Chapter 4.7, the decision was made to employ the MOCABA procedure for thermal system calculations for calibrating cross-sections relevant to HTGRs. It was demonstrated that the posterior distributions are inherently multivariate normal. However, there remains uncertainty regarding the validity of GLLS's linear approximation of cross-section sensitivities in thermal systems with resonances. Since MOCABA is not affected by the curse of dimensionality as SMC-ABC, it was decided to calibrate many more cross-sections than in Section 4.7. The MOCABA algorithm is based on the mathematical description from Chapter 2.2. It was implemented in Python 3.8 by the author of the dissertation.

5.1 Relevant cross-sections and assimilated systems

Since MOCABA is not affected by the curse of dimensionality as SMC-ABC, it was decided to calibrate many more cross-sections than in Section 4. All the cross-sections belonging to U-234, U-235, U-238, graphite, B-10, and B-11 were calibrated, along with the chi and nubar parameters of the uranium isotopes. That makes a total of 1904 parameters. The list of reactions with calibrated parameters for each isotope is presented in Table 3. As in Section 4, the cross-sections were not explicitly calibrated, but their perturbation factors were defined in Eq. 4.1. The experiments for assimilation were selected based on the occurrence of isotopes of interest and the presence of thermal neutron spectrum. Thirty-four experiments from three series of experiments were selected from the ICSBEP [47] Handbook. The experiments are listed in Table 4.

Table 3: List of reactions whose parameters were selected for calibration

U-234	U-235	U-238	B-10	B-11
elastic	elastic	elastic	elastic	elastic
n, n'	n, n'	n, n'	n, n'	n, n'
n, 2n	n, 2n	n, 2n	n, gamma	n, 2n
fission	fission	fission	n, p	n, gamma
n, gamma	n, gamma	n, gamma	n, d	n, p
nubar	nubar	nubar	n, α	n, t
chi	chi	chi		n, α

Table 4: List of experiments selected for assimilation

System type	Series	experiment number
Highly Enriched Uranium Thermal Solution Systems	HEU-SOL-THERM-001	001-010
Highly Enriched Uranium Thermal Solution Systems	HEU-SOL-THERM-028	001-014
Low Enriched Uranium Thermal Compound Systems	LEU-COMP-THERM-039	001-010

The complete experimental designation is constructed by joining the series' name and number with a dash in between. The HEU-SOL-THERM-001 is a series of experiments consisting of minimally reflected cylinders of highly enriched uranyl nitrate solutions. They were performed in the mid-1970s at the Rocky Flats Plant, which was operated at that time by Rockwell International. The photo of the experimental setup is presented in Fig. 18 .

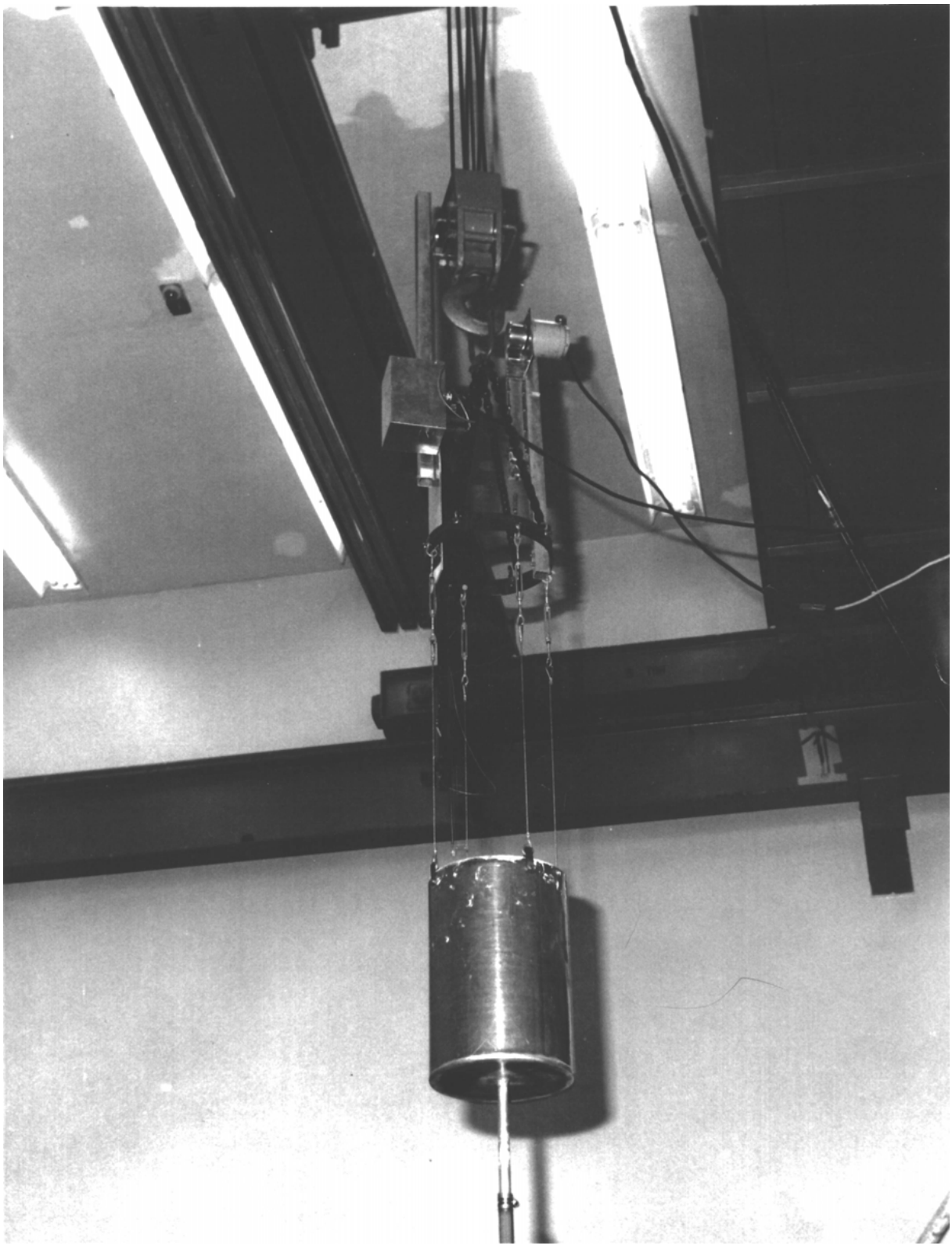

Figure 18: Photo of HEU-SOL-THERM-001 experimental setup, taken from ICSBEP [47]

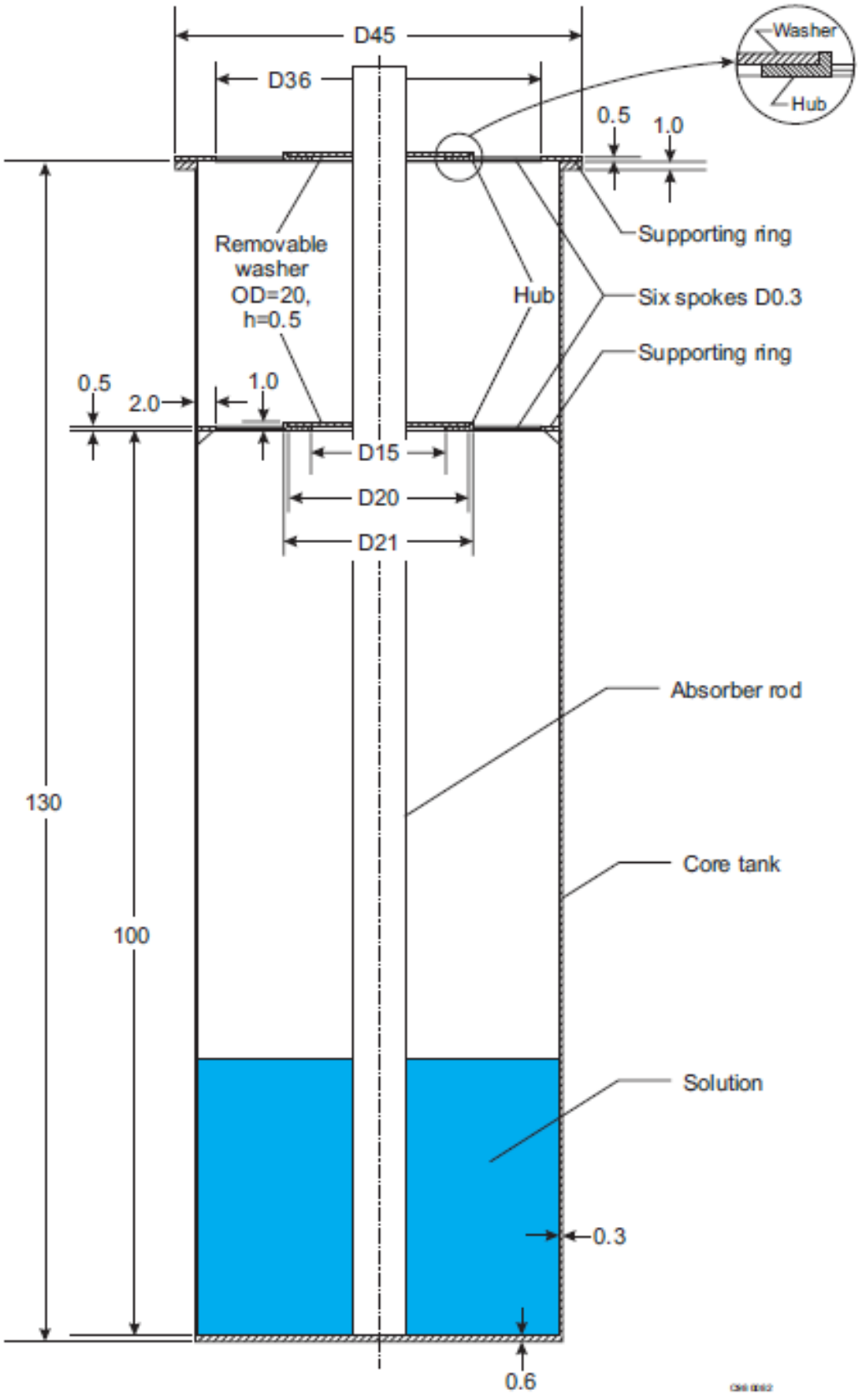

Figure 19: Schematic drawing of a cross-section of HEU-SOL-THERM-028 experimental setup's tank and solution, taken from ICSBEP

The individual experiments differed by the solution composition and the tank material. For each experiment, the critical height of the solution was obtained by interpolating between the measurements of subcritical and supercritical states with k_{eff} very close to 1. The documentation outlines all uncertainty sources and the correlations between measured errors for all experiments. The uncertainties for individual experiments range from 380 to 600 pcm.

The HEU-SOL-THERM-028 series comprises uranium (89% 235-U) nitrate solutions with a central boron carbide absorber rod. The experiments were conducted in the 1960s at the Solution Physical Facility of the Institute of Physics and Power Engineering, Obninsk, Russia. The schematic drawing of the cross-section of the experimental setup is presented in Figs. 19 and 20, due to lack of photos. The individual experiments differed by solution composition and tank dimensions. Some experiments had a boron absorber rod placed in the middle of the tanks, while some did not. The experiments' descriptions contained sufficient descriptions of measurement uncertainties and error correlations for the experiments to be appropriate for Bayesian assimilation. The uncertainties of k_{eff} range from 230 to 580 pcm.

The LEU-COMP-THERM-039 series are experiments made of incomplete arrays of water-reflected 4.738-WT.%-enriched uranium dioxide fuel-rod arrays. The experiments were carried out at Institut de Protection et de Sûreté Nucléaire in C.E.A. in 1978. Figs. 21 and 22 present the arrays submerged in a water tank and outside of the water tank.

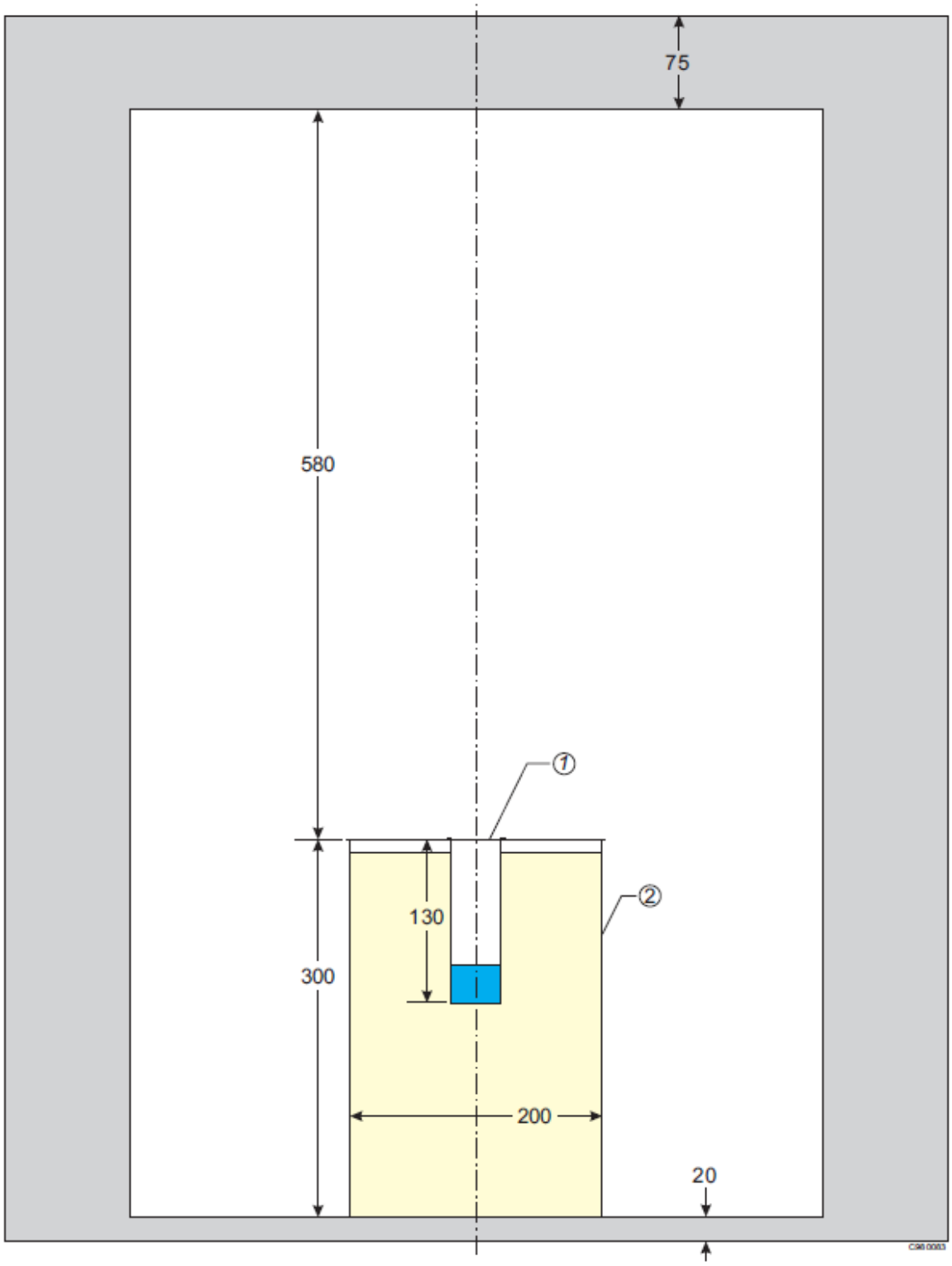

Figure 20: Schematic drawing of a cross-section of the whole HEU-SOL-THERM-028 experimental setup, including tank (1), water reflector (2) and surrounding concrete walls. Drawing taken from ICSBEP.

Figure 21: A photo of the experimental setup of LEU-COMP-THERM-039 series. A complete array of fuel rods is visible, while the experiments had different configurations of rods removed.

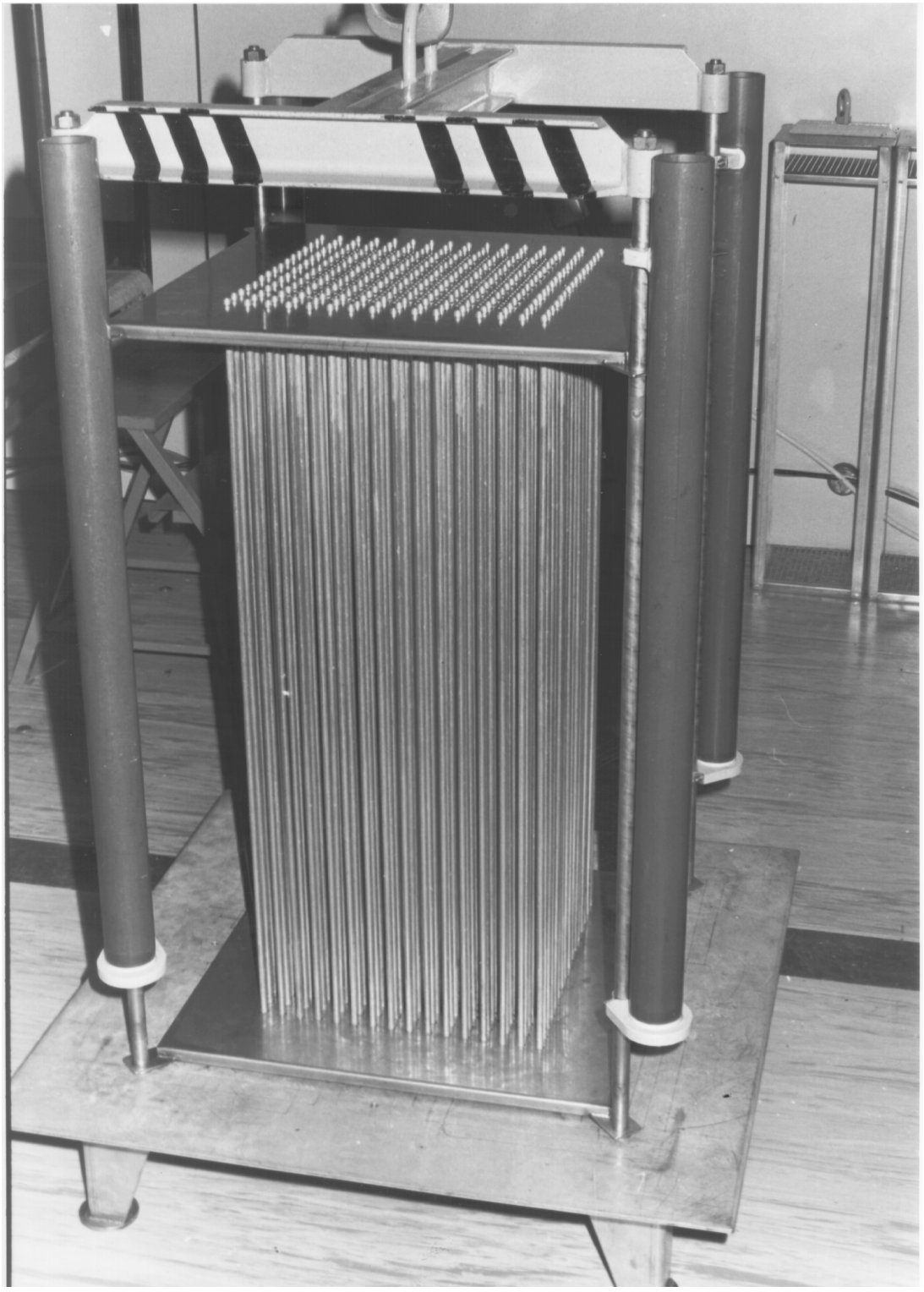

Figure 22: A photo of the full fuel rod array removed from the water tank from the experimental setup of LEU-COMP-THERM-039 series.

5.2 Prior distribution

Prior distribution $P(\alpha_0, C_{\alpha\alpha})$ takes the form of a multivariate distribution with prior means of perturbation factors made of a 1904-long vector of "1" values and the corresponding relative covariance matrix. Any non-zero covariances between cross-sections of different reactions (like between U-235 fission and U-238 (n, gamma)) were included. The covariances are taken from the 56-group relative covariance library from the SCALE software package (see Chapter 3.2).

5.3 Mathematical Model and uncertainties

The software chosen for the simulation of experiments was SCALE's CSAS5. Each simulation runs until a predefined Monte Carlo uncertainty of 0.0002 is reached. Similarly, as described in Section 4.3, the model discrepancy consists of the Monte Carlo uncertainty (0.0002 in this case) and the uncertainty from the usage of a multigroup library instead of a continuous energy library. The uncertainty from the multigroup collapse is calculated in accordance with Algorithm 2, but separately for each of the four series of experiments. This approach was needed because the experiments in individual series were similar in composition and geometry, leading to a correlated model discrepancy. An ability to generate perturbed CE libraries would be required to calculate the exact correlations between model discrepancies of individual experiments. That was out of the scope of this research. Instead, it was assumed that this error would be 70 % correlated within each experimental series. The summary of the uncertainties due to multigroup collapse is presented in Table 5.

Table 5: Uncertainties due to multigroup collapse

Experimental series	Uncertainty in ± 1 sd
HEU-SOL-THERM-001	0.00193
HEU-SOL-THERM-028	0.00141
LEU-COMP-THERM-039	0.00031

The uncertainty from the uncalibrated cross-sections is calculated with the Monte Carlo method rather than the sandwich method described in Section 4.3. This is because the correlations due to geometrical and isotopic uncertainties also had to be computed, and this could only be done with the Monte Carlo method for the largest sources of such uncertainties. They could have interacted non-linearly with the uncalibrated parameters' uncertainties. Three hundred libraries and three hundred inputs with randomized uncertain geometrical and isotopic components were generated for this purpose. The uncertain input parameters with lower impacts on k_{eff} or input parameters that would be too difficult to implement in the Monte Carlo method were considered with a different procedure. Their influence was modeled by simple randomization of errors with standard deviation calculated by ICSBEP authors. These errors would also be randomized 300 times and added to the respective results of the three hundred simulations.

To combine information on uncertainties from all components: the model discrepancy, the benchmark experiment uncertainty, and uncertainty from uncalibrated cross-sections, the model discrepancy was also randomized and added to the three hundred results. The covariance and correlation matrices were then computed analogously to Eq. 2.23. The resulting covariance and correlation matrices are presented in Figs. 23 and 24. The abbreviated names of experiments are used; for example, HEU-SOL-THERM-028-011 is designated as HST-028-011.

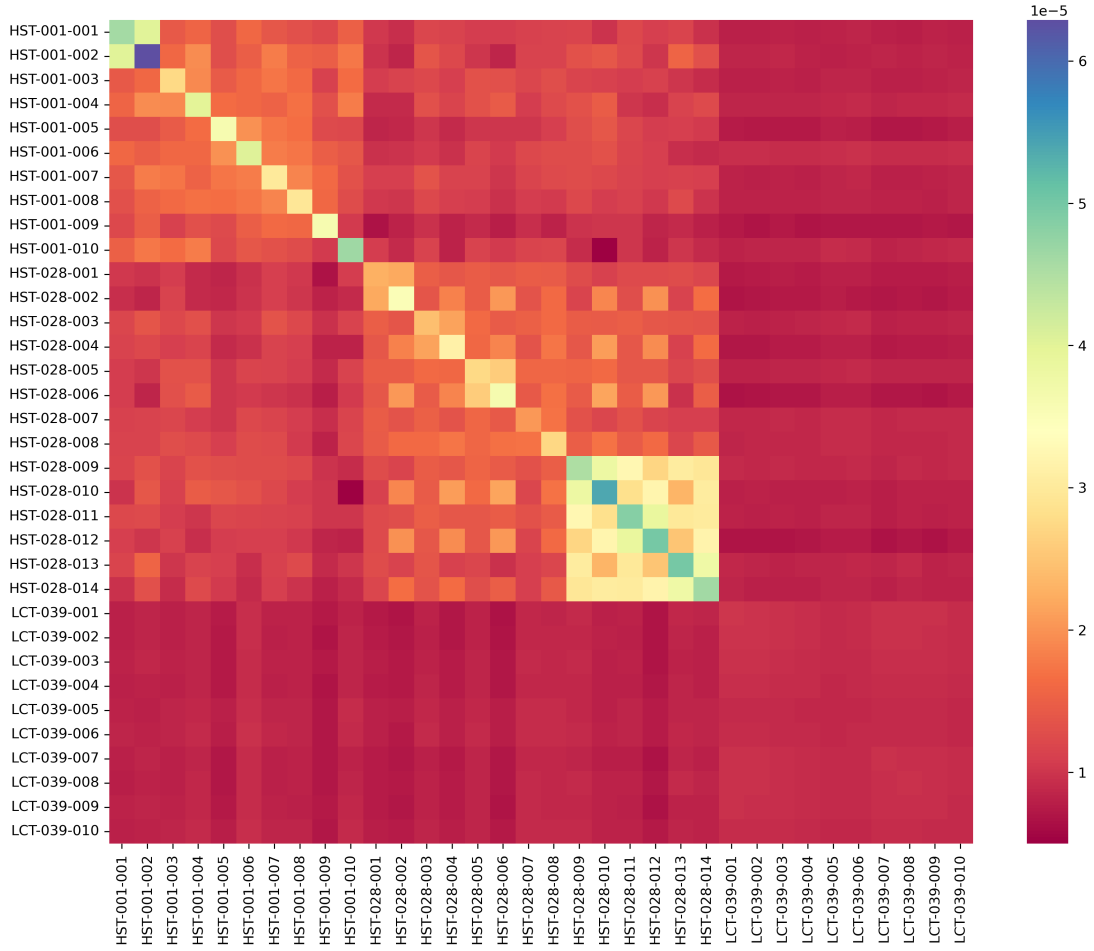

Figure 23: Covariance matrix of the HEU-SOL-THERM-001, HEU-SOL-THERM-028, and LEU-COMP-THERM-039 experiments.

It is visible on the correlation plot that the LEU-COMP-THERM experiments have very large correlations within their groups. It is also notable that despite there being no correlated systematic uncertainties between different experimental series, there are still correlations present between them. Those correlations are due to uncalibrated cross-sections' correlated errors.

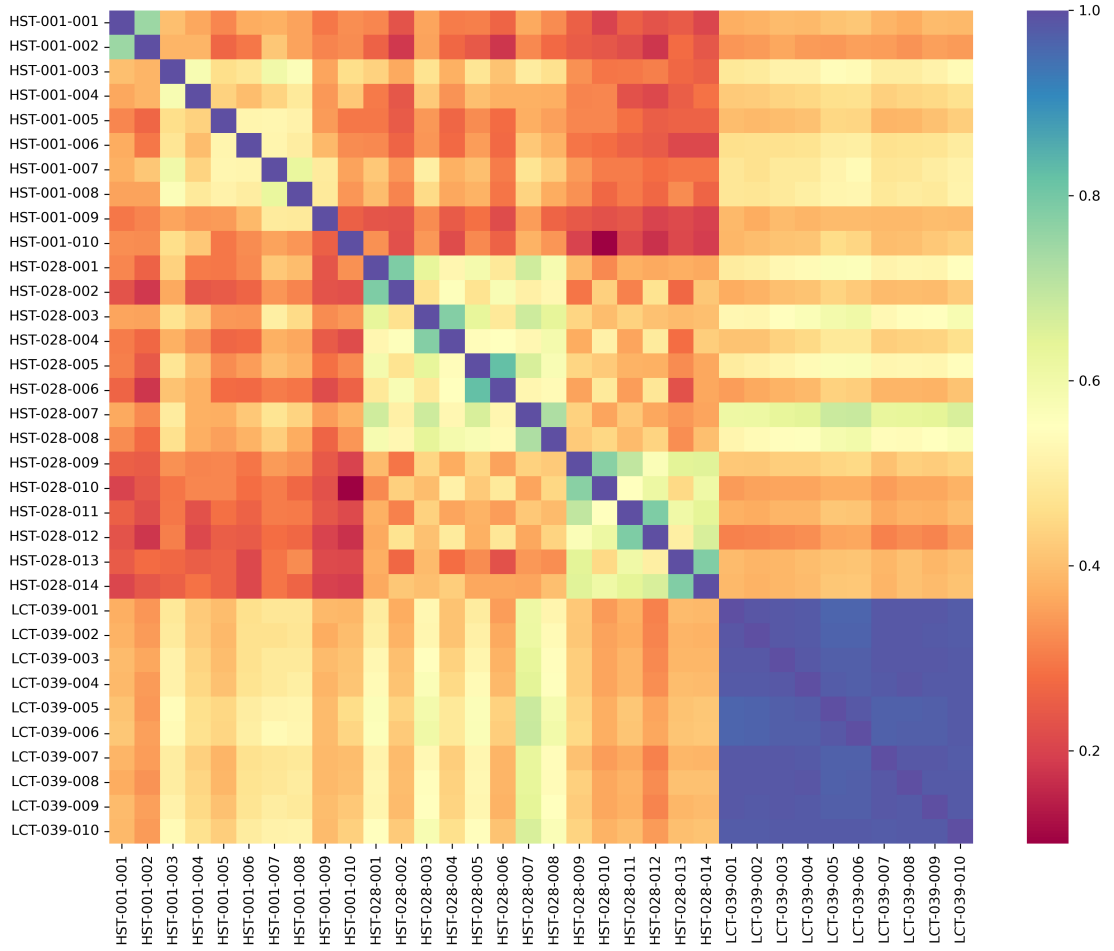

Figure 24: Correlation matrix of the HEU-SOL-THERM-001, HEU-SOL-THERM-028, and LEU-COMP-THERM-039 experiments.

5.4 Algorithm settings

Just as in Chapter 4, the only notable adjustable settings for the MOCABA algorithm is the number of samples generated, as shown in Eq. 2.20 and the transformation function in case that prior k_{eff} values are non-normal. Based on pre-calculations with MOCABA using linear TSUNAMI-derived sensitivity-based models, it was decided that 2,000 samples would be generated. The prior k_{eff} values calculated with SCALE CSAS5 passed the normalcy test, so the transformation was not required. The direct perturbation sensitivity validation (see Chapter 3.4) failed in the case of the systems HEU-SOL-THERM-001, HEU-SOL-THERM-028, and LEU-COMP-THERM-039, but the calculated sensitivities could still be used as the

basis for a metamodel used for the sole purpose of calculating the Monte Carlo uncertainty. This failure also disables the possibility of conducting the GLLS calculations and comparing the results with MOCABA.

5.5 Synthetic experiments study

5.5.1 Creation of good quality synthetic experiments and their application

The larger number of calibrated parameters and assimilated experiment requires a slightly different approach to the result presentation than the one applied in Section 4. There is no point showing 1904 calibrated cross-sections without knowing which were calibrated well and which were probably overfitted. To achieve this, we first need to conduct synthetic experiments. Fig. 25 shows the prior and posterior k_{eff} values after assimilation of synthetic experiments. The synthetic experiments were generated using the 56-MG SCALE SAMPLER library designated as "Sample1".

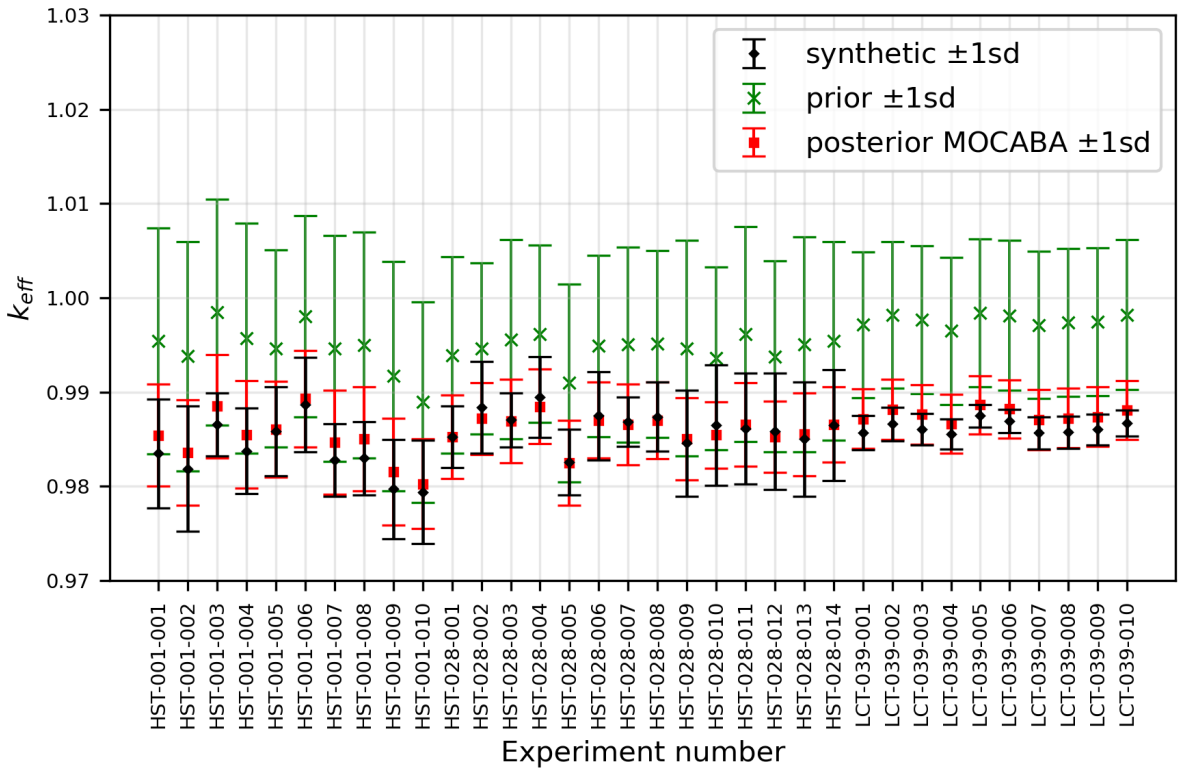

Figure 25: Comparison of k_{eff} results for prior simulation, posterior simulation, and synthetic experiment.

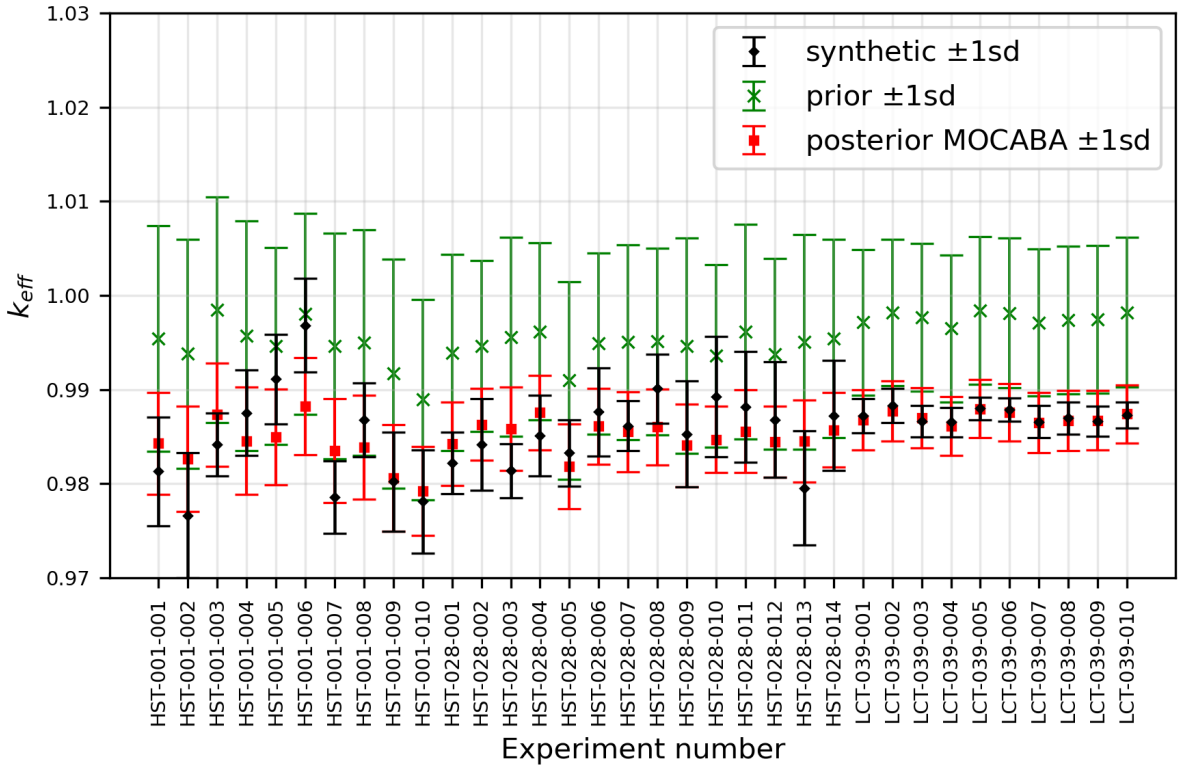

Figure 26: Comparison of k_{eff} results for prior simulation, posterior simulation, and synthetic experiment with perturbed values.

In Fig. 25, the agreement between the prior and posterior benchmark k_{eff} values is excellent, but this set of synthetic experiments is a little unrealistic. Notice that if we created a continuous curve from prior values and then separately did the same for experimental values, then the curves would look almost as if they differed by a free constant. Experimental measurements exhibit significantly greater levels of complexity and noise. To make the synthetic experiments look more like real experiments, we need to additionally perturb them by considering the experimental uncertainties - geometrical, isotopic, etc. The comparison between prior and posterior can then look as shown in Fig. 26. The posterior k_{eff} values don't differ by much, even though it is visible that some synthetic values are significantly perturbed in some cases. Such a result is expected and is evidence of the robustness of the Bayesian algorithms.

5.5.2 Comparison of synthetic parameters with the calibration results

Now, we can investigate how the posterior cross-sections look in relation to synthetic cross-sections. We shall start with the most significant contributor to the k_{eff} uncertainty, the U-235(chi) parameter. The calibration results are presented in Fig. 27. It is clearly visible in Fig. 27 that for most of the energy groups, the posterior U-235(chi) is closer to the synthetic U-235(chi), so in this instance, the calibration was successful. The only exceptions are for the two fastest energy groups. This is likely due to the larger groups having a low influence on k_{eff} of assimilated synthetic experiments and these two parameters being partially anti-correlated to the parameters from groups 5-32. The posterior relative uncertainty was somewhat reduced.

The second largest contributor, the nubar parameter, will be investigated. The calibration results are presented in Fig. 28.

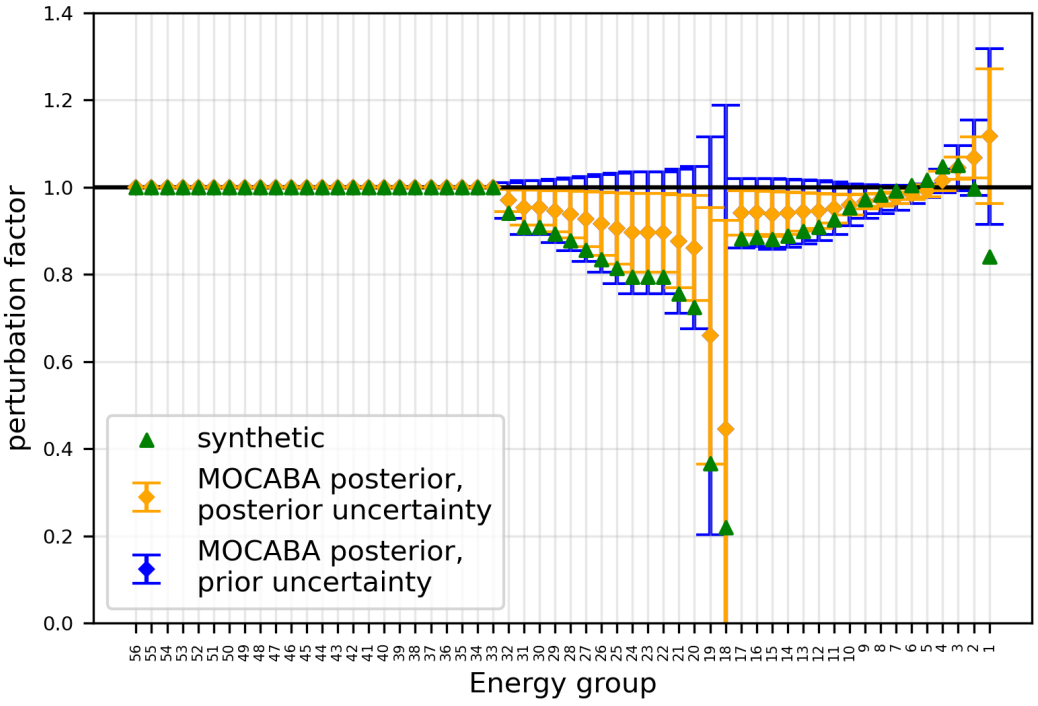

Figure 27: Comparison of posterior U-235(chi) parameters with synthetic U-235(chi) values along with a comparison of corresponding prior and posterior uncertainties.

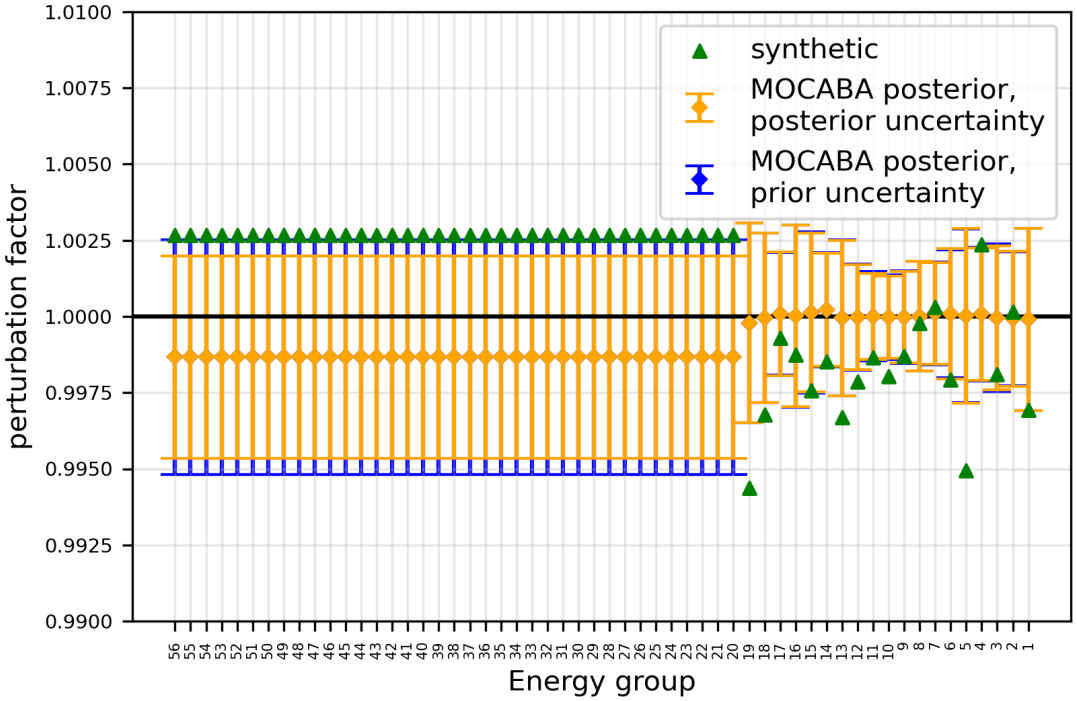

Figure 28: Comparison of posterior U-235(nubar) parameters with synthetic nubar parameter values along with a comparison of corresponding prior and posterior uncertainties.

The results visible in Fig. 28 are overfitted. There was a slight reduction in uncertainty for groups 20-56, but the posterior values moved away from the synthetic one. The calibration of the nubar parameters was therefore unsuccessful.

The third largest contributor to the k_{eff} uncertainty depends on the experiment. For the low enriched uranium (LEU-COMP-THERM) experiments, it is U-238(n, n') reaction. The calibration results are presented in Fig. 29. The calibration of the U-238(n, n') cross-sections was mainly successful. Nearly all of the posterior cross-sections are closer to the synthetic ones. The exception to that are cross-section 10-15, which moved in the opposite direction of the synthetic cross-section values. However, the uncertainties for energy group 10-15 did not change, and the shift was small.

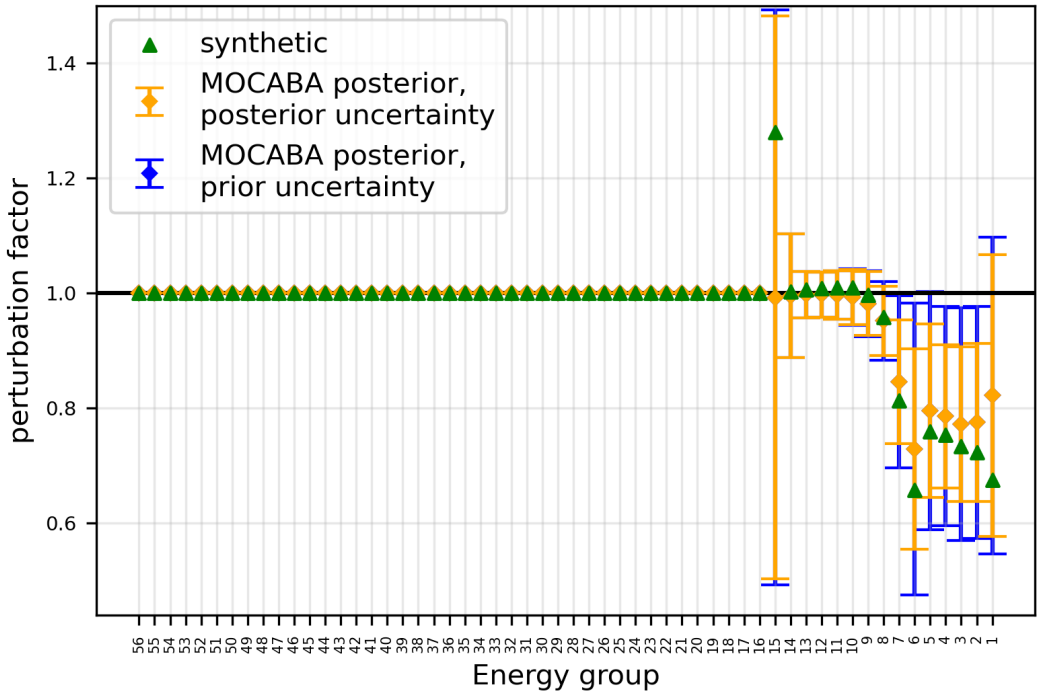

Figure 29: Comparison of posterior U-238(n, n') cross-sections with synthetic U-238(n, n') values along with a comparison of corresponding prior and posterior uncertainties.

Next, the synthetic calibration results will be presented for the U-235(n, gamma) reaction in Figs. 30 and 31. The results must be presented on two figures due to the much lower relative uncertainty of the cross-sections in the thermal region. The posterior cross-sections are overfitted for the thermal neutron energy range. For the fast range, the cross-sections shifted in the correct direction, but not enough to know whether the shift resulted from overfitting or correct calibration.

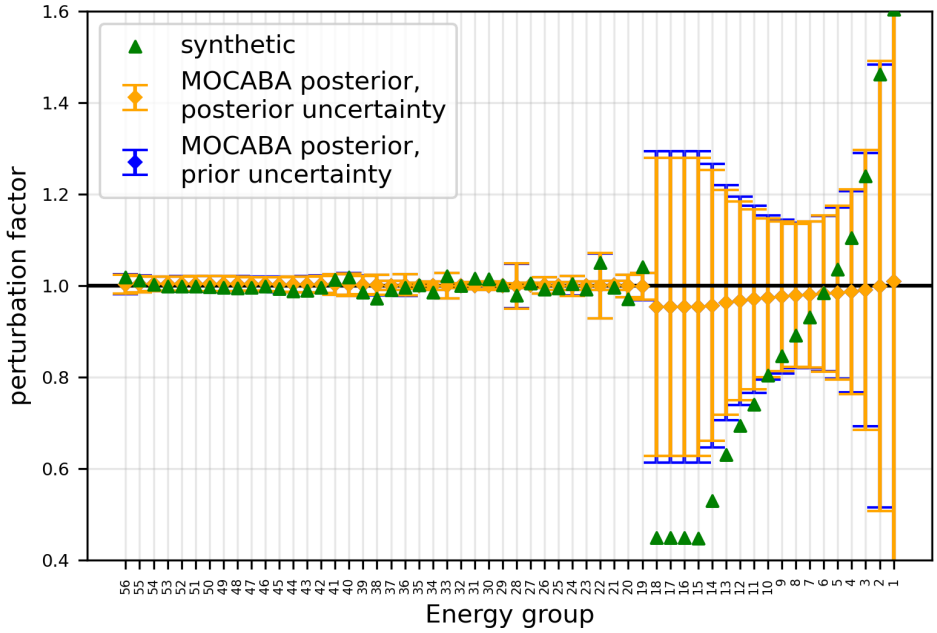

Figure 30: Comparison of posterior U-235(n, gamma) cross-sections with synthetic U-235(n, gamma) values along with a comparison of corresponding prior and posterior uncertainties.

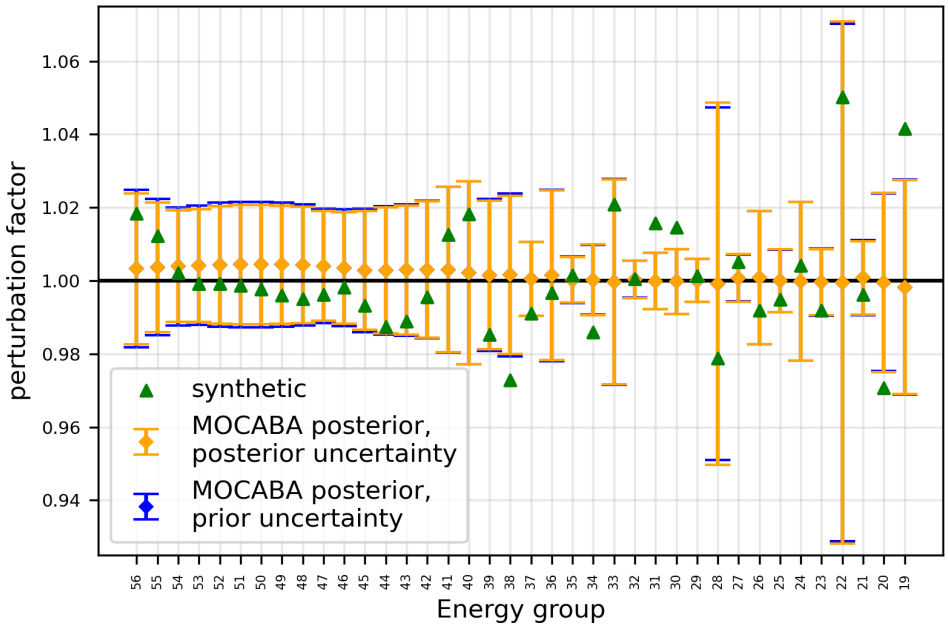

Figure 31: Comparison of thermal posterior U-235(n, gamma) cross-sections with synthetic thermal U-235(n, gamma) values along with a comparison of corresponding prior and posterior uncertainties.

So far, only the U-235(chi) and U-238(n, n') parameters were shown to have the potential to be calibrated correctly (i.e., not overfitted), and these were the 1st and 3rd largest contributors to the k_{eff} uncertainties. The lower the contribution to the uncertainty, the lower the chance of a cross-section to be calibrated successfully. The U-235(n, gamma) already had a much lower contribution to the k_{eff} uncertainties than the U-235(chi) and U-238(n, n'). One more reaction will be analysed. If it is also proven to be overfitted in the current calibration, then all the remaining ones will also be assumed to be overfitted. We can see in Fig. 32 that the cross-sections either stayed in place or shifted very little, with no tendency to move more often in the direction of the synthetic values than away. The U-238(n, gamma) cross-sections are therefore concluded to be calibrated unsuccessfully.

It has been established that the only parameters whose posterior values move in the direction of their true values are U-235(chi) and U-238(n, n'). For the rest, if they shift towards their true value, it is by chance. The substantial reduction of the posterior uncertainty in the k_{eff} is due to many cross-sections' uncertainty being successfully reduced, despite being overfitted. Such an outcome will lead to the calculated k_{eff} values closer to the experimental ones and with lower uncertainties but will likely negatively influence other integral parameters. For example, if fission cross-sections are overfitted, then the precision of fuel depletion calculations will be negatively impacted despite more accurate k_{eff} prediction. It is, therefore, desirable that either all or the vast majority of posterior cross-sections move in the direction of their true values, not just that their uncertainty gets reduced.

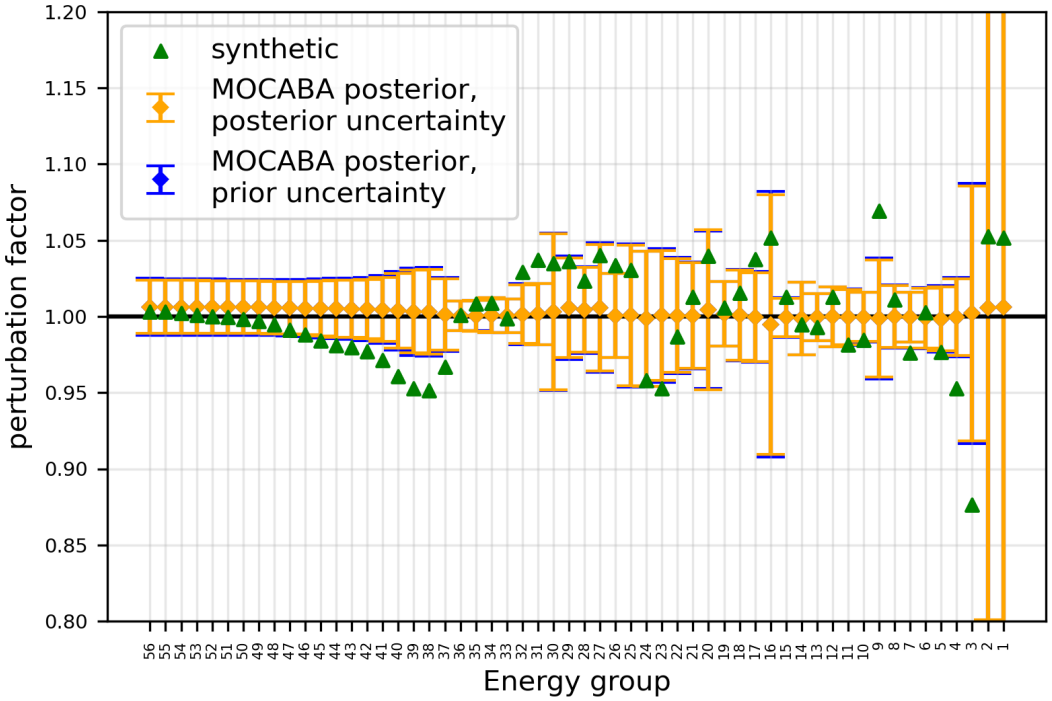

Figure 32: Comparison of posterior U-238(n, gamma) cross-sections with synthetic U-238(n, gamma) values along with a comparison of corresponding prior and posterior uncertainties.

5.5.3 Study of the influence of inclusion of experimental uncertainty correlations

Researchers attempting Bayesian calibration usually take into account the experimental uncertainties and the correlations between the experimental errors but fail to consider the correlations from uncalibrated parameters (examples: [25], [33]). In this work, it will be shown that such an approach might lead to a serious underestimation of the uncertainty of the calibrated parameters. To illustrate how the neglected correlations from uncalibrated parameters can influence the results, we will analyse a toy example. This example is introduced because it is simple and can easily illustrate how the treatment of uncalibrated input parameters affects the results. After its presentation, the influence of uncalibrated cross-sections' treatment will be investigated.

Consider the three following parameters described by normal distributions with specified means and uncertainties:

$$\begin{aligned} a &= 50 \pm 5, \\ b &= 40 \pm 7, \\ c &= 15 \pm 3. \end{aligned} \tag{5.1}$$

An experimenter builds three experiments with measurable quantities x_1, x_2, x_3. The measured quantities are related to the parameters as follows:

$$\begin{aligned} x_1 &= a + 2 * b + 3 * c, \\ x_2 &= 2 * a + 2 * b + 2 * c, \\ x_3 &= 4 * a + b + c. \end{aligned} \tag{5.2}$$

The quantity c clearly has the lowest influence on the results, having the lowest value. The experimenter decides that he wants to calibrate a and b since they have the largest impact on uncertainty. The true values of the parameters unknown to the experimenter are 43, 36, and 12 for a, b, and c, respectively. The measurement device used to measure the x_1, x_2, x_3 integral parameters has 0.1 uncertainty. The measurement errors are uncorrelated. The measurements yield the following values: 151.2, 181.9, 219.7 (the true experimental values, unknown to the experimenter, are 151, 182, 220). The experimenter neglects the influence of the c parameter on experimental uncertainties, so his experimental covariance matrix C^I_{mm} has diagonal elements equal to 0.1^2 and off-diagonal elements equal to 0. He applies the MOCABA algorithm and obtains the posterior values:

$$\begin{aligned} a^I &= 43.26 \pm 0.032, \\ b^I &= 32.033 \pm 0.0486. \end{aligned} \tag{5.3}$$

Both of the posterior mean values are way further than 5 standard deviations away from their true values, even though the posterior values of x_1, x_2, x_3 got much closer to the experimental measurement yielding 152.33, 180.57, 220.08 compared to their priors of 175, 210, 255. This is a clear

example of overfitting, with the added unacceptable problem of underestimated posterior uncertainties.

What if the experimenter included the uncertainty and correlations coming from c in the experimental values? By applying a Monte Carlo sampling, the covariance now takes the form:

$$C_{mm}^{II} = \begin{bmatrix} 92.18 & 61.41 & 30.72 \\ 61.41 & 40.92 & 20.46 \\ 30.72 & 20.46 & 10.25 \end{bmatrix}. \tag{5.4}$$

The experimenter applies the MOCABA algorithm again and now obtains the posterior values of:

$$\begin{aligned} a^{II} &= 42.92 \pm 0.04, \\ b^{II} &= 35.80 \pm 0.22. \end{aligned} \tag{5.5}$$

Both of the posterior mean values lie within 3 standard deviations of their true values, which is the desired result.

Another component that cannot be omitted is the correlations between uncertainties. Consider the same scenario as in formula 5.4, but with off-diagonal elements equal to zero. We would get the covariance matrix:

$$C_{mm}^{III} = \begin{bmatrix} 92.18 & 0 & 0 \\ 0 & 40.92 & 0 \\ 0 & 0 & 10.25 \end{bmatrix}. \tag{5.6}$$

From such a covariance, we would arrive at the following results:

$$\begin{aligned} a^{III} &= 43.03 \pm 1.19, \\ b^{III} &= 33.13 \pm 3.06. \end{aligned} \tag{5.7}$$

Even though the true values of the parameters are within three standard deviations of the posterior mean values, the uncertainty is significantly increased. Also, one parameter lies much further away from its true value than if correlations were included. However, the example does not prove

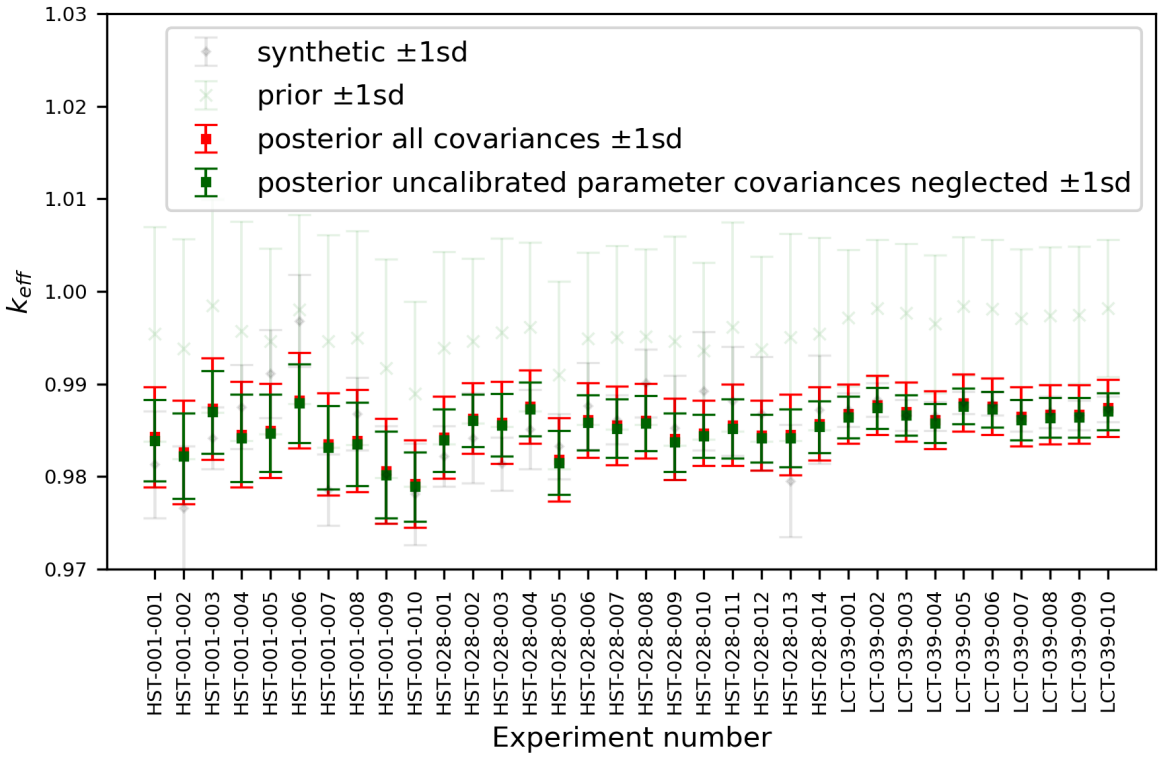

Figure 33: Comparison of posterior k_{eff} values for cases where uncalibrated parameter uncertainty was included and neglected.

that the neglect of correlations between experiments will lead to less successfully calibrated parameters. In other cases, it might lead to the underestimation of posterior uncertainty, just as it was shown in Section 4.6.2. The effect of neglecting the influence of the uncalibrated parameters has been analysed for the same synthetic experiments as in Section 5.5.1. Fig. 33 shows the comparison between the posterior with the influence of the uncalibrated cross-sections included and the case where they were neglected. The posterior uncertainty for both cases is obtained by applying Eq. 2.19 and then adding the uncertainty from uncalibrated parameters calculated with the Monte Carlo sampling. The synthetic experiment and the prior values were made semi-transparent for clarity, but they are the same as in Fig. 26. We can see that the posterior values are very similar, but the posterior covariance is visibly different. The average posterior uncertainty in simulated k_{eff} of the assimilated experiments is 421 pcm

when uncalibrated parameter influence is included and 316 pcm when it is neglected. It is a substantial difference.

Figs. 34 and 35 show how neglecting covariances influenced the posterior cross sections for the U-235(chi) and nubar parameters. We can see that in both of the figures, the posterior uncertainty is slightly lower for the case where uncalibrated parameters' influence is neglected. In Fig. 34, the posterior values are slightly shifted towards synthetic values, while in Fig. 35, they are shifted away from the synthetic parameters, although by a minuscule amount. No conclusions can be drawn from these posterior parameter shifts. The most important observation is the combined influence of all posterior parameter uncertainty underpredictions in k_{eff} of 24.9 % discussed below in Fig. 33. This observation further solidifies the conclusion of the necessity of inclusion of uncalibrated parameters' variances and covariances in the experimental data.

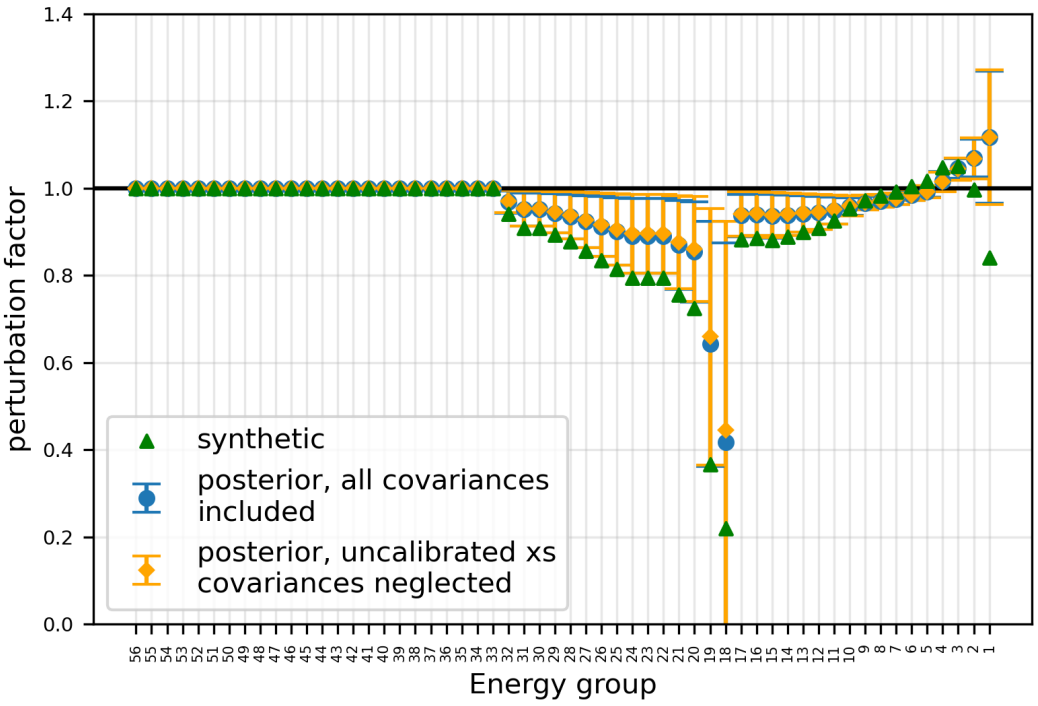

Figure 34: Posterior mean U-235(chi) values after real experiment assimilation, with prior uncertainty presented alongside posterior uncertainty to illustrate the uncertainty reduction.

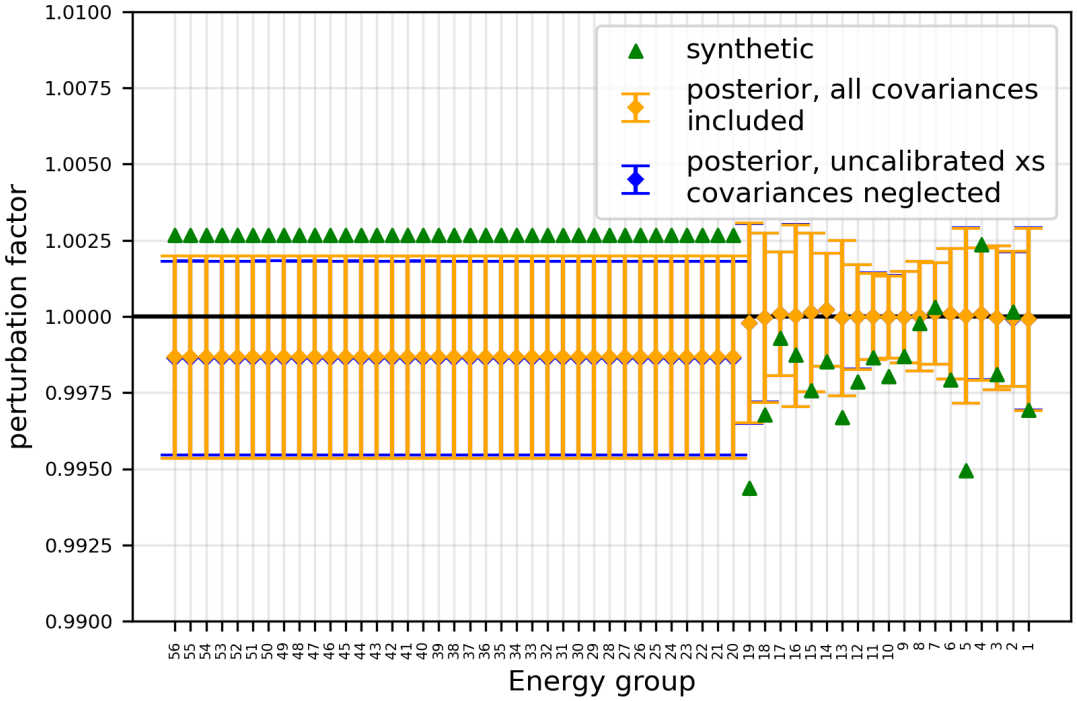

Figure 35: Posterior mean U-238(n, n') values after real experiment assimilation, with prior uncertainty presented alongside posterior uncertainty to illustrate the uncertainty reduction.

5.6 Results using real experiments

Based on the conclusions from Section 5.5, the correct approach to calibrating real experiments would be to limit the calibration to the U-235(chi) and U-238(n, n') parameters while adding the uncertainty from the remaining cross-sections to the experimental uncertainties. However, such an approach would require the repeat of the expenditure of large computational resources - namely, the generation of 2000 cross-section libraries and calculating k_{eff} of the experiments chosen for assimilation. The already finished MOCABA computations are good enough to let us estimate how far the real U-235(chi) and U-238(n,n') parameters are from the values currently used in the 56-MG cross-section library and whether the true values are smaller or larger. There is no possibility to extract just these well-calibrated perturbation factors for later use in other calculations. That

is due to the fact that as a result of the MOCABA procedure, there are now non-zero covariances between these parameters and all the others. So either all should be extracted for later use, or none of them.

The results of the prior and posterior calculations are shown for the experimental k_{eff} values in Fig. 36. It is visible that the currently available best estimates of the U-235(chi) values are lower than their real values, while the U-238(n, n') the best estimations are above their real values.Figs. 37 and 38 show the posterior perturbation factors for U-235(chi) and U-238(n,n') reactions.

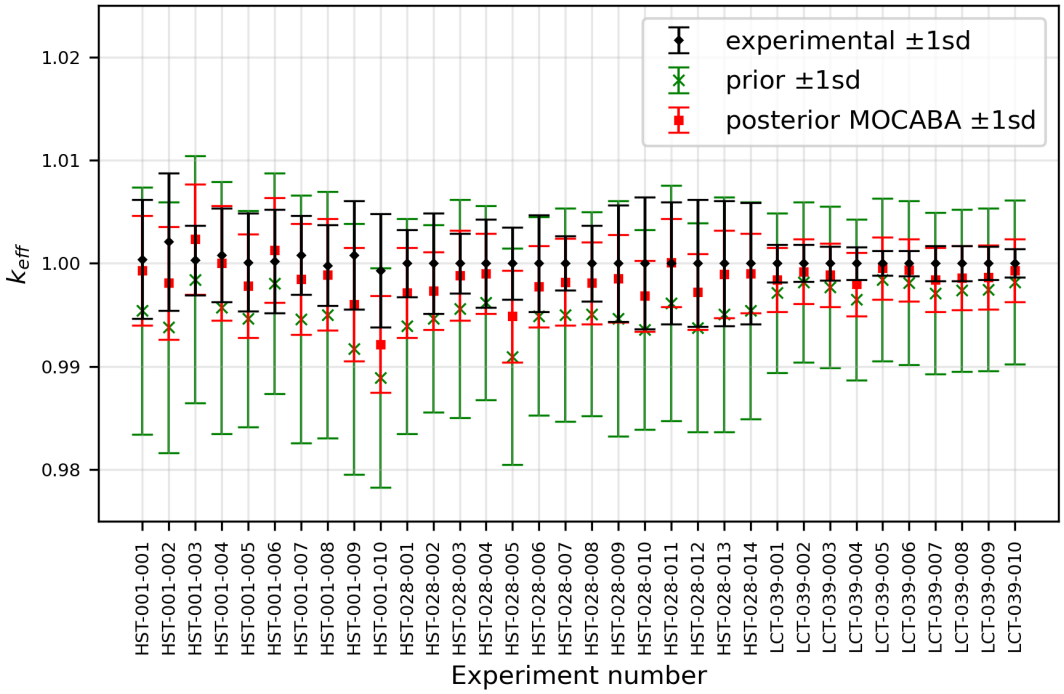

Figure 36: Comparison of k_{eff} results for prior simulation, posterior simulation, and real experiment.

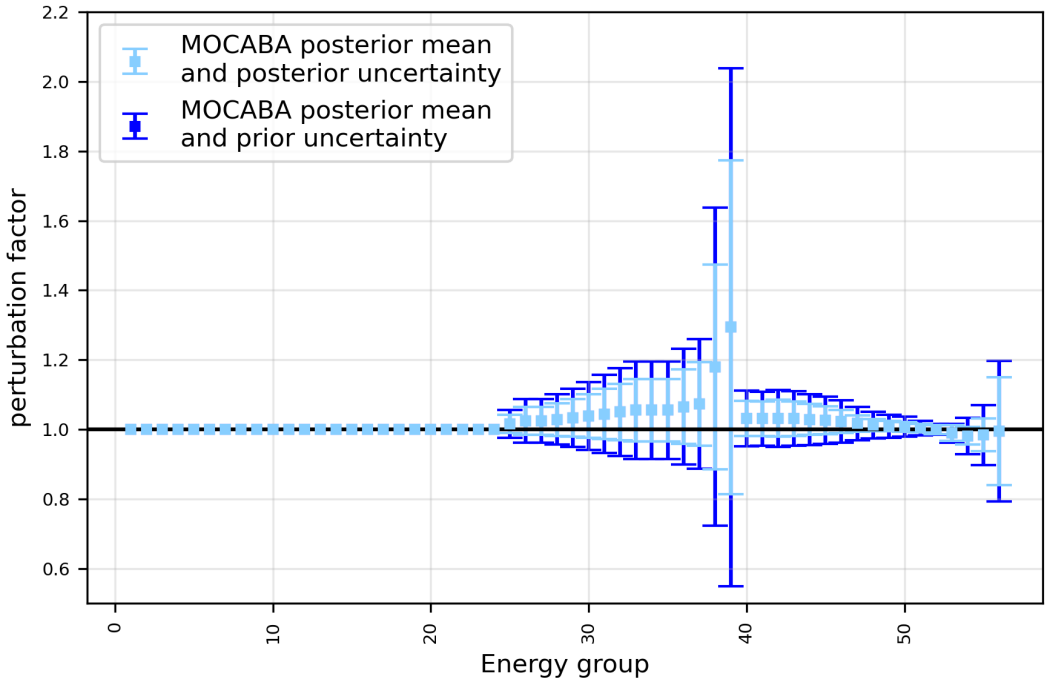

Figure 37: Posterior mean U-235(chi) values after real experiment assimilation, with prior uncertainty presented alongside posterior uncertainty to illustrate the uncertainty reduction.

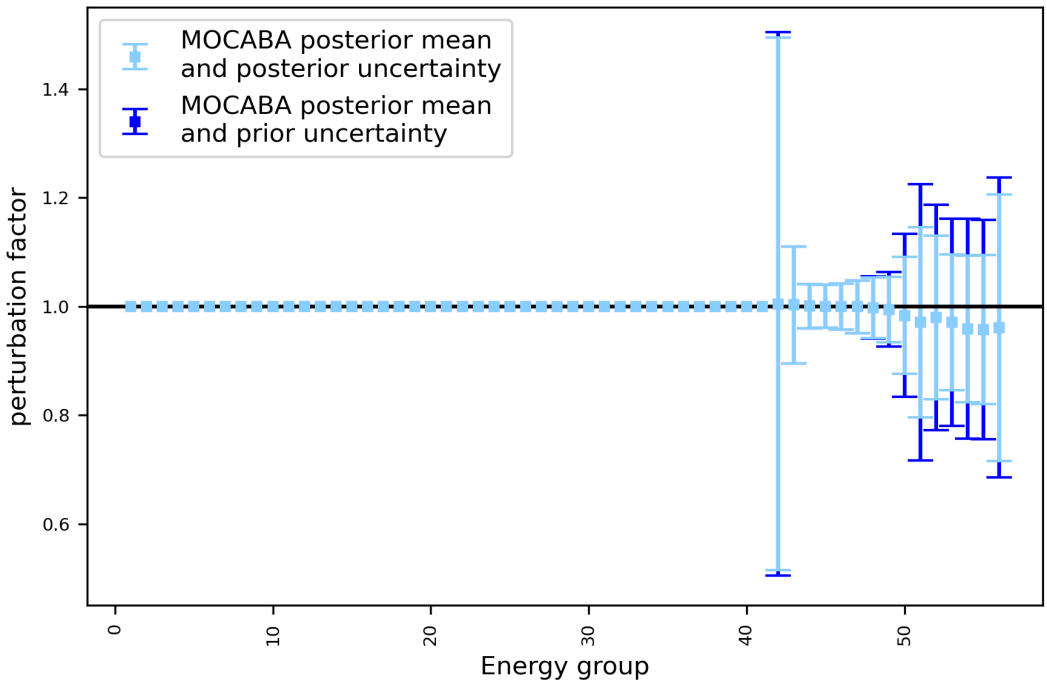

Figure 38: Posterior mean U-238(n, n') values after real experiment assimilation, with prior uncertainty presented alongside posterior uncertainty to illustrate the uncertainty reduction.

Given the conclusions of the synthetic parameter study in Section 5.5, where it was established that only the U-235(chi) and U-238(n, n') parameters are fully successfully calibrated (both their uncertainty is reduced and their posterior values get closer to their real values), it was decided not to conduct further validation exercises. If the synthetic study concluded that all or nearly all cross-sections are successfully calibrated, then further validation should be conducted, just as in Section 4.6.1. Ideally, integral parameters other than just k_{eff} should be used for validation. A non-exhaustive list of examples of such integral parameters are reactor power distribution measurements, fuel depletion, boron letdown curve in a pressurized water reactor, and neutron energy distribution at specified points in critical systems.

5.7 Summary

In this chapter, the calibration of 1,904 neutron cross-sections with the MOCABA algorithm is attempted. It was found by using an enhanced (in comparison with Chapter 4.6) synthetic experiment validation procedure that only the cross-sections contributing the most to k_{eff} uncertainty are successfully calibrated. It was concluded that only the cross-sections that can be successfully calibrated should undergo calibration, while the uncertainty from the rest should be included in the experimental covariance matrix. If a cross-section is chosen for calibration, all the cross-sections correlated with it must also be calibrated. No reliable mathematical treatment could be applied to find the posterior covariance between calibrated and uncalibrated cross-sections. An accelerator-driven system could increase the sensitivity of k_{eff} for some cross-sections, like for the fastest (n, gamma) or fission energy groups, to make their calibration possible. This might be too difficult for other cross-sections, such as (n, 2n'). The case for including the uncertainty from uncalibrated cross-sections was made using a toy example and a neutron cross-section calibration problem.

6 Outline of best practices for neutron cross-section calibration and conclusions

The findings gathered from the research described in Sections 4 and 5 allow for the creation of a best-practices algorithm for reliable calibration of neutron cross-sections. Successful calibration not only reduces the cross-section uncertainties but also results in the means of their posterior distributions being closer to the true cross-section values than their prior means. The summary of these findings is presented in the next three paragraphs.

It is not necessary to use the rigorous but computationally expensive SMC-ABC to calibrate neutron cross-sections through the assimilation of measurements of integral parameters, as was shown in Section 4.5. The posterior means and standard deviations look almost the same and are within the Monte Carlo uncertainty with each other. It is necessary, however, to include the non-linearity of responses of k_{eff} to cross-section changes by using MOCABA, not GLLS. The non-linear behavior is not present when small changes in cross-section take place, but it does happen when its values are far away from the prior mean, as discussed in Chapter 4.5. The GLLS procedure also suffers from one major flaw. The method for calculating sensitivities, which is based on adjoint calculations, is not universally reliable, as it is mentioned in Chapter 3.4. Even if the total sensitivities for isotopes generated by TSUNAMI pass the direct perturbation test in CSAS5, it is not a guarantee that the sensitivities of individual cross-sections are correct. Furthermore, the sensitivity validation procedure is done by manually modifying CSAS5 inputs, so it is prone to human error. Another important finding is related to MOCABA. It is found that even a minor skew in the prior distribution from the normal one will result in noticeable differences in posterior k_{eff}. It is, therefore, essential to run a reliable normalcy test, not only visually gauge if the prior distribution of the assimilated parameter looks normal. The application of the rigorous

SMC-ABC to neutron cross-section calibration and comparison of it with MOCABA and GLLS is novel.

The synthetic experiments validation has the ability to verify whether the posterior cross-section means are closer to their true values or not. It was shown both in Sections 4.6 and 5.5.1 that while the cross-section uncertainties may be reduced during Bayesian calibration, it is not always guaranteed that they will move towards their true values. To make sure that we obtain the posteriors with means closer to their real values, a diverse set of experiments backed by synthetic experiment validation is required. It is likely that for some cross-sections, experiments from other sources than ICSBEP are needed. For example, k_{eff} has low sensitivity to the fastest groups because of the relatively low number of generated neutrons in that range. It might be the case that accelerated-driven experiments could be used for that purpose. The accelerator could increase the relative number of neutrons in specific ranges, thus increasing the k_{eff} sensitivity to corresponding cross-sections. The synthetic experiment validation is novel in the context of nuclear engineering inverse problems. It is an improvement on currently used validation procedures, which proves part of the thesis statement presented in Chapter 1.4.

It is not possible to calibrate all cross-sections that influence the integral parameters of experiments. While accelerated-driven systems may be a solution for some of the cross-sections' successful calibration, the others' influence is too low for any remedy. An example of that is the U-235(n, 2n') reaction. In this case, the uncertainty from this cross-section must be included in the experimental covariance matrix. Its neglect will, in the best case, slightly underestimate the posterior uncertainty of the calibrated cross-sections. In the worst case, it will underestimate this uncertainty so much that the calibrated cross-section value will be more than 3 standard deviations away from the true value. While it is unlikely that this would happen during cross-section calibration, it was shown in the toy example

in Section 5.5.3, that it is a possible outcome in Bayesian calibration problems. The practice of some authors in the field of Bayesian statistics of neglecting the uncertainties of uncalibrated input parameters is incorrect. The rigorous treatment of the uncalibrated input model parameters presented in 5.5.3 is novel. It provides improved results, which proves part of the thesis statement presented in Chapter 1.4. In conjunction with the improved validation with synthetic experiments, the entire thesis statement is proven.

All the findings above are combined and presented in Algorithm 4 and 5, which shows how to conduct a successful calibration of neutron cross-sections.

Algorithm 4 Step-by-step instruction on how to successfully calibrate neutron cross-sections, Part 1

1. Make an initial decision on which cross-sections will be calibrated. The higher the uncertainty contribution of a cross-section to accessible experiments, the easier it is to calibrate it successfully. All cross-sections whose uncertainties are correlated with a chosen cross-section must also be calibrated. There is no reliable mathematical treatment that can compute the posterior correlation value when one of the initially correlated parameters was calibrated and another was not, as discussed in Section 4.

2. Choose a set of experiments for assimilation. Create models calculating the measured integral parameters.

3. Start the MOCABA algorithm. If possible, first make a few dozen runs on coarser, for example, linear models to estimate how many libraries are needed to achieve desirably low Monte Carlo error in posterior means. Create a sample of N neutron cross-section libraries and run all models for every sampled library.

4. Calculate the uncertainties and their correlations (an error covariance matrix) for all experimental integral quantities with the Monte Carlo method. Include the geometrical and material sources, as well as the uncalibrated parameters' contribution and model discrepancy error. Make calculations for enough samples to have a desirably low Monte Carlo uncertainty in calculated variances and covariances.

5. Generate a sample of synthetic cross-sections. Use them to generate synthetic experiments. Perturb the generated synthetic integral quantity values in accordance with the experimental covariance matrix described in step 4.

Algorithm 5 Step-by-step instruction on how to successfully calibrate neutron cross-sections, Part 2

6. Check if the prior distributions of the modeled integral parameters form normal distributions. If they don't, fit them into the Johnson distribution and transform them into normal ones using the standard Johnson-to-normal transformation. Assimilate the synthetic experiments with the MOCABA algorithm. Check if all of the posterior cross-sections are closer to synthetic cross-sections. If they are not, find additional experiments for assimilation, calculate their measured integral quantities with libraries generated in step 3, compute the uncertainty and correlations by using the libraries generated in step 4, compute the synthetic integral parameter values with library generated in step 5, and check if all cross-sections are closer to their synthetic values. Repeat step 6 until all cross-sections are closer to their synthetic values. Due to some cross-sections having a very low influence on some integral parameters, like the fastest neutron group chi parameter, accelerator-driven experiments might have to be designed and applied.

7. Check if any synthetic values are more than four posterior standard deviations away from the posterior mean values. If so, some uncertainties were likely erroneously calculated. If more than 1 in 400 is more than three standard deviations away, then the same applies. In such a case, review the step 4 uncertainty calculations.

8. Once the calibration using synthetic experiments is proven to be successful, assimilate real experiments.

9. Validate the posterior cross-sections generated in step 8 with the experiments not used during assimilation. Use as many experiments as possible and check as many integral parameters as possible. The calculated integral parameters must always be within three standard deviations away from experimental values (more precisely 399 out of 400 within three standard deviations).

10. Once the validation is successful, the new library will consist of the updated cross-sections and the uncalibrated cross-sections. The covariance library will be updated for the calibrated cross-sections. Every calibrated neutron cross-section will have a non-zero correlation to every other since they were calibrated together. After that, the new library is ready for deployment in engineering applications.

The cross-section Bayesian calibration has a great application potential not only for the reduction of the uncertainty of the integral experiment parameters like k_{eff}. It might be possible to use them for calibration of the continuous energy neutron cross-section libraries. The results of multigroup calibration provide information on the integral average of neutron cross-sections in specific energy ranges and its uncertainty, which might be possible to incorporate in continuous energy library generation as a constraint. The author of this thesis plans to investigate this possibility in the future.

The algorithms 4 and 5 can be slightly modified and applied to other Bayesian calibration problems (for example with the use of SMC-ABC if non-normal posterior distributions are expected). The Bayesian calibration algorithms see any mathematical models as black boxes, which is why the same statistical tools are applied in fields even as distant as biology and geology. As the computational power of computers and clusters grows much quicker than the accuracy of direct measurement devices, the computationally demanding indirect measurements, which is what Bayesian calibration essentially is, will likely become more and more popular. It is vital that researchers applying Bayesian calibration procedures do that in a standardized, rigorous way. This thesis helps establish these standards, with a focus on the application of Bayesian calibration of neutron cross-sections.

References

[1] Nuclear Energy Agency. Meeting Climate Change Targets: The Role of Nuclear Energy. *OECD Publishing*, 2022.

[2] United Nations Framework Convention on Climate Change. Paris agreement, 2015.

[3] P Anzieu, R Stainsby, K Mikityuk, et al. Gas-cooled fast reactor (GFR): overview and perspectives. *Paris, France 9-10 September 2009*, 127, 2009.

[4] Alessandro Alemberti, Valery Smirnov, Craig F Smith, and Minoru Takahashi. Overview of lead-cooled fast reactor activities. *Progress in Nuclear Energy*, 77:300–307, 2014.

[5] Jérôme Serp, Michel Allibert, Ondřej Beneš, Sylvie Delpech, Olga Feynberg, Véronique Ghetta, Daniel Heuer, David Holcomb, Victor Ignatiev, Jan Leen Kloosterman, et al. The molten salt reactor (MSR) in generation IV: overview and perspectives. *Progress in Nuclear Energy*, 77:308–319, 2014.

[6] Kazumi Aoto, Philippe Dufour, Yang Hongyi, Jean Paul Glatz, Yeong-il Kim, Yury Ashurko, Robert Hill, and Nariaki Uto. A summary of sodium-cooled fast reactor development. *Progress in Nuclear Energy*, 77:247–265, 2014.

[7] Mohammad Mizanur Rahman, Ji Dongxu, Nusrat Jahan, Massimo Salvatores, and Jiyun Zhao. Design concepts of supercritical water-cooled reactor (SCWR) and nuclear marine vessel: A review. *Progress in Nuclear Energy*, 124:103320, 2020.

[8] Shohei Ueta, Jun Aihara, Kazuhiro Sawa, Atsushi Yasuda, Masaki Honda, and Noboru Furihata. Development of high temperature gas-

cooled reactor (HTGR) fuel in Japan. *Progress in Nuclear Energy*, 53(7):788–793, 2011.

[9] GIF. IV generation nuclear forum resources, 2023. Accessed: 13.09.2023.

[10] Ladislav Bělovskỳ, J Gadó, B Hatala, A Vasile, and G Wrochna. The ALLEGRO experimental gas cooled fast reactor project. In *International Conference on Fast Reactors and Related Fuel Cycles Next Generation Nuclear Systems for Sustainable Development, Yekaterinburg*, pages 26–29, 2017.

[11] Eleonora Skrzypek, Dominik Muszyński, Maciej Skrzypek, Piotr Darnowski, Janusz Malesa, Agnieszka Boettcher, and Mariusz P Dąbrowski. Pre-Conceptual Design of the Research High-Temperature Gas-Cooled Reactor TeResa for Non-Electrical Applications. *Energies*, 15(6):2084, 2022.

[12] GIF. IV generation nuclear forum IV generation systems outline, 2023. Accessed: 13.09.2023.

[13] Plompen A. *Accuracy of Measurements*. OECD/NEA, Paris (France), 2008.

[14] Romojaro, Pablo, Alfonso, Ciro, Fiorito, Luca, Cuesta-Matesanz, Alejandro, Guillamot, Juan Carlos, Hernandez-Solis, Augusto, Stankovskiy, Alexey, and Van den Eynde, Gert. Nuclear Data Uncertainty Analysis to Meet the Target Accuracy Requirements on the MYRRHA keff. *EPJ Web of Conf.*, 284:08012, 2023.

[15] Filip Osuský, Štefan Čerba, Jakub Lüley, Branislav Vrban, Ján Haščík, and Vladimír Nečas. On gas-cooled fast reactor designs – Nuclear data processing with sensitivity, uncertainty and similarity analyses. *Progress in Nuclear Energy*, 128:103450, 2020.

[16] MICHAEL F. L'ANNUNZIATA. 1 - NUCLEAR RADIATION, ITS INTERACTION WITH MATTER AND RADIOISOTOPE DECAY. In Michael F. L'Annunziata, editor, *Handbook of Radioactivity Analysis (Second Edition)*, pages 1–121. Academic Press, San Diego, second edition edition, 2003.

[17] Patrick Talou, T. Kawano, and P. Young. Covariance matrices for ENDF/B-VII 235,238 U and 239 Pu evaluated files in the fast energy range. *http://dx.doi.org/10.1051/ndata:07679*, 2008.

[18] Xu Wu, Ziyu Xie, Farah Alsafadi, and Tomasz Kozlowski. A comprehensive survey of inverse uncertainty quantification of physical model parameters in nuclear system thermal–hydraulics codes. *Nuclear Engineering and Design*, 384:111460, 2021.

[19] Xu Wu, Tomasz Kozlowski, Hadi Meidani, and Koroush Shirvan. Inverse uncertainty quantification using the modular bayesian approach based on gaussian process, part 1: Theory. *Nuclear Engineering and Design*, 335:339–355, 2018.

[20] *U.S. NRC, 2014. TRAC/RELAP Advanced Computational Engine (TRACE) V5.840 USER'S MANUAL Volume 1: Input Specification, US NRC.* Washington, DC, 2014.

[21] D Neykov, F Aydogan, L Hochreiter, H Utsuno, F Kasahara, E Sartori, and M Martin. NUPEC BWR Full-size Fine-mesh Bundle Test (BFBT) Benchmark: Volume I: Specifications. *OECD*, 6(7):1–132, 2006.

[22] Dan G Cacuci and Erkan Arslan. Reducing uncertainties via predictive modeling: FLICA4 calibration using BFBT benchmarks. *Nuclear Science and Engineering*, 176(3):339–349, 2014.

[23] Ph Fillion et al. FLICA4: Reference manual of modules and procedures. *User Guide Version*, 1, 2007.

[24] Paolo Mason. Approximate Bayesian Computation of the occurrence and size of defects in advanced gas-cooled nuclear reactor boilers. *Reliability Engineering & System Safety*, 146:21–25, 2016.

[25] Pieterjan, R., Tiernan, C., Christopher, M., Cooper, M. W. D., Sophie, B., Giovanni, P., Dong-Uk, K., Md Ali, M., Tonks, Wirth, M., Andersson, B., Ragnar, A. D., & Habib N. Calibration of the Diffusivity Predictions of Centipede Using Approximate Bayesian Computation and Applications in Nyx (Engineering Scale) and Xolotl-MARMOT (Meso-Scale) Simulations. *Osti*, 2021.

[26] Cody J Permann, Derek R Gaston, David Andrš, Robert W Carlsen, Fande Kong, Alexander D Lindsay, Jason M Miller, John W Peterson, Andrew E Slaughter, Roy H Stogner, et al. MOOSE: Enabling massively parallel multiphysics simulation. *SoftwareX*, 11:100430, 2020.

[27] Indranil Hazra, Mahesh D Pandey, and Noldainerick Manzana. Approximate Bayesian computation (ABC) method for estimating parameters of the gamma process using noisy data. *Reliability Engineering & System Safety*, 198:106780, 2020.

[28] Piotr Kopka and Anna Wawrzynczak. Framework for stochastic identification of atmospheric contamination source in an urban area. *Atmospheric environment*, 195:63–77, 2018.

[29] Piotr Kopka, Anna Wawrzynczak, and Mieczyslaw Borysiewicz. Application of the Approximate Bayesian Computation methods in the stochastic estimation of atmospheric contamination parameters for mobile sources. *Atmospheric Environment*, 145:201–212, 2016.

[30] William A. Wieselquist, Robert Alexander Lefebvre, and Matthew A. Jessee. SCALE Code System. Technical Report ORNL/TM-2005/39 Version 6.2.4, Oak Ridge National Laboratory, 4 2020.

[31] Christopher C Paige. Computer solution and perturbation analysis of generalized linear least squares problems. *Mathematics of Computation*, 33(145):171–183, 1979.

[32] Axel Hoefer, Oliver Buss, and Jens Christian Neuber. How confident can we be in confidence intervals for the computational bias obtained with the generalized linear least squares methodology?-a toy model analysis. In *Proceedings of the International Conference on Nuclear Criticality, ICNC*, 2011.

[33] A. Hoefer, O. Buss, M. Hennebach, M. Schmid, and D. Porsch. MOCABA: A general Monte Carlo–Bayes procedure for improved predictions of integral functions of nuclear data. *Annals of Nuclear Energy*, 77:514–521, 2015.

[34] RN Hwang. Topics in data adjustment theory and applications. Technical report, Argonne National Lab., IL (USA), 1988.

[35] T.G. Trucano, L.P. Swiler, T. Igusa, W.L. Oberkampf, and M. Pilch. Calibration, validation, and sensitivity analysis: What's what. *Reliability Engineering '&' System Safety*, 91(10):1331–1357, 2006. The Fourth International Conference on Sensitivity Analysis of Model Output (SAMO 2004).

[36] A. Hoefer and O. Buss. Assessing and improving model fitness in MOCABA data assimilation. *Annals of Nuclear Energy*, 162:108490, 2021.

[37] James F Slifker and Samuel S Shapiro. The Johnson system: selection and parameter estimation. *Technometrics*, 22(2):239–246, 1980.

[38] David T. Frazier, Worapree Maneesoonthorn, Gael M. Martin, and Brendan P.M. McCabe. Approximate Bayesian forecasting. *International Journal of Forecasting*, 35(2):521–539, 2019.

[39] Mark A. Beaumont, Jean-Marie Cornuet, Jean-Michel Marin, and Christian P. Robert. Adaptive approximate bayesian computation. *Biometrika*, 96(4):983–990, 2009.

[40] Jarno Lintusaari, Michael U. Gutmann, Ritabrata Dutta, Samuel Kaski, and Jukka Corander. Fundamentals and Recent Developments in Approximate Bayesian Computation. *Systematic Biology*, 66:e66–e82, 09 2016.

[41] PyMC Contributors. Approximate Bayesian Computation. In: PyMC examples. Ed. by PyMC Team. 10.5281/zenodo.5654871.

[42] PyMC Contributors. Sequential Monte Carlo. In: PyMC examples. Ed. by PyMC Team. 10.5281/zenodo.5654871.

[43] S. S. Vallender. Calculation of the Wasserstein Distance Between Probability Distributions on the Line. *Theory of Probability & Its Applications*, 18(4):784–786, 1974.

[44] Michael G. B. Blum. Approximate Bayesian Computation: A Nonparametric Perspective. *Journal of the American Statistical Association*, 105(491):1178–1187, 2010.

[45] Anand Patil, David Huard, and Christopher J Fonnesbeck. PyMC: Bayesian stochastic modelling in Python. *Journal of statistical software*, 35(4):1, 2010.

[46] Afaque Shams, Dante De Santis, Adam Padee, Piotr Wasiuk, Tobiasz Jarosiewicz, Tomasz Kwiatkowski, and Sławomir Potempski. High-performance computing for nuclear reactor design and safety applications. *Nuclear Technology*, 206(2):283–295, 2020.

[47] OECD Nuclear Energy Agency. International criticality safety benchmark evaluation project handbook, 2019.

[48] S. M. Bowman. Scale 6: Comprehensive nuclear safety analysis code system. *Nuclear Technology*, 174(2):126–148, 2011.

[49] Jagjit Singh Matharu and Vidya Devi. Uncertainty propagation in neutron activation cross-section measurement using unscented transformation method. *Nuclear Science and Engineering*, 193(3):314–324, 2019.

[50] Xu Wu, Koroush Shirvan, and Tomasz Kozlowski. Demonstration of the relationship between sensitivity and identifiability for inverse uncertainty quantification. *Journal of computational physics*, 396:12–30, 2019.